Detection and Discrimination of Bacteria and Pathological Analytes using Photoacoustic Flow Cytometry

By

Robert H. Edgar

B.S. Biology & B.A. Biblical Studies, Geneva College, PA 2002

M.A.T & M.S. University of Pittsburgh, PA 2003, 2013

Submitted to the Graduate Faculty of the

Swanson School of Engineering in partial fulfillment

of the requirements for the degree of

Doctor of Philosophy

University of Pittsburgh

2022

UNIVERSITY OF PITTSBURGH

SWANSON SCHOOL OF ENGINEERING

This dissertation was presented

by

Robert H. Edgar

It was defended on

December 13th , 2021

and approved by

John Kellum, M.D., Professor, Department of Critical Care Medicine

John A. Viator, Ph.D., Professor, Department of Engineering, Duquesne University

Dr. William Federspiel., Professor, Department of Bioengineering

John Hempel Ph.D., Retired

Dissertation Director: Partha Roy, Ph.D., Associate Professor, Department of Bioengineering

Detection and Discrimination of Bacteria and Pathological Analytes using Photoacoustic Flow Cytometry

Robert H. Edgar. PhD

University of Pittsburgh, 2022

Infections caused by antibiotic-resistant bacteria, such as *Clodostrium difficile*, *Acinetobacter baumannii*, carbapenem-resistant *Enterobacteriaceae*, and methicillin-resistant *Staphylococcus aureus* (MRSA), are increasing worldwide and cause significant strain on the healthcare system. Without early intervention, bacteremia can progress to sepsis, a potentially lethal condition. Rising prevalence of resistant bacteria have necessitated a move towards more rapid and quantifiable diagnostic tools, as time is of the essence in effective treatment. Current treatment relies on prescribing broad-spectrum antibiotics until blood cultures can be completed, a process which usually takes days to complete. Furthermore, sub-populations of seemingly isogenic bacteria may exhibit a range of antibiotic susceptibilities, often called heterogeneous resistance. These heterogeneous antibiotic-resistant infections are often misdiagnosed as hospital-acquired secondary infections because there are no clinically used tests that can differentiate between homogeneous and heterogeneous antibiotic resistance.

To address the need to improve rapid diagnostics for antibiotic-resistant "superbugs," we describe the development and proof of concept of rapid bacterial identification using photoacoustic flow cytometry and labeled bacteriophages with the characterization and differentiation of heterogeneous antibiotic resistant bacterial infections. Bacteriophages are viruses that infect bacteria, using specialized attachment proteins called tailspikes, to specifically bind to their target bacterial cell-surface proteins. We exploit this bacteriophage-host interaction specificity conferred

by tailspikes, along with other specific proteins such as antibodies and bacteriocins, by attaching these proteins to streptavidin-coated chromophores and passing them through the photoacoustic flow cytometer. In this setup, pulsed laser light is delivered to a sample containing tagged bacteria flowing past a focused transducer, with tagged particles absorbing laser light to create a photoacoustic response. We illustrate the ability of this technique to discriminate and enumerate any bacterial population using a bacteriophage-chromophore tag through a proof-of-principle experiment detecting and differentiating *Salmonella* from *Escherichia coli*. This research presents an innovative way of identifying and differentiating bacterial strains and sub-populations of antibiotic sensitivity. This method can be further developed for use with other bacterial pathogens in blood cultures representing a major step forward in clinical practice, speeding up delivery of effective treatment to patients by eliminating the need to culture samples.

Table of Contents

List of Tables

List of Figures

Preface

I am very grateful to all the members of my dissertation committee - Profs. Viator, Kellum, Hempel, Roy, Federspiel – for their support and willingness to advise me over my years at the University of Pittsburgh. I would like to express particular thanks to Dr. Kellum, Viator, and Hempel for believing in me when others did not and for allowing me the freedom to make mistakes and still build something great. Dr. Hempel has been one of my longest friends and supporters and a constant promoter of my dreams and even a financial supporter of my endeavors. Dr. Kellum likewise has used his connections and knowledge to allow me the opportunities to succeed. Dr. Viator has mentored me in both science and life and I can truly call a friend. Dr. Federspiel and Dr. Roy have both been most valuable in times of need and listened and helped me at the beginning and end of my time at the University of Pittsburgh.

1.0 Bacterial Detection

1.1 Current Methods

Bacterial contamination is part of all medical and industrial services. Detection of bacterial contamination early and accurately is imperative to reduce negative impacts of patients, production, and general well-being. The two main areas of bacterial diagnostics occur in the manufacturing/food industry and in the medical field. In both sectors, rapid determination of bacterial type and species as well as antibiotic sensitives are required. Many of the current methods have been derived to speed up the process of identification.

Culturing bacteria directly from a patient or sample is the "gold standard" whereby all other detection methods are judged but this process has its roots in ancient practices. Culturing of bacteria for production of food stems from at least 7000 B.C. with the production of cheese[4] and other fermented foods. As humans developed various methods of food fermentation and preservation, so did their understanding of the effects of bacteria upon food production and preventing spoilage. Although the people producing cheese and yogurt did not have the technical ability to recognize and fully understand the microorganisms responsible for these activities, they were able to understand the effects that bacteria can have upon food in terms of spoilage and fermentation. It is this understanding of bacteria's effects that have led to some of our modern detection techniques.

Two main advantages of using bacterial cultures are reproducibility and the ability to separate bacteria for further cultures or testing. A bacterial culture consists of millions of individual bacterial cells, which can be subdivided for future tests, including antibiotic sensitivity. Culturing

of bacteria in a clinical diagnostic laboratory consists of inoculating a patient sample into liquid or solid. If bacteria are present in the sample, they will grow and divide rapidly until a suitable number are present for visual or biochemical identification. Once a culture grows to appropriate density, a smear can be prepared and examined using light microscopy and staining procedures to identify bacterial shape and arrangement. In the clinical microbiology lab, gram staining is often used in one of the first steps in the culture-based bacterial identification process. This process, developed by Hans Christian Graham in 1884, was the first advancement in bacterial identification[5]. Gram Staining involves staining a bacterial smear with crystal violet-iodine complex, rinsing with alcohol, and applying safranin counter stain. This method can be used to classify bacteria based on cell shape, cell arrangement, and the biochemical nature of the bacterial cell wall. Gram-negative microorganisms have a high lipid content and low peptidoglycan content compared to Gram-positive bacteria. The differential nature of the Gram stain method results in Gram positive bacteria retaining the crystal violet-iodine complex within their cell walls while Gram negative bacteria fail to retain the stain during alcohol rinse. Gram-negative bacteria will appear red/pink under the light microscope due to the safranin counter stain while Gram-positive bacteria will appear purple. Because antibiotic therapy often depends on the biochemical nature of the bacterial cell wall, determining the Gram reaction of clinical samples is very critical for medical diagnosis.

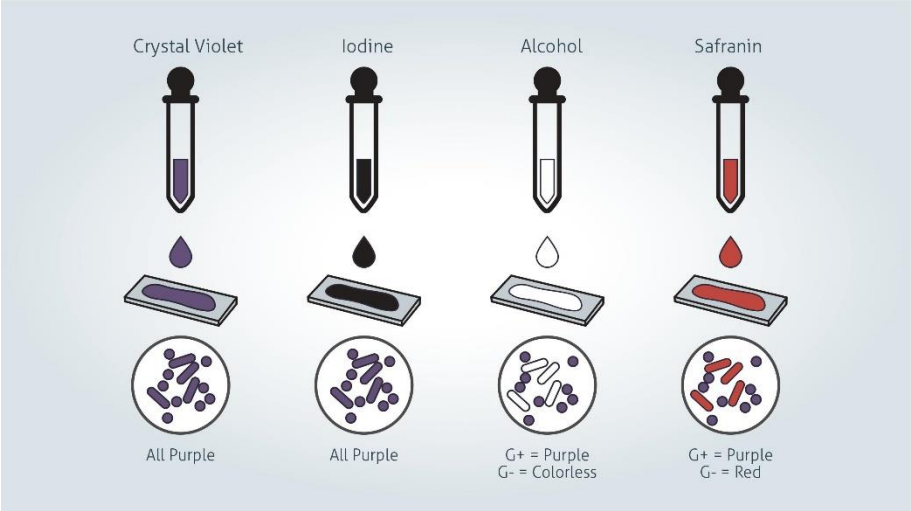

Figure 1 Graham staining procedure. Taken from

https://www.technologynetworks.com/immunology/articles/gram-positive-vs-gram-negative-323007

Bacterial cultures can also be grown in selective media for further classification and identification purposes. Selective media either contains inhibitors to prevent the growth of certain bacteria or a unique carbon source that only the desired bacteria can use. Recent advancements in media have led to the development of chromogenic media[1]. Chromogenic media allow the identification of pathogenic species of bacteria based on each bacteria's unique enzyme activity. Colonies of various bacterial species will metabolize synthetic chromogenic enzyme substrates in the media, resulting in color changes in the bacterial colonies. Bacterial hydrolases, often glycosidases such as ß-galactodase[6], are the most common targets for the development of chromogenic media. The chromogens produced from the enzyme cleavage are insoluble and remain localized on the bacterial colony, enabling interpretation of color changes to support bacterial infection. The produced insoluble chromogen are exogenous to the bacterial cell and therefore this method cannot be used with fluorescent flow cytometry. Chromogenic media are

now primarily used to screen for antibiotic resisitance targeting the ß-lactamases used by methicillin-resistant *S. aurres* (MRSA) or carbapenemases used in vancomycin-resistant enterococci (VRE)[1].

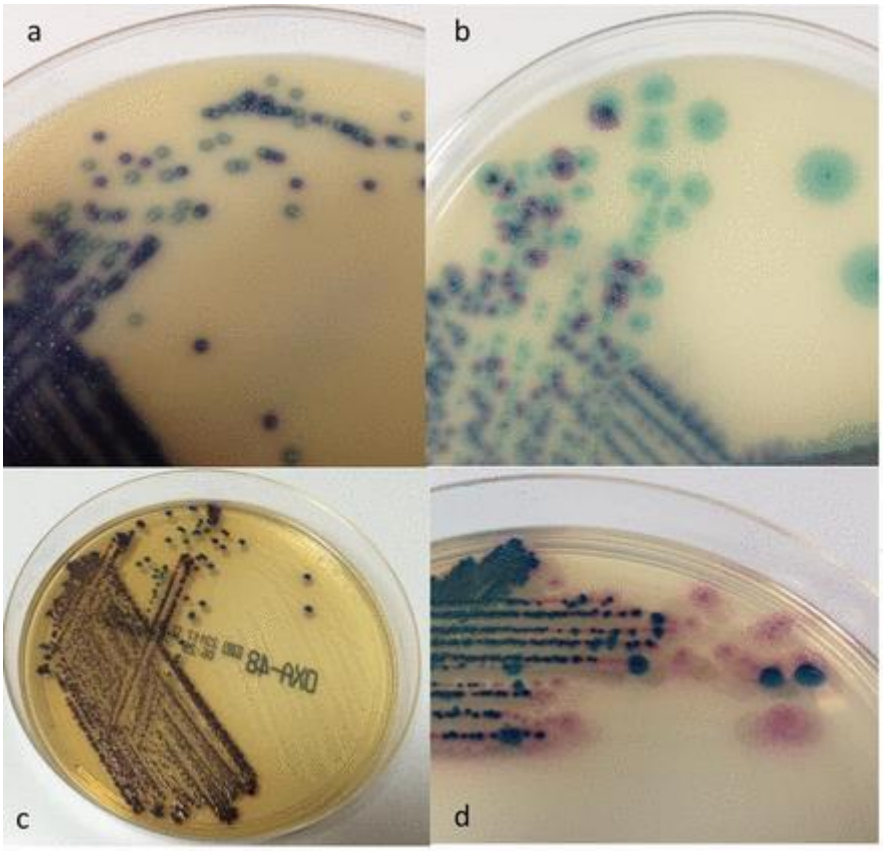

Figure 2 Examples of chromogenic media for detection of antimicrobial-resistant pathogens. (a) Enterococcus faecium and faecalis (b) Klebsiella pneumoniae with and Escherichia(c) K. pneumoniae and E. coli (d) Carbapenemase-producing K. pneumoniae with and E. coli

While numerous advances have been made in bacterial culturing technology, the growth rate of bacterial cultures places a significant disadvantage upon culture-based methods of bacterial identification to support a medical diagnosis or treatment plan. Bacteria often grow slower in selective media, therefore lengthening the amount of time required for identification. Due to these

long growth times (16-48hrs), chromogenic media is often coupled with Mass Spectrometry. Mass spectrometry identifies a pattern of bacterial peptides from a sample and this can be compared against known samples. This method can be used to accurately identify bacterial species from positive cultures.

1.1.1 Advanced Current Methods

Matrix assisted laser desorption/ionization-time of flight mass spectrometry (MALDI-ToF) has become a powerful tool in bacterial identification. Clinical use of MALDI-ToF developed in the last decade is powered by shared databases of previous samples, resulting in a powerful repertoire to support clinical diagnosis. MALDI-ToF requires a matrix treated sample to be irradiated by a laser and the ionization of analytes, which are separated based on time of flight to the detector. MALDI-ToF is very economical per test compared to other culture-based methods, once the upfront cost of the equipment is eliminated[7], because hundreds of species-level identifications from patient samples can be determined per day.

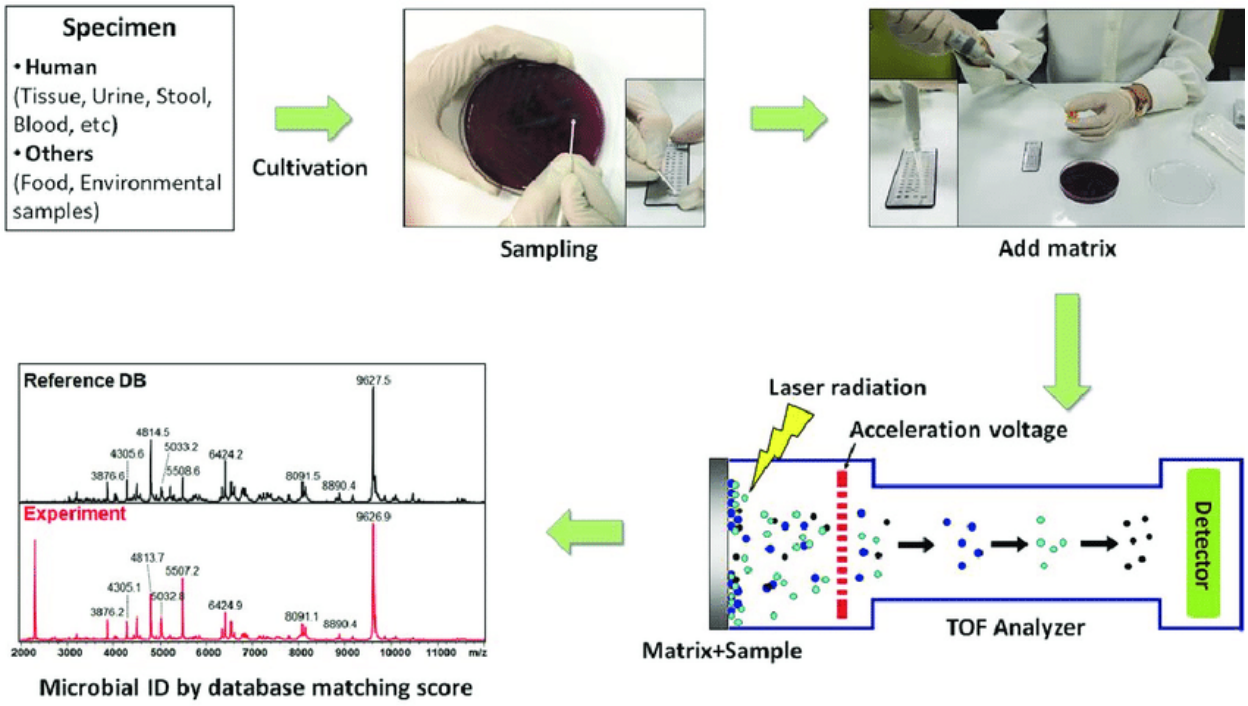

Figure 3 Workflow of microbial identification using MALDI-ToF MS

Despite the power of MALDI-ToF, this approach is still unable to differentiate highly similar bacteria or strains. For this reason, MALDI-ToF is often coupled with other methods such as culture, chromogenic media, or molecular techniques. Recent advancements in MALDI-ToF have reduced the amount of time needed for positive identification of bacteria. Traditional plate cultures take 24-48 hours and MALDI-ToF coupled with smudge plate reduces that time to 16-18 hours[8]. Although these advancements have improved the ability of MALDI-ToF in the clinical laboratory setting, the limitations of relying upon bacterial culturing techniques for accurate identification still pose significant impediment to diagnosing a patient's infection before hospital discharge[9].

Several molecular methods for bacterial identification are currently used in clinical laboratories. Most molecular methods analyze genomic markers and target species-specific genes

or antibiotic resistance genes. Hybridization methods use single or double stranded synthetic DNA fragments that are labelled with fluorescent dyes. These labelled fragments will bind due to their complementarity DNA targets and fluorescence detected. Fluorescence can either be detected *in situ*, such as in Fluorescence *In Situ* Hybridization (FISH), or bound to a microarray. FISH has found to be 96.5% accurate and take as little as 2.5 hours when tested on bacteremia patients[10]. Unfortunately, commercially available FISH probes have shown a higher than acceptable false negative rate (4.1% to 22.1%) when used alone and therefore require multiple probes to ensure accuracy[11]. One method of increasing accuracy is to massively multiplex the analysis using multiple tags against multiple targets. This is often done using microarrays and microchip designs. There are several commercially available systems targeting a variety of pathogens such as Nosochip (pneumonia causing bacteria, 5 gram-positive and 18 gram-negative)or FilmArray® Blood Culture panel (25 pathogens, 4 antibiotic resistance genes within 1 hour)[12, 13]. Though each of these molecular methods achieve high specificity and sensitivity they each require positive blood cultures and therefore still have a 18-20 hour response time.

Many other molecular methods rely fundamental on the core technology of Polymerase Chain Reaction (PCR). PCR is a way of amplifying a particular short piece of DNA using a DNA polymerase repeatedly to exponentially increase the target DNA. Most commercially available bacterial contamination test rely on quantitative real-time PCR (RT-qPCR) that uses labelled oligonucleotides and the detection of the change in fluorescence from the beginning of the run till the end to quantitate starting DNA concentration. Most PCR cycles require 20-35 cycles and take roughly 2 hours with an overall detection time ranging from 5 to 24 hours[14]. There are many commercially available PCR based tests available offering very high rates of sensitivity but each of them plagued by the possibility of contamination or unknown sample conditions. PCR has been

an invaluable tool in molecular biology laboratories but has had a slow transition into clinical laboratories. PCR, though highly sensitive, can often fail due to unknown concentrations in samples, secondary and tertiary DNA structures, and additional polymerase inhibitors such as EDTA and immunoglobulins[15]. Despite these drawbacks and high failure rates, PCR technologies have been particularly useful in difficult to isolate and slow growing microorganisms such as *Mycoplasma pneumoniae* and *Legionella* spp.[16].

Recent advancements in genome sequencing have allowed for rapid and cost effective whole genome sequencing. Genome sequencing combined with metabolomics provides invaluable information about specific bacterial contaminants, their antibiotic resistance genes, the expression level of those genes, and allows for tracing of bacterial outbreaks. This approach, though increasingly more cost effective, still requires culturing of bacteria from a sample and the amplification of DNA. Genome sequencing and metabolomics provide the most complete information of any method but still take days instead of hours. Despite the immense amount of powerful information generated from whole genome sequencing, it lacks the speed and consistency of other methods, and is rarely used as a standalone diagnostic.

There are several commercially available rapid diagnostic methods for bacterial identification. The majority of these rapid identification tests, such as Verigene and FilmArray, require a positive blood culture to be grown[17]. Accelerated diagnostics produces one of the most successful new rapid diagnostics with the PhenoTest BC. PhenoTest BC technology relies upon micro colony observation using in-situ hybridization and morphokinetic cell analysis by dark field imaging for identification and determination of antibiotic sensitivity [18]. Using this method, PhenoTest BC is able to identify bacteria within 1.5 hours and antibiotic sensitivity in 7 hours after a positive blood culture. Few technologies do not require a positive blood culture. T2 Biosystems

is a notable exception with it technology based on magnetic resonance. T2 Biosystems promises to deliver results in 3-6 hours straight from patient samples[19]. T2 Biosystems tests have proven cost prohibitive with their initial machine costs and each test costs range from $140 to $200. Compared to plate culture ($6-8 per test[20]), commercially available rapid diagnostic methods pose a cost barrier to treatment.

Table 1 Comparison of rapid diagnostics currently on market

Table 1 **Test**	**Culture time**	**Test time**	**Cost**	**Sensitivity**	**Specificity**	**Reference**
Selective media	16-48 hours	Visual inspection	$2-8	91.9-99%	97.1-99%	[1]
Chromogenic media	16-48 hours	Visual inspection		67.5-99.7%	91-100%	[1]
Multiplex PCR	5-18 hours	2 hours	$18.30-80	100%	94%	[21]
MALDI-ToF	16-18 hours	1-2 hours	$3-4	85%	93%	[22]
FISH	11.2 hours	2.5 hours	$377	96.50%	96.50%	[23]
Microarray	16-48 hours	1-3 hours	>$100	96%	98%	[24]
Sequencing	0	18-24 hours	$83	100%	100%	[25]
PhenoTest BC	0	1.5 – 7 hours	$200	97.40%	99.30%	[18]
T2 Biosystems	0	3-6 hours	$140-$200	95%	100%	[26]

1.2 Need for Improved Rapid Diagnostics

Resistance to antibiotics is a natural process that has been accelerated by human use of antibiotics in medicine and agriculture. In an effort to slow the rate of antibiotic resistance, rapid identification of contaminating bacteria is essential. New antibiotics have been slow to develop with only two completely novel antibiotics brought into use in the 75 year, high regulatory hurdles, and small economic value to the developing company[27]. From food processing plants to hospital beds, the speed at which bacterial contamination can be identified is the most important factor in treatment and control. Rapid bacterial identification negates the need for broad-spectrum antibiotic use and allows for targeted therapy. An estimated 90% of human antibiotic use is broad spectrum prescribed by general practice doctors[28]. Hospital acquired infections are implicated in 99,000 deaths per year in the United States and the World Health Organization estimates 7.1% of all patients admitted to hospital in Europe acquire a bacterial infection. In the United States, an estimated $30 billion is spent annually on dealing with antibiotic resistant bacteria[28]. One subset of bacteria is primarily responsible for the majority of multi drug resistant infections. The ESKAPE pathogens (*Enterococcus faecium, Staphylococcus aureus, Klebsiella pneumonia, Acinetobacter baumannii, Pseudomonas aeruginosa, and Enterobacter*) are responsible for the majority of nosocomial infections and mostly likely to be multi drug resistant[27]. Detection of these pathogens not only requires their identification but also the susceptibility to antibiotics. Ideally, rapid bacterial detection and identification of resistance would be fast enough to negate the use of broad-spectrum antibiotics, therefore allowing point of care facilities to test, and not require expensive equipment.

2.0 Bacteriophage

2.1 Bacteriophage Ecology

Viruses are ubiquitous and represent the bulk of genetic material present on earth. Viruses that infect bacteria, or bacteriophages (phages), comprise the majority of viruses in the biosphere and play a major role within food webs, and act as agents of gene transfer between bacterial cells [29-32]. Bacteria are the obligate hosts of phage and the two can have either a parasitic or a cooperative relationship [33]. Phage also play a central role and influence human immune system as well as non-host-derived immunity of metazoans [34, 35]. Through phagocytosis and cytokine response phage have been shown to directionally modulate mammalian innate immunity. Phage mediated infection and lysis of pathogenic bacteria increases antibody production and primed immune response similar to that of a human derived vaccine [35-37]. Lytic phage present in our soft mucosal membranes target and lyse invading pathogenic bacteria providing initial protection as well as providing inactivated bacterial antigens allowing human immune system to raise targeted antibodies[38, 39].

There are three possible infection cycles for bacteriophage [40, 41]. Temperate phages undergo either the lytic or the lysogenic cycle. During the lysogenic cycle, temperate phages, integrate their DNA into the chromosome of their bacterial hosts, forming lysogens. Phages in the lysogenic cycle do not reproduce, since the phage-encoded genes required for replication and lysis are silenced during this phase. Integrated temperate phages (prophages) require an induction event to induce chromosomal excision, phage replication, and eventual lysis of their bacterial host[42]. When prophages are present in bacterial genomes, they provide immunity to their bacterial hosts

against infection by genetically similar phages, and some prophages provide additional host immune defenses against infection by unrelated phages[43-45]. This immunity can allow for increased growth of lysogen-containing bacteria and bacterial blooms in various environments where phage infection normally controls bacterial growth [46]. Virulent (lytic) phage lack the machinery to integrate into bacterial genomes and therefore always lead to direct lysis of bacterial hosts as a consequence of phage replication. The presence of lytic phage in an environment suppress the growth of susceptible bacterial populations driving increased bacterial diversity and the coexistence of competing bacteria [47, 48]. Additionally, the lysis of bacterial cells plays a critical role in global nutrient cycles through the recycling of nutrients and the release of fixed carbon from dead bacterial cells [49]. The third possible infection cycle for a bacteriophage is the phage carrier state, a newly discovered scenario in which bacterial cells harbor episomal phage DNA elements that segregate asymmetrically upon bacterial divisions [50]. Although the phage carrier state is similar to the lysogenic cycle of a temperate phage, little is currently known about the advantages of a carrier state or its evolutionary role.

Central to bacterial evolution are phage that transfer host-derived genetic material at a rate of 10^{23} infections per second globally [51, 52]. The vast majority of all genetic material is transferred via temperate phages through the process of transduction [53]. High rates of recombination are observed through phylogenetic comparison and noted that non-random DNA fragments are transferred, with observed recombination boundaries correlating directly with predicted open reading frames(Genes

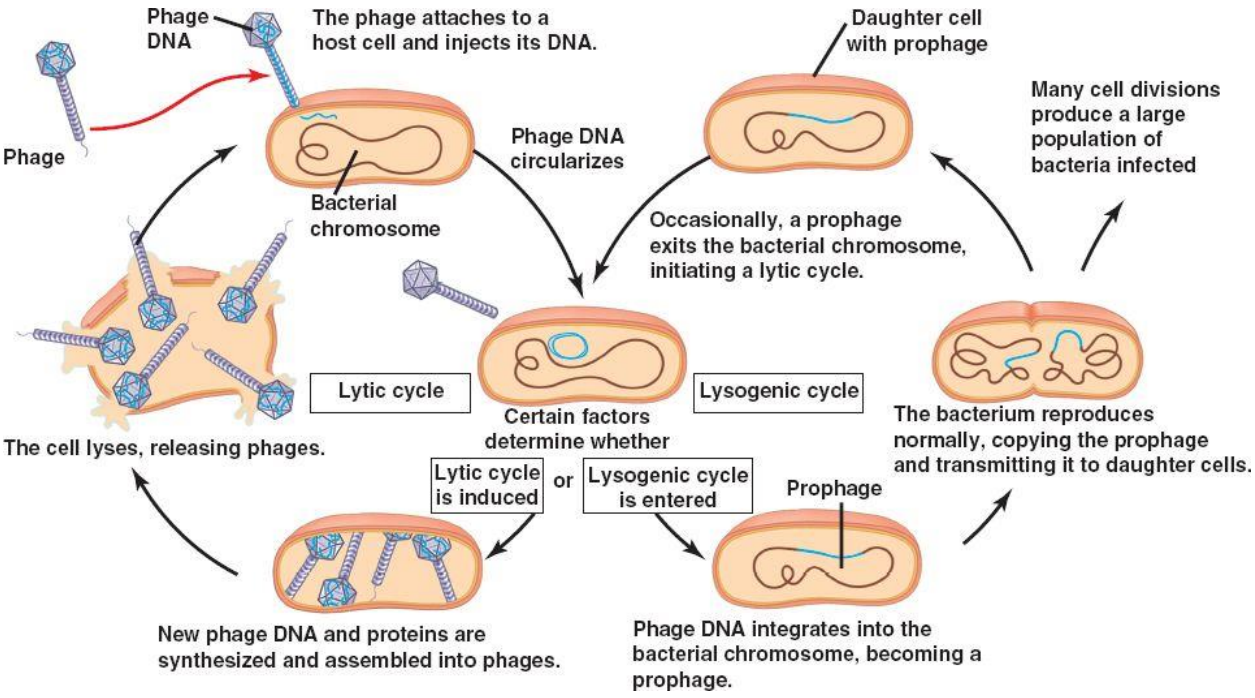

Figure 4Bacteriphage lytic and lysogenic lifecycles. Campbell Biology ninth Edition

predicted from genomic sequence) [54]. Virulent phage genomes show linear ancestry while temperate phage are highly mosaic in nature owing to their high rates of recombination. Virulent phage usually have well defined areas of recombination often associated with host range expansion[55, 56]. The large amount of genetic transfer means that any individual phage likely possess genes from multiple diverse evolutionary lineages [57].

Successful phage infection requires attachment to a host followed by penetration of the cell wall or outer membrane. Subsequent to attachment, injection of phage DNA is required to begin the co-opting of host machinery to produce phage encoded DNA and phage structural proteins. Lastly, phage encoded lysin proteins are produced allowing newly formed phage particles to exit the host cell[56]. Once phage have exited a cell, they are poised to infect a new bacterial cell. The majority of phage have a narrow host range, but a growing number of recently discovered phages

have evolved mechanisms allowing for more broad host ranges[58]. Some phage like Det7, which infects over 70% of *Salmonella* sarovars, have a broad host range within a single species. Other phage, such as phiSboM-AG3 that infect *Shigella* and E.*coli*, have broad host ranges that include multiple bacterial species. Host-attachment proteins of phage demonstrate diversity in specificity demonstrating phages adaptation for their target bacteria, fostered in mainly by high recombination rates in regions involved in host attachment [56, 57, 59].

2.2 Bacteriophage Structure

Bacteriophages are the best studied viruses, and a host of structural information has been amassed since their initial discovery. Most of early microbiological investigations and breakthroughs were made through the study of phage[60]. Rosalind Franklin's famous x-ray diffraction pattern used by Watson and Crick to elucidate the structure of DNA was in fact DNA from phage Lambda. Watson was a phage biologists working in the lab of Salvador Luria (for whom LB media was named) before accepting a post-doctoral position with Max Delbruck (leader of the Phage Group)[61]. Phage were in part chosen for their ease of manipulation and growth in the lab setting and their simplicity in structure. Phage structure is comprised of three main parts, the capsid where DNA is stored, the tail used to transfer DNA from phage into bacteria, and the host attachment apparatus. These three structures correlate with the three main historical ways that phage were identified and classified; capsid size, tail morphology, and host range[62]. With advancement in genome sequencing phage cladistics(classification) has changed dramatically based on gene relatedness and recombination and ordered by the International Committee of taxonomy of Viruses (ICTV) [63].

2.2.1 Capsid

Phage are primarily divided into two structural groups: Filamentous phage and tailed phage. Tailed phage consist of a tail position on one vertex of an icosahedral capsid and represent the majority of identified phage. Filamentous phage produce only a single capsid protein that wraps around the double stranded DNA of the phage to form a long filament. Filamentous phage are used in molecular biology for phage display libraries with the most commonly used ones being phage M13, F1, and Fd[64, 65].

Phage capsids posed an early fundamental problem and helped determine the information capacity of DNA. Shortly after the structure of DNA was solved, people became interested in elucidating the information inherent in the genetic code. Working from the assumption of the triplet non-degenerate coding ratio of base pairs to amino acids, it was noted that the amount of information transmitted by a virus could be determined by the size of the DNA that it carried [66]. Watson and Crick noted that if three base pairs coded for a single amino acid, then the information contained inside the viral capsid would be insufficient to code for a capsid large enough to contain it. The basis of this observation is evident when one considers that the average size of a codon is 2,100 Daltons, whereas one amino acid is on average only 110 Daltons. It was therefore postulated that viral capsids must be built from repeating subunits. Though these viruses infect a variety of hosts and exist in extremely different environments, many of them share a common icosahedral capsid architecture. Each of these icosahedrons is constructed from repeating protein subunits, comprised primarily of a single type of polypeptide: the major capsid protein. Despite the large range of viral capsid sizes (~30 - 400nm in diameter), the major capsid proteins of many viruses are relatively the same size and share a common fold. The precursors of these viruses established a way to build different size capsids using the same protein building blocks by modulating the

number of subunits. In addition, it was noted that the use of one repeating subunit would require that those subunits would exist in identical environments, where each subunit was identically bonded to its neighbor. A structure with identical subunits in identical environments is limited to what has been commonly referred to as the platonic solids: tetrahedrons, hexahedrons, octahedrons, dodecahedrons, and icosahedrons. Of the five platonic solids, only dodecahedrons and icosahedrons possess two, three, and five-fold symmetry. In addition, these shapes allow for the largest ratio of internal volume to surface area. An icosahedron is the most spherical of the platonic solids and therefore allows for the most efficient packaging of DNA and the lowest free energy structure. Each icosahedron is built from 20 triangular faces with 12 vertices, and 30 edges corresponding to its three, five, and two-fold symmetry axes [67]. Each of the 20 faces can be further divided into three asymmetric but identical facets to give a total of sixty possible subunits. By the time of the publication of Caspar and Klug's seminal paper on virus construction [68], it had already been demonstrated that several viruses seemed to display icosahedral symmetry. Oddly enough, some of those viruses seemed to possess far more than sixty subunits. This deviation requires flexibility in the bonding between subunits. As Pauling noted in 1953 [69], there is a flexibility in bonds of about 5^{o} in any direction from the average bond length. This flexibility allows for slight "deformations" in the identical bonds that hold each of the subunits to its neighbors. In order to have more than 60 subunits on the surface of an icoshahedron one must allow flexibility in the bonding angles and "environments" that those subunits possess. Caspar and Klug labeled this theory "quasi-equivalence". By allowing for quasi-equivalence, Caspar and Klug were able to show how "an infinite range of capsid sizes could be 'constructed' by combining 60T subunits [70]." The T number corresponds to the area occupied by each of the 20 faces and thus the size of the icosahedrons and can be derived from the formula $T= h^2 + hk + k^2$ [71]. Some

phage capsids have an elongated icosahedron like the prolate capsid of T4. These capsids are determined to have a triangulation number based on the arrangement of the pentamers and hexamers in the proximal and distal caps. The elongated portion in-between is defined as having a Q number.

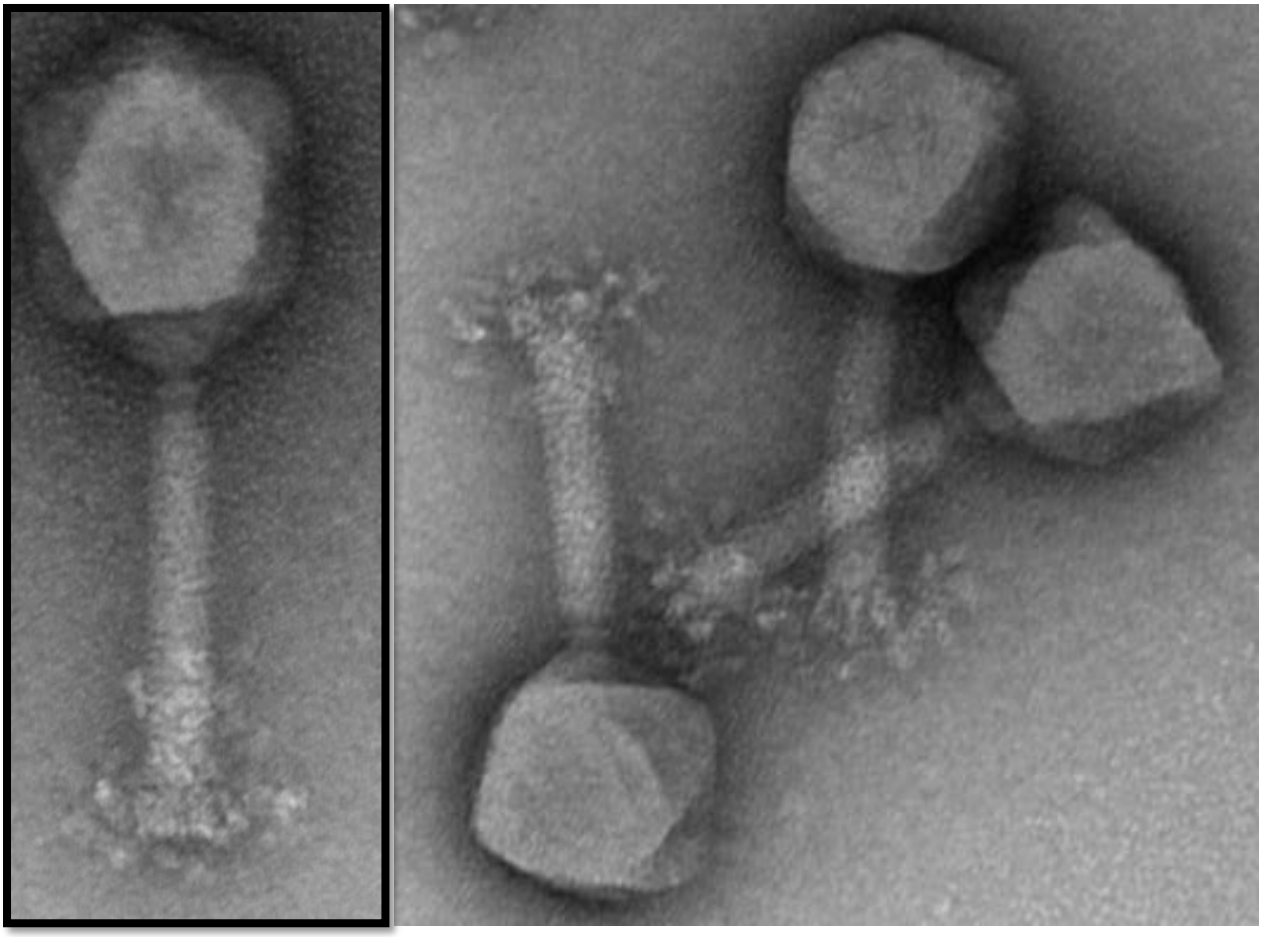

Figure 5Bacteriophage Det7 EM micrograph at 140,000 magnification displaying the equilateral triangles of the mature T=16 capsid. EM taken by R.H. Edgar

Since the publication of Caspar and Klug's theory of quasi-equivalence and description of icosahedral structures using triangulation numbers there have been several viruses that seem to

have structures that do not fit into their model. The elucidation of SV40's structure called into question the rules proposed by Caspar and Klug because it is built completely from pentamers with no hexamers. In addition, the phage HK97 prohead was puzzling because its hexamers were partially skewed to look like two trimers that had slid past each other. The identification of structures with apparent T=2 structures (a disallowed T number) also seemed to be exceptions to the rule. Viral tiling theory was proposed to more fully model the structures that have been identified specifically to account for the structures of the virus family *Papovaviridae.* Viral tiling theory describes the locations and bonds between subunits based on a mathematical concept of quasicrystals [72]. In contrast, Caspar and Klug's theory describes where the symmetry positions are located and makes no judgments on how the virus will accommodate that symmetry.

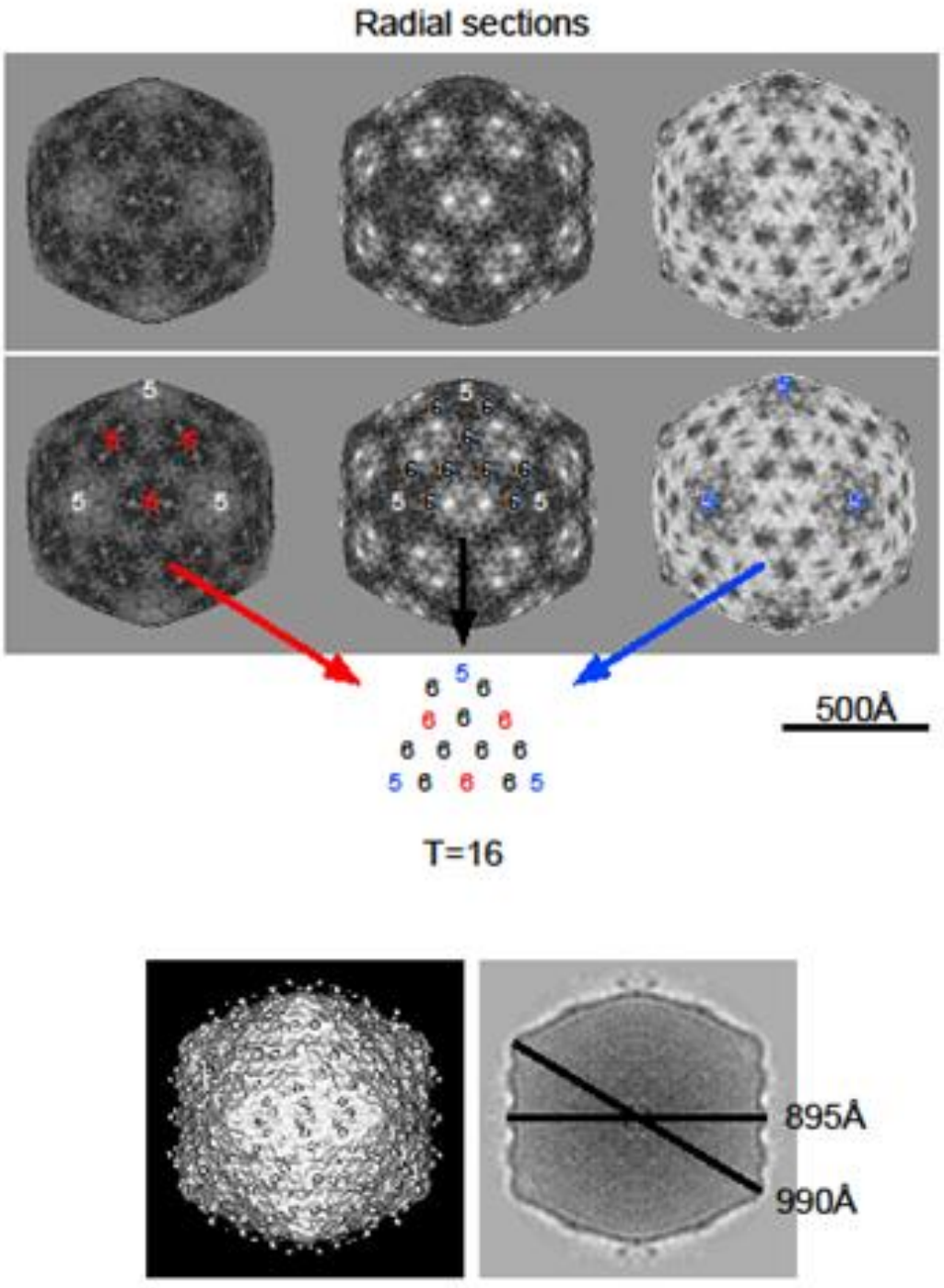

Figure 6 CryoEM reconstruction of Det7 Capsid demonstrating icosahedral symetery and T=16 triangulation number. Reconstruction performed by Dr. James Conway

There are many examples of structures that seem to be "exceptions" to the rules developed by Caspar and Klug as well as viral tiling theory. While some of these exceptions are real; others appear to be so simply from a lack of information. Those that are truly exceptions demonstrate the myriad ways that viruses and, fundamentally, proteins, can achieve stability. The viruses are unaware of the rules of triangulation that we have set up for them and are constantly about the business of finding new and novel ways to more efficiently build and maintain structures to protect their precious genetic cargo.

The size of a viral capsid specifies the amount of genetic material that can be packaged and transported by the virion. An increase in the capsid size allows for a larger amount of DNA or other proteins to be packaged and transported. For some bacteriophages, an increase in capsid size results in a corresponding increase in genetic material packaged due to the packaging mechanism. Many phage package their DNA using a pressure sensing mechanism termed head-full packaging[73]. In the case of phage T4, DNA is replicated as long concatimers inside the bacterial host and packaged until the mature capsid is full. Eiserling *et al.* were able to produce mutants that packaged upwards of ten complete copies of the T4 genome[74]. Some phage like Lambda use a system of DNA packaging where specific recognition sites in the DNA molecule called *cos* sites are used. Lambda cuts the DNA at these *cos* sites and only packages the amount of DNA from one *cos* site to the next[75].

Despite little conclusive evidence, studies of several model viruses yielded clues about how capsid size is determined. Much of the early work was done using T4 as the model phage. Each of the capsid proteins and scaffolding proteins were identified and manipulated by gene dosage experiments as well as deletion mutations. T4 was able to produce mature capsids without the aid of the core but at a dramatically reduced efficiency. In addition, the scaffold formed without the

aid or restriction from the major capsid protein. When expression of gp22 (the major scaffolding protein) was increased or gp24 (corner protein) was decreased, abnormally long particles were formed. In some cases long open-ended tubes were formed that suggested the scaffold inhibited distal closure while gp24 promotes distal closure [76]. In addition to T4, studies of several other model viruses have yielded clues into how capsid size is determined. Bacteriophage P2 has an icosahedral capsid with a triangulation number of 7 and a 33kb genome size. Satellite phage P4 produces an icosahedral capsid using the same major capsid protein (N) as P2 but with a triangulation number of 4. P4 packages an 11.6kb genome into its capsid that is roughly 1/3 the volume of the T=7 capsid of P2. The P4 satellite phage has no sequence similarity to the P2 genome except for 19 base pair cohesive ends and does not code for its own capsid or tail proteins[77]. P2 encodes gpO that acts as an internal scaffolding protein to determine the capsid as a T=7 icosahedron. P4 alternatively encodes Sid that acts as an external scaffolding and restricts the size of the capsid to T=4 icosahedron. Wang *et al.* found that gpO was completely dispensable in the presence of Sid for the formation of P4 capsids but was essential for producing P2 capsids in the absence of Sid[78]. In the case of P2/P4 it seems that capsid size is determined by the scaffolding proteins and their interaction with the growing capsid structure[79]. We learn from P2 and P4 that the capsid proteins do not necessarily possess in themselves a specification for triangulation number.

The coliphage P1 normally produces three variant capsid sizes named P1B (big), P1S (small), and P1M (minute) [80]. The tails all seem to be identical and each plaque-forming unit produces the same proportion of variant capsid sizes. The capsid sizes have recently been determined (Bob Duda, personal communication) to be T=13 for the P1B, T=7 for P1S, and T=4 for P1M. Only the P1B particles package a complete genome with P1S particles packaging about

less than 60% of the complete genome. P1B particles are fully infectious whereas the P1S and P1M particles only form plaques with multiple infections. At this point very little is known about what determines the size variation in P1 but it is interesting that the same major capsid protein is used in each of the three structures, therefore reiterating that size determination is not completely specified by the major capsid protein itself.

The *Bacillus subtilis* phage φ29 has also been used to delve into the determinants of capsid size and morphology. φ29 has been shown to have an internal scaffold constructed from gp7 and also to require the formation of a portal (gp10) to form wild type T=3 prolate capsids. When either scaffolding proteins or portal proteins are limited or deleted, aberrant structures are formed. In these situations larger T=4 prolate capsids are formed as well as smaller T=3 and T=4 icosahedral capsids. The evidence from φ29 suggests that the scaffold plays an important but non-essential role in stabilizing the skew of the hexameric capsomers [81]. φX174 also uses scaffolding proteins to assist in the formation of its icosahedral capsid. Interestingly though, φX174 has both an internal and external scaffold built around its T=1 capsid. In this odd case, the internal scaffold is built from 60 subunits to form a T=1 icosahedron identical to that of the capsid itself. The external scaffold for φX174 is built from more subunits and is a great deal more complex then the final mature capsid. In addition, the external scaffold, formed from 240 copies of protein D, does not have a typical T=4 arrangement because the subunits are not in quasi-equivalent positions. With its tiny T=1 capsid it carries a single stranded DNA genome of only 5386 base pairs that is so complex it was thought to be of extraterrestrial origin[82]. φX174 continues to be an exception which shows that scaffolding proteins are not used only for specifying larger capsid sizes. T=1 particles have been shown to self-assemble *in vitro* at a very high degree of efficiency and should not need the additional support and structure provided by either an internal or an external scaffold.

The precise reason that φX174 requires these scaffolding proteins has yet to be determined, but it could be postulated that perhaps the native environment of this virion is such that it could not successfully assemble without their aid.

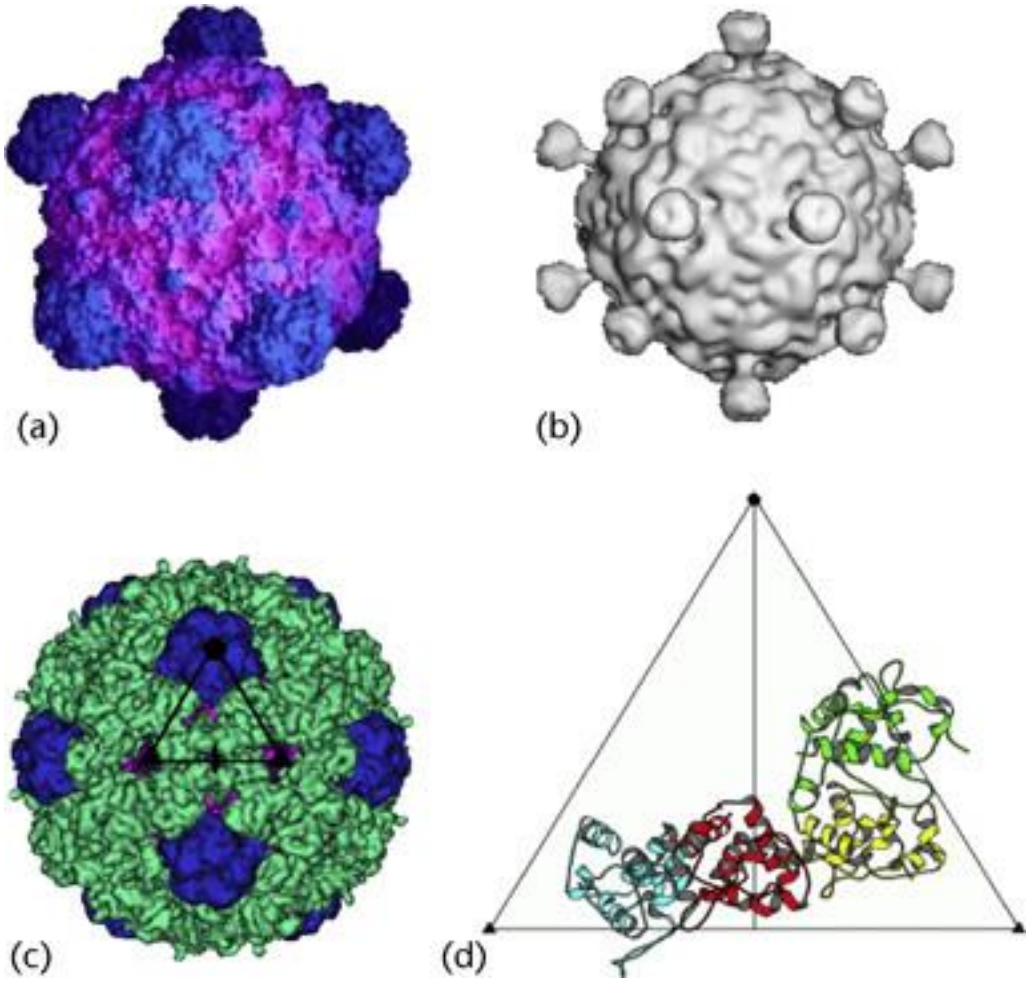

Figure 7 Virion and procapsids structures. (a) Atomic structure of ϕX174, a microvirus. (b) CryoEM image reconstruction of SpV4, a gokushovirus. (c) CryoEM image reconstruction of the ϕX174 procapsid. The external scaffolding protein is shaded in light green, the major spike protein in blue, and the viral coat protein in magenta. The triangle forms an asymmetric unit, which contains one coat, one major spike and four external scaffolding proteins. (d) the atomic structure of the four D proteins found in the asymmetric unit. Cherwa et al. [83]

Scaffolding proteins are commonly seen in capsids greater then ~500A^{o} in diameter but expelled from the capsid prior to DNA packaging [84]. For capsids that are T=7 or larger, it seems that additional help is required to stabilize interactions or specify geometry. In many cases this is accomplished by an internal or external scaffold built from encoded proteins that differ from the major capsid protein. In still other cases, that stabilization is produced by a part of the major capsid protein that is later cleaved and no longer present in the mature capsid. Although one might be led to believe that scaffolding proteins hold the key to capsid size determination, this certainly cannot be the case for all capsids. Both HK97 and T5 lack any gene encoding a scaffolding protein. Instead, both HK97 and T5 employ a second mechanism of proteolytic removal of the N-terminal portion of the major capsid protein [84]. This part of the major capsid protein, termed the Δ domain, is present during capsid maturation but is cleaved off by a protease and exits the capsid prior to DNA packaging. Interestingly, in the case of these two phages, the Δ domains of T5 which produces a T=13 capsid, is ~70% larger than that of HK97 which produces a T=7 capsid, though the major capsid protein of each is strikingly similar in size. It seems evident that the Δ domain plays a specific role in positioning and stabilizing of the major capsid proteins during maturation similar to that of the scaffolding proteins.

PRD1 has yet another way of stabilizing interactions and specifying the orientation of particular parts of its capsid structure. The capsid of PRD1 has an external structure with a pseudo T=25 lattice and contains a linear double stranded DNA genome of 14,927 base pairs surrounded by a lipid membrane. Recently, the complete structure was resolved at near 4A^{o} and revealed a new twist in capsid structure. An overlying lattice of 60 copies of a single protein was identified in the structure that extended from one vertex to the next. This minor capsid protein (P30) appears to act as a molecular tape measure in defining distance from one vertex to the next [85]. Molecular

tape measure proteins have long been known in relation to phage tails but never in specifying capsid size. It is likely that PRD1 is not the only virus to use such a mechanism as other large capsid viruses, such as PBCV-1 and adenovirus, share other structural similarities.

Scaffolding proteins, Δ domains, and tape measure proteins all share the common feature of assisting or aiding in the building of a proper sized capsid. It seems evident at this point that the major capsid proteins themselves, though often able to build the appropriately sized capsid, do not hold all the information to determine the size. The analogy has often been made between scaffolding proteins and chaperones that help proteins fold properly. The difference in the case of viral capsids is that the information is not inherent in only one protein but is imbedded in a collection of proteins, not all of which remain in the final structure, which specify the correct structure of the capsid. Scaffolding proteins, Δ domains, and tape measure proteins share analogous roles and we could therefore postulate some lineage among them or ancestral relationship but the futility would quickly become evident by the sheer number of differing plausible possibilities.

Phage capsids are the largest structural portion of bacteriophage and built from repeating subunits. The repeating subunits means that attachment of dyes or specific ligands are easy and predictable. The ridged structure and size of the capsids provides a reliable photo absorber for photoacoustic flow cytometry. Additionally, phage capsids can be emptied of their DNA to allow the uptake of dyes creating even better absorbing particles for use with photoacoustics. Due to the predictable and measurable size of phage capsids they provide a way to differentiate between multiple bound phage and single free floating phage particles. For photoacoustic detection single free floating particles are well below the detection threshold at normal laser energies. When multiple phages are brought into close proximity by binding to a single bacterial cell the

cumulative effect is much higher than the detection threshold. This differentiation is key to developing useful diagnostic assays using photoacoustic flow cytometry and bacteriophage.

2.2.2 Tail Structure

The capsid is essential to protect and store the phage genome, but is useless without the tail structure. Phage tails allow for controlled delivery of the genetic material into a bacterial host. This host selection and selectivity is what gives bacteriophage their marked advantage over static objects such as antibodies or protein ligands[86].

All phage tails share a similar attachment point on the bacteriophage capsid. A specialized portal vertex fulfills a multifunction role as both tail attachment and molecular motor. The specialized portal vertex is a multi-protein structure that replaces a capsid pentamer. In all phage, this connector serves as the docking site for preassembled tails[87]. The portal complex is a pentameric ring with a head completion protein inserted in the center. The ring serves as the tail-docking site as well as a conduit for DNA pressure release into the tail. The head completion protein is positioned in the center of the ring and retains the internal pressure of the packaged DNA until conformational changes allow for its release[87]. The ring and head completion protein are commonly referred to as the portal proteins and crystallography of multiple portal complexes has confirmed related 3D structures strongly suggested they are related evolutionarily[88]. All portal proteins contain four distinct domains; clip, stem, wing and crown [89] as conformed by over 40 x-ray structures.

All phage employ an ATP driven molecular motor to pump genetic material into capsids. The DNA-translocation machinery in centered around the portal complex with a packaging enzyme as well as recognition subunit[90]. The packaging enzyme, often referred to as the large

terminase is one of the fastest and strongest molecular motors discovered [91]. Phage T4's large terminase pumps DNA into its capsid at a rate of 2000 base pairs per second[92]. The packaging enzyme pumps genetic material into the phage capsid to near crystalline form and pressures ten times higher than that of a bottle of champagne or 60 atmospheres[93]. The stored kinetic energy from the pressure is released during phage infection allowing for rapid and total insertion of the phage genome into its bacterial host. Packaging of phage genetic material is initiated by the small terminase and completed by the large terminase. The small terminase possesses a three domain structure. The N-termianal domain serves as the DNA-binding domain while the C-terminal domain binds with the large terminase[94]. The central domain of the small terminase enzyme acts as an oligomerization domain causing many subunits to form between 8 fold and 14 fold symmetry[95]. The small terminase requires hydrolysis of one ATP molecule for every 2 base pairs of DNA translocated[90]. Multiple small and large terminase subunits form the portal complex, which also serves for the phage tail connecter.

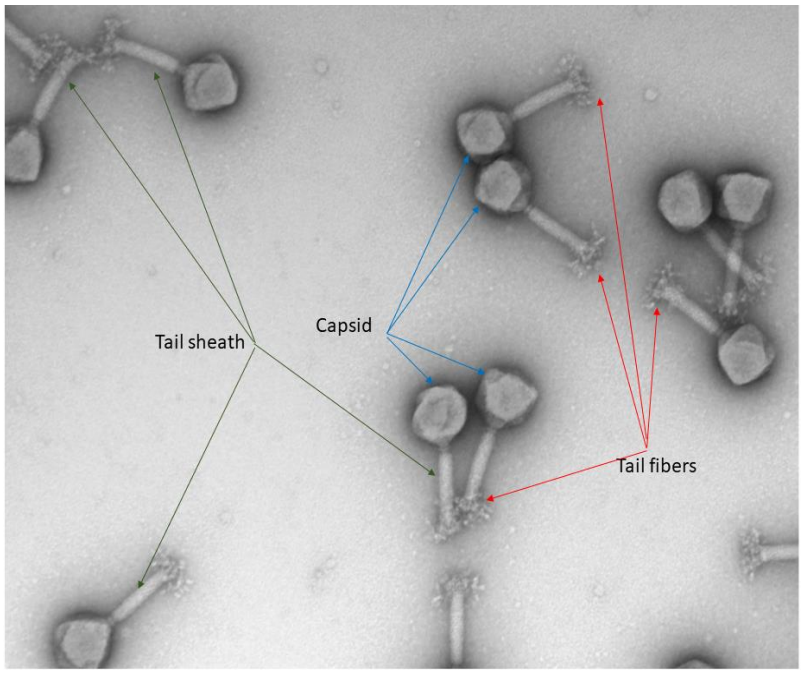

Figure 8 Figure 4Bacteriophage Det7 with capisd, Tail, and tail fibers/tail spikes marked. Picture by R. H. Edgar at 56000 magnification

Traditional classification of phage has been morphological in nature and primarily based on the types of tails they possess have classified them. Modern cladistics and genetic analysis have shown that related phage can swap tail types. Despite this, physical characterization of virion particles is still the primary way of classification. Phage tails are separated into three categories: Short tails, long flexible tails, and contractile tails. Phage P22 is the architype phage of the *Podovirdae* family. Like all members of the *Podovirdae* family, P22 fully assembles its capsid separate from its tail structure. Once the capsid structure is complete and DNA is fully packaged the tail proteins are then added sequentially. Both P22 and T7 have been had their tail assembly pathways elucidated by cryoEM and x-ray crystallography. Both tails follow an identical assembly pathway thus suggesting that all *Siphovirdae* follow the same general assembly pathway.

In each case, the connector proteins of the large and small terminase bind to the immature capsid allowing for the packaging of DNA. Upon completion of packaging the adaptor protein (gp11) binds to the connector allowing for binding of the nozzle proteins(gp12) and tail fiber proteins (gp17)[96]. All identified members of the *Podovirdae* family share a 6-fold symmetry of their tail structures.

Siphoviridae (long flexible tails) and *Myoviridae* (contractile tails) differ in their assembly from *Podovirdae* in that they fully assembly separately from capsid completion. In each case, the tail baseplate/ tip complex forms independently by self-assembly. Self-assembled baseplates have 6-fold symmetry and serve as a platform for the tail tube [97]. A tape measure protein also attaches to the baseplate and allows regulation of the tail tube polymerization [98]. The physical length of the tape measure gene regulates the length of the tape measure protein that determines the length of the completed phage tail complex [99]. Tail tube proteins oligomerize around the tape measure protein forming stacks of hexameric rings. Growth of the tail tube is stopped by the attachment of the tail tube terminator protein to the tape measure and tail tube [100]. It is at this point that the assembly of *Siphoviridae* and *Myoviridae* diverge. *Siphoviridae* flexible tail assembly is finished with the addition of the terminator protein but *Myoviridae* contractile tails require addition of several additional proteins. In *Myoviridae* tails the tail sheath forms around the growing tail tube propagating from the baseplate towards the terminator protein assembly. The sheath protein assembles into a 6-star helix around the tail tube. Each hexameric ring of the sheath protein is rotated relative to the next ring producing the 6-star spiral [101]. The head attachment proteins bind to the end of the sheath protein tube and serves as the head attachment site. This arrangement allows for contraction of the sheath protein as part of the DNA ejection mechanism.

The baseplate sits at the distal end of each tail and serves as an attachment point for host interacting proteins. Adsorption, where specialized phage proteins bind to bacterial cell receptors, is the first step in phage infection. Host attachment is mediated by specialized proteins called tail spikes or tail fibers presented on the posterior tip of tailed phages. These proteins attach to specific structures on the outer surface of host bacteria. Lipopolysaccharides (O-antigens), flagellin, teichoic acids, capsular polysaccharides (K-antigens), and specific membrane proteins such as nutrient transporters can be used as attachment sites [102]. The ability of a phage to attach to specific cell surface molecules is considered the primary determinant of host range. There are other physiological or genetic properties of cells that influence the ability of certain phage to replicate in them, for example the presence of a restriction enzyme or a CRISPR system, and these can in principle influence host range. The best studied host attachment protein is the tail spike of *Salmonella* phage P22 (P22TSP). The cell surface receptor of the P22TSP was shown to be the O-antigen of *Salmonella enteric* subsp. *enterica* , serovar Typhimurium [103]. Further investigation demonstrated that P22TSP recognizes the O-antigen α-D-Gal-(1-2)-α-D-Man-(1-4)-α-L-Rha-(1-3) repeats and cleaves the 3,6-dideoxyhexoses[104]. Each phage particle carries multiple homotrimeric tail spikes allowing for multivalent attachment and essentially irreversible binding [105]. O-antigen binding is much faster than hydrolysis suggesting the primary importance of binding the phage particle to the bacterial surface [106, 107]. Tail spike proteins are always trimeric and incredibly stable ensuring host binding is preserved above all else [108].

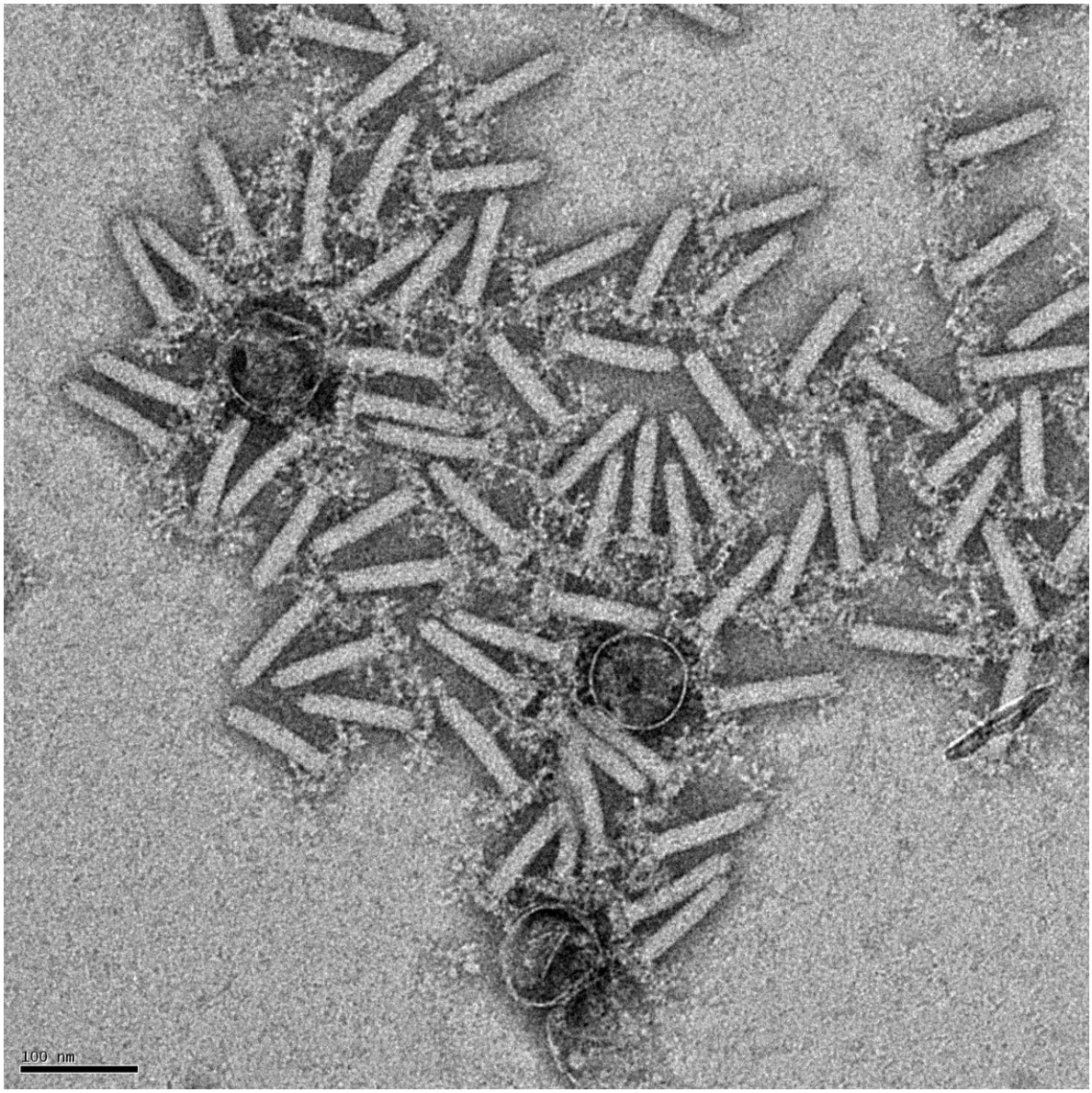

Figure 9: Bacteriophage Det7 Tails imaged by Alexis Huet. Tail preparation by R. H. Edgar

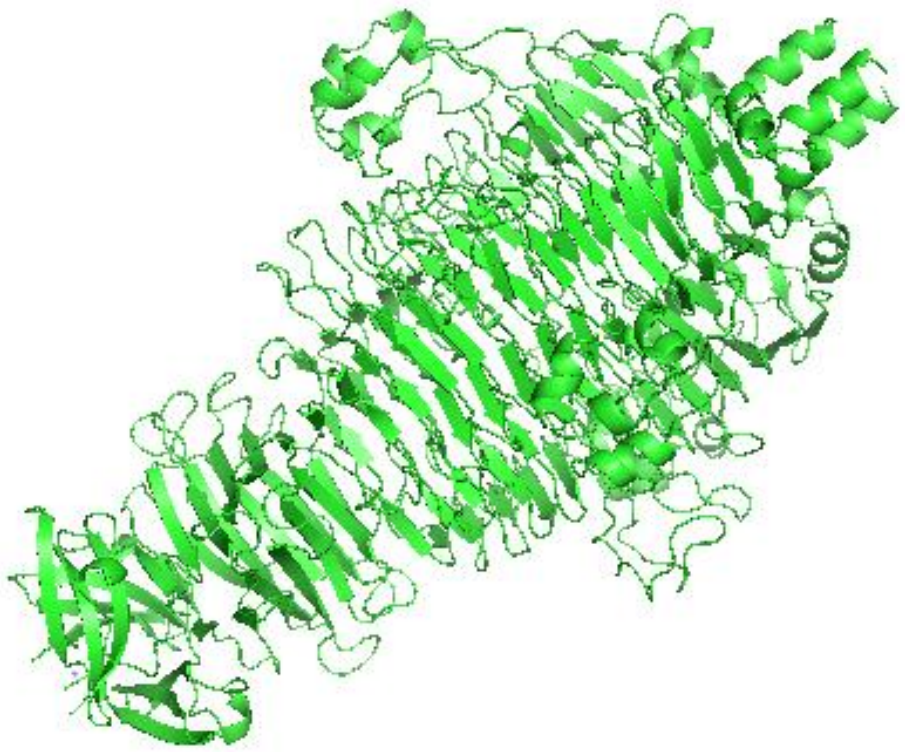

Figure 10 Reconstruction of Det7 Tail spike similar to P22 tail spike. Reconstruction made using HHpred by R. H. Edgar

Bacteriophage have evolved several mechanisms for injecting their genetic material into host cells. Depending on the type of cell wall and complexity, simple puncturing mechanisms to complicated hydrolysis of peptidoglycan through enzymatic activity have evolved. These multiple systems have been reviewed previously by Inamdar *et al.[109],* Xu *et al.* [110], and a host of others [111, 112].

Phage tails structures are essential to the survival and reproduction of bacteriophage. The host attachment proteins have evolved to rapidly and specifically bind only to their bacterial hosts. This specific binding allows from extremely high sensitivity and specificity from phage tail binding. When used with photoacoustic flow cytometry these tails are essential. The tails can be

combined with microspheres to produce bacterial binding particles that do not cause lysis of the target cell. Tails from multiple phages with different host ranges can create functionalized microspheres with any combination of host specificity. The stability of tail spikes means that these functionalized microspheres are stable and do not degrade when stored at room temperature for long periods of time unlike most other molecular probes.

2.3 Bacteriophage Therapy

Phage therapy is the commonly used name for the therapeutic use of bacteriophage in humans. Despite bacteriophage being ubiquitous in the environment, Phage therapy is the targeted use of bacteriophage against pathogenic bacteria in humans.

2.3.1 History of Bacteriophage Therapy

The discovery of bacteriophage is most often ascribed to French Canadian Félix d'Herelle and English Frederick Twort in 1916 and 1915 respectively. Though Twort preceded in discovering what would eventually be identified as bacteriophage he neither followed up on his observations or identified them as a replicating virus. Twort wrote up his observations of "glassy spots" but was unable to further investigate the cause [113]. Félix d'Herelle took a decidedly different approach and from his initial observations he published his seminal paper describing the effect and postulating the existence of bacteriophage[114]. "On an Invisible Microbe Antagonistic to the Dysentery Bacillus" was published in the French academy of Science in September of 1917. In it, d'Herelle argued that the invisible antagonist must be a microscopic virus that he named,

with the help of his wife, bacteriophage (*Les Périgrinations d'Un Microbiologiste.* Unpublished manuscript (FdH: 144)). D'Herelle continued to study and use bacteriophage for the rest of his life. He primarily focused on the application of bacteriophage as therapeutics for dysentery and typhoid fever. d'Herelle started his work with bacteriophage therapy by fighting multiple Cholera epidemics in India, researching at Yale university and the Pasteur Institute, and eventually agreeing to live and work at the Eliava Institute in Tiblishi, Georgia [115].

Bacteriophage research had a rocky start from the beginning. Controversy over priority of discovery and the exact nature of bacteriophage continued for almost 20 years following their discovery. The directory of the Pasteur Institute, Nobel laureate Jules Bordet, opposed d'Herelle's conclusion and postulated that bacteriophage were not viruses but "self-replicating lytic enzyme"[116]. In 1931 d'Herelle had to get a court order to allow his challenge of Bordet to be published. It wasn't until the invention and subsequent publication of electron micrographs of bacteriophage by H. Ruska that d'Herelle's position as bacteriophage as viruses was vindicated[117]. Much of the clinical and medical research of bacteriophage was ad hoc at best but d'Herelle prided himself at being an excellent experimentalist and using robust experimental design. In one of d'Herell's books, he brags of his experimental prowess: "In discussing this question with my colleague, Professor Einstein, he told me, as a physicist, he would consider this experiment as demonstrating the discontinuity of the bacteriophage. I was very glad to see how this deservedly-famous mathematician evaluated my experimental demonstration, for I do not believe that there as a great many biological experiments whose nature satisfies a mathematician" [118]. Despite the work of d'Herelle, many bacteriophage experiments, especially on the clinical side, were poorly designed and executed. The concepts of double blind studies and appropriate sample size were not yet common in clinical science. Three reviews published by the American

Medical Association in 1934[119], 1941[120], and 1945[121] all noted the "contradictory and confusing" nature and outcomes of bacteriophage therapy trials [116]. D'Herelle left his position at Yale University in 1934 to help establish the Eliava Institute of Bacteriophage Therapy in Tbilisi, Georgia, which was under communist Soviet control. Bacteriophage were widely used by the Soviet and German armies during World War II, since the Allied forces did not share their medical knowledge freely. d'Herelle did not last long in Tbilisi, especially after his friend and former colleague George Eliava was executed by the Russian secret police[115].

2.3.2 Bacteriophage Modern Uses

Despite the negative press and review bacteriophage received early on, they have consistently remained part of our scientific and healthcare world. Bacteriophage have consistently been a key tool in biological research. Rosalind Franklin used bacteriophage DNA in her crystallography "photo 51" that was used to determine the double helix structure of DNA[122]. Much of modern microbiology and virology was built upon bacteriophage research. The majority of structural virology uses bacteriophage or similar icosahedral viruses. Virology in general started with the T-even bacteriophage (bacteriophage T2, T4, and T6) as their model organism and expanded into other uses of bacteriophage. M13 bacteriophage is widely used in phage display and the high throughput screening of novel proteins and polypeptides[123]. Additionally, several groups take advantage of phage capsids to design drug delivery systems[124].

The single largest advance in microbiology and possibly modern medicine has been the discovery of CRISPR-Cas9 gene editing system [125]. The discovery of CRISPR as a bacterial defense mechanism against bacteriophage infection was first made by bacteriophage researchers and has since been widely adapted into other organisms for real time editing of living cells[126].

Large palindromic repeating sequences that matched bacteriophage sequences were found in bacterial genomes. These sequences were initially thought to be connected to dead prophage until Francisco Mojica showed the repeating sequences matched active bacteriophage genomes [127]. Advances in many of the CRISP-Cas9 have led to discovery of RNAi based systems in eukaryotes as well as commercial gene editing kits.

Another use of bacteriophage is in the detection and classification of bacteria. Phage typing has historically been used to differentiate morphologically similar bacterial strains. Phage typing is of particular use for bacterial strains such as *Salmonella* with over 2600 serovars. Advancements in bacterial sequencing and PCR techniques have largely taken over much of the bacterial typing. Despite this, there are many instances where phage typing is both cheaper and quicker than other biochemical techniques. Several companies and labs have expanded phage typing into a more robust test and even added antibiotic sensitivity testing using phage mutants. In 1987 Ulitzur and Kuhn used recombinant bacteriophage for rapid detection of specific bacteria and determination of antibiotic susceptibilities [128]. By 2006 Ulitzur and Ulitzur developed a method of where they were able to accurately determine antibiotic sensitivity as low as 40 CFU/ml in as low as four hours [128]. Bacteriophage have also been utilized in agriculture to discriminate pathogenic bacteria as well as control bacterial populations to maximize crop yield. Svircev et al have reviewed several methods of using bacteriophage in agriculture extensively *[129].* Several companies have also begun producing bacteriophage products for agriculture. Phageguard, based in the Netherlands, produces several agricultural bacteriophage products against Listeria, Salmonella and E.coli (www.Phagegurad.com). Intralytix (www.intralytix.com) has the widest range of bacteriophage based agriculture products targeting several species and combating many

veterinary specific pathogens such as *Salmonella, Clostridium difficile, Acinetobacter baumanii* and *Pseudomonas aeruginosa*.

Bacteriophage use as a human therapeutic has increased dramatically recently with the rise of multi-drug resistant bacteria. The rise of immunosuppressed people has also lead to an increased interest in using bacteriophage to treat bacterial infection in humans. Bacteriophage are also used prophylactically to ward off initial infection in patients. Several of the original products produced by the Eliava Institute, and still produced today, are prophylactic preparations of bacteriophage. Pyobacteriophage is a sterile filtrate from of lysates containing a mixture of bacteriophage that are active against *Staphylococcus, Streptococcus, E.*coli, *Pseudomonas,* and *Proteus*. Pyobacteriophage is used in "the treatment and prophylaxis or purulent inflammatory and enteric infectious diseases caused by above enlisted microorganisms" (http://phage.ge/products/pyo-bacteriophage/). The Eliava Institute produces several other bacteriophage preparations that can be used for acute treatment as well as prophylactically such as Intesti Bacteriophage, SES Bacteriophage, FERSIS Bacteriophage, and ENKO Bacteriophage.

Despite the overwhelming positives of bacteriophage and their uses in therapy and detection, there are some potential drawbacks or caveats. Some of the strengths of bacteriophage can also be some of their weaknesses in different situations. Specifically, the host range or specificity of bacteriophage is both a strength and a potential weakness. Bacteriophage are specific for their target hosts. Some bacteriophage have broad host ranges, meaning they infect a large number of bacterial types. Bacteriophage Det7 and the other bacteriophage of the VIunalikevirus genus typically have broad host ranges infecting multiple bacterial species or a majority of serotypes [55, 56, 130, 131]. Bacteriophage are limited to infecting bacteria that express as outer antigen or protein that can be recognized by the bacteriophages host recognition proteins.

VIunalike bacteriophage accomplish a broad host range by carrying multiple types of host recognition proteins. The advantage of possessing a broad host range is counterbalanced by the evolutionary cost of carrying extra genetic material and therefor a larger capsid. The majority of known bacteriophage poses only a single type of host recognition protein and thus have a much narrower host range. Bacteriophage Lambda has a single host recognition protein named J protein that attaches to the LamB receptor found on E.coli B. Bacteriophage Lambda has a very narrow host range due to the fact that it is restricted to bacterial cells that carry the LamB receptor [132]. The host range of bacteriophage Lambda can be artificially expanded by inserting a plasmid expressing the LamB receptor into other E. coli strains [133]. Despite this expansion, bacteriophage Lambda, like the majority of known bacteriophage, has a very narrow host range. In addition, because of narrow host range, bacteriophage are often mistakenly used against non-target bacteria. Simply administering an *E.* coli bacteriophage for and *E.* coli infection is not specific enough. The bacteriophage may not infect that particular strain of *E.* coli and therefore be useless at eliminating the infection. Bacteriophage cocktails have traditionally been used to circumvent this problem by combining multiple bacteriophage that infect the same types of bacteria. Recently, several studies have shown that this method can lead to increased bacterial resistance and ineffective long-term prophylaxis [134-136]. For bacteriophage clinical trials and bacteriophage therapy to be successful and robust and precise determination of bacterial susceptibility to a particular bacteriophage needs to be determined.

Photoacoustic flow cytometry coupled with bacteriophage can provide an essential element to modern phage therapy. Real time testing of patient samples against banks of bacteriophage to determine suitable phage for individualized therapy. Once appropriate phage are identified, photoacoustic flow cytometry can be used to determine the number of bacteria in a patient sample

and proper dosage of phage to be given to patient. These two features of photoacoustic flow cytometry will allow for safe and effective controlled use of bacteriophage as an alternative to antibiotics for initial care.

3.0 Photoacoustics

3.1 Physics of Photoacoustics

Plane waves are simplified idealizations of electromagnetic waves. Plane waves do not describe any physical phenomenon but instead are used to develop understanding and as approximations for localized regions of larger phenomena. Plane waves are used to derive general properties of electromagnetic waves but are mathematically easier to handle because variation is constrained to a single dimension. Planar waves are transverse electromagnetic waves that are invariant over a plane normal to the direction of propagation. Electromagnetic waves have both electric ($\bar{E}$) and magnetic ($\bar{H}$) fields that are perpendicular to each other and the direction of propagation. Specifically, in planar waves the direction of the electric and magnetic fields form a right handed triad. In order to be classified as a planar wave the magnitude must be invariant and orientation must be oriented toward the direction of propagation[137]. The generalized formula of a plane wave can be written as

Equation 3.1

$$\boldsymbol{F}(\vec{\boldsymbol{x}}, \boldsymbol{t}) = \mathbf{G}(\vec{\boldsymbol{x}} * \vec{\boldsymbol{n}},\ \boldsymbol{t})$$

where $\vec{n}$ represents the unit-length vector and $\vec{x}$ represent any position in space and any time (t).

There are three special types of plane waves used to approximate more complex wave functions. A standing plane wave is expressed as the product of two functions where one is

dependent only on position and the other only on time and a scaler function. A standing plane wave therefore can be expressed as

Equation 3.2

$$F(\vec{x}, t) = \mathrm{G}(\vec{x} * \vec{n},\ t)S(t)$$

where S is the scaler function of time. A monochromatic or sinusoidal plane wave is one where the profile is a sinusoidal function. Where A is defined as the amplitude of the wave and the scalar coefficient *f* is the "special frequency". The phase of a sinusoidal wave is represented as ϕ. Sinusoidal waves can be written as

Equation 3.3

$$F(\vec{x}, t) = A\sin(2\pi f(\vec{x} * -ct) + \varphi)$$

True plane waves cannot physically exist but are used as a model in physics to approximate waves emitted by a finite source with infinite extent into a large homogeneous space.

When the source of a wave is smaller than the wavelength emitted by it, it can be described as a point source. Point source is described as radiating sound waves equally well in all directions. Usually described as being a sphere whose radius alternatively expands and contracts in a sinusoidal fashion. When the point source, or monopole, expands it creates a pressure wave that is transmitted outward in all directions. Contraction of the point source follows and creates waves of high and low pressure radiating outward from the center. As the waves moves further from the source the amplitude decreases. This relationship can be described with the simple equation

Equation 3.4

$$I = \frac{W}{A}$$

The intensity (*I*) is the power (*W*) of the wave divided by the area (*A*) of the wave front. Since the wave front is assumed to be a sphere the following equation can be derived by substituting the area of a circle for A.

Equation 3.5

$$I = \frac{W}{4\pi\, r^2}$$

Moving further from the point source increase the radius and the intensity decreases. The intensity decreases as an inverse-square with distance. Therefore, the acoustic amplitude of the spherical wave is proportional to $1/r^2$.

Photoacoustics is fundamentally the induction of sound waves produced optically. The primary mechanism of inducing sound waves is through thermoelastic expansion though other mechanisms do exist. Radiation pressure, dielectric breakdown, vaporization and ablation are also mechanism of optically inducing sound waves. Radiation pressure is described as the mechanical pressure that is exerted upon an object due to the exchange of momentum, in this case, the exchange of momentum between the object and the electromagnetic field. Johannes Kepler identified radiation pressure, also called radiation pressure force, by observing that comets tails always pointed away from the sun[138, 139]. In comparison with these other forces, the force of radiation pressure is negligible[140]. Dielectric breakdown is a voltage threshold where currents above the threshold flow through the insulator. When used for lasers, this is only important for transparent mediums and for high laser intensities of the order of 10^7 V cm^{-1}[141]. Photoacoustic signals can be generated using dielectric breakdown and found to be proportional the laser pulse energy[142]. For laser energies below the dielectric breakdown threshold, vaporization and thermolelastic effect are the dominant processes [143]. Vaporization occurs at energy levels below dielectric breakdown and above thermoelastic expansion. When enough energy is deposited in a short enough time to exceed thermoelastic expansion time the particle is vaporized and turned to gas. Thermoelastic expansion occurs when optical energy is absorbed by a material and dissipated acoustically. When the optical energy is absorbed in a period of time smaller than the amount of

time required for the acoustic wave to travel the absorption depth, a condition referred to as stress confinement is produced. When a laser pulse is stress-confined the result is heating from the adsorption of optical energy which causes a stress on the material. The relation of absorption depth (δ)and speed of sound in the material (C_s) determines the stress confinement and can be expressed as a relationship[144]. Stress confinement can be understood from the equations:

Equation 3.6

$$\mathrm{T}_{ac} = \frac{\delta}{C_s}$$

and

Equation 3.7

$$\mathrm{T}_{th} = \frac{\delta^2}{4\mathrm{K}}$$

K is defined as the thermal diffusivity which is the thermal conductivity divided by the specific heat capacity and density of object. Simply, K is a measurement of the rate of heat transfer of a material[145].

The ratio between pulse duration to relaxation time of stress (T_{ac}) and temperature (T_{th}) represent the relative importance of photothermal effect versus that of the photomechanical effect.

When a laser pulse is stress-confined this results in heating of the region, creating stress on the object, and ultimately the generation of acoustic waves[146]. When laser pulse duration is less than $\frac{\delta}{C_s}$, it is considered stress confined. The reciprocal of the optical absorption coefficient is the absorption depth and is defined as the depth where optical energy is attenuated by $1/e$. An object is stress confined when meets the following equation:

Equation 3.8

$$\mathrm{T} < \frac{\delta}{C_s}$$

Stress confinement is an essential part of producing the photoacoustic effect. When laser energy is delivered and vaporization does not occur, the production of sound is exclusively due to the thermoelastic process[141].

When an object or cell is under stress confinement the resulting heating causes expansion and rapid contraction creating an acoustic wave. The size and shape of an object determines the shape of a resulting acoustic wave. When the cell or material under stress confinement is much smaller than the wavelength of sound emanating from it, it is described as a point source or monopole [147]. An acoustic point source will radiate sound waves with spherical symmetry, or equally in all directions as from a point. Compression waves are followed by a pulse of lower density or rarefaction causing a repeating pattern of high and low pressure waves. It is these pressure waves that can be detected by transducers and converted into electrical impulses and used in photoacoustics based diagnostics and imaging.

3.2 Uses of Photoacoustic Effect

3.2.1 Biomedical Photoacoustic Imaging

Photoacoustic imaging, also known as optoacoustics, is one primary use of the photoacoustic effect. Photoacoustic imaging combines the high contrast of optical imaging with the resolution obtained from ultrasound[148]. Development of techniques utilizing the photoacoustic effect can be traced back to Alexander Graham Bell and his observations of sound created by absorption of modulated sunlight[149]. It was not until the development of lasers in the 1960's that powerful monochromatic light was available to develop photoacoustic sensing[150].

For photoacoustic imaging optical wavelengths between 550 and 900 nm are most often used and offer the greatest depth penetration[151]. After suitable laser light was available, photoacoustic imaging became possible and lead to developments in image reconstruction and acoustic ultrasound transducers[152]. In photoacoustic imaging, a small temperature rise is created by the rapid absorption of photons by specific chromophores. Chromophores such as melanin, hemoglobin, lipids, and other water containing tissue are used. The rapid conversion of heat is well below the amount that would damage or change the targeted tissue (usually less than 0.1 K). This temperature change leads to a pressure increase and relaxation, which produces low amplitude acoustic waves. The broadband acoustic waves that are produced are and usually in the tens of megahertz range. These acoustic waves propagate to the surface where they can be detected. Detection of acoustic waves and time of arrival can be detected by either a single transducer or an array of transducers. The detected acoustic waves combined with other acquired data can be used for image formation. Many reconstruction techniques have been developed and new deep learning models are producing advances in image formation and resolution[152-155]

Photoacoustic imaging provides contrast based on the amount of absorption of each type of tissue or molecule. This fundamental difference in contrast differentiates photoacoustic imaging from ultrasound imaging. In photoacoustic imaging, optical scattering produced by soft tissue eliminates the ability to focus the excitation light in anything over 1mm deep. Ultrasound imaging, on the other hand, produces localization by focusing the excitation ultrasound wave. To achieve localization in photoacoustic imaging, the receiving transducers function independently to determine signal localization[156]. Despite the possible limitation of light scattering, photoacoustic imaging produces greater tissue differentiation and specificity than ultrasound

imaging. This is primarily due to the differences in optical absorption of different tissues types, which is more differentiated than the acoustic impedance difference[157].

Photoacoustic tomography is the most general form and least restrictive form of photoacoustic imaging. In photoacoustic tomography a large diameter, pulsed laser irradiates the whole sample area and produces a large tissue volume bathed in diffuse light. Large arrays of ultrasound transducers and calculating the speed of sound in the tissue can then be used to spatially resolve, back-project and reconstruct a three-dimensional image[158]. Ultrasound arrays positioned as spheres or cylinders for smaller objects or arrayed in a planar geometry for larger objects are most common. Several commercially available ultrasound arrays can be easily adapted for use with photoacoustic tomography though image quality can be limited. Commercially available ultrasound arrays operate in the sub-10 MHz range. For this reason, custom ultrasound arrays with center frequency ranges around 30 MHz are used to obtain better image quality in photoacoustic tomography[159]. By combining traditional ultrasound imaging and photoacoustic tomography deep tissue imaging of sentinel lymph node in breasts have been successful. The combined ultrasound/photoacoustic systems have been able to achieve real time imaging with 10 frames per second frame rate[160].

3.2.2 Photoacoustic Microscopy

Photoacoustic microscopy produces an image by using a focused transducer or a focused laser and producing an image directly from acquired A-lines. Acoustic-focused refers to the use of a focused transducer to produce acoustic-resolution photoacoustic microscopy (AR-PAM). Optical-focused refers to the use of a focused laser beam to produce optical-resolution photoacoustic microscopy (OR-PAM). To maximize image sensitivity photoacoustic signal are

generated from the overlap in acoustic foci and optical focal points[161]. This imaging modality holds advantages over light microscopy in that the image depth acquired. Photoacoustic microscopy can image several centimeters, deeper even than photoacoustic tomography[161]. As a non-invasive and non-destructive imaging technique, photoacoustic microscopy offers superior resolution and acquisition speed[162]. *In vivo* uses of photoacoustic microscopy are somewhat limited to surface structure such as mouse ears and mouse brain tissue with cranial openings in clinical applications[163]. Clinical applications broaden immensely when using photoacoustic technology with endoscopic devices. Among the targeted applications are detection of prostate cancer, intestinal cancer, and coronary artery disease [164-166]. The list of applications grows every year with advancement and miniaturization of acoustic transducers and cheaper lasers.

3.2.3 Photoacoustic Doppler Flowmetry

The photoacoustic Doppler effect is a specific manifestation of the Doppler effect created using the modulation of light intensity to create a photoacoustic wave in a moving particle. The shift in frequency provides and basis for calculating the velocity of object creating the photoacoustic effect[167]. This simple principle, when applied using photoacoustics, can be used to measure blood flow in a non-invasive manner without the use of contrast agents. Because the signal is emitted from the red blood cells, as opposed to being reflected by them, there is a significant signal-to-noise advantage. For this reason photoacoustic Doppler flowmetry lends to the measurement of low flow microvessles in the microvasculature[168]. Using focused transducers with a defined spot size near that of a single red blood cell (RBC) it has been possible to follow individual RBC's. Following a single RBS allows resolution within 0.1 mm s^{-1} and velocities up to 7.4 mm s^{-1} [169]. Combining photoacoustic Doppler flowmetry data with oxygen

saturation measurements produces a reliable measure of oxygen consumption of a specific tissue[170]. Individual tissue blood flow and oxygen saturation present a new level of diagnostics and targeted treatments in patients never before seen.

3.2.4 Photoacoustic Spectroscopy in Trace Gas Monitoring

Photoacoustic detection is well adapted to measurements of dilute and transparent samples. It is also well adapted to measure the light absorption spectrum of these samples. This becomes particularly useful in measuring trace gases in very low concentrations. Minimum detection levels in the part-per-trillion range have been achieved[171]. Using pulsed laser light of differing wavelengths, local heating of the target molecules is achieved, generating thermal expansion, which generates an ultrasound pressure wave. The detection of these pressure waves by miniaturized ultrasound transducers has been the greatest advancement in photoacoustic spectroscopy.

There are two main types of photoacoustic spectroscopy gas monitoring systems: Direct and indirect, both types rely on the photoacoustic effect but differ in their setup. Indirect systems use a smaller remote sealed gas chamber that acts as the photoacoustic cell. The acoustic signal is generated when the emission spectrum matches the absorption spectrum of the gas encased in the chamber. In this way, selectivity is introduced into the setup. Direct photoacoustic setups achieve selectivity solely by modulating the laser light into the gas chamber[172]. The majority of gas spectroscopy is done in the infrared spectrum (above 700 nm) for target gasses like Carbon Dioxide (CO_2) and ethylene (C_2H_4)[173]. Direct photoacoustic systems have been developed for *in situ* air quality monitoring in industrial and rural environments to measure the spread of trace compounds[174]. In environmental situations, detection ranges were in the parts-per-billion range

but increased by using continuous laser sources. Monitoring volatile organic compounds (VOC's), particularly from vehicle exhausts, is another major use of photoacoustic gas monitoring[174]. The uses and applications of photoacoustic trace gas monitoring continue to grow particularly with cheaper and more powerful LED laser systems.

3.3 History of Cytometry

Cytometry is the measurement and characterization of cells. Hemocytometers, the earliest cell counting devices, were developed near the end of 19th century. The ability to image and characterize individual cells was enhanced by the invention of the ultraviolet light microscope by scientists working for Zeiss and Leica, two of the largest companies producing microscopes to this day[175]. Although the use of ultraviolet light microscopy led to advances in cytometry, the unforeseen difficulty of autofluorescence posed challenges to imaging biologically active substances. Solving the problem of autofluorescence created a new line of investigation that eventually developed such early instruments as spectrophotometers, automated cell counters, and pulse cytophotometry[176]. The first commercially available machine that could be called a flow cytometer, called the Coulter counter, used electrical impedance to enumerate and classify particles under flow[177]. The following years saw many innovations and advancements for detection of particles under flow. Flow Cytometry as we know it now was developed in the 1960's from work at Los Alamos and Lawrence Livermore National Laboratories[178].

Flow cytometry requires a few fundamental parts to operate: electronics for detecting, computers for analyzing detections, optics for light sources and capture, and fluidics for sample movement[178]. Flow cytometry is most widely associated with fluorescent flow cytometry in

which laser light is used to induce light signals from particles under flow. Illumination source lasers are used due to their ability to deliver intense illumination and ability to be focused to a point. Early lasers used in fluorescence flow cytometry were single wavelength argon ion lasers. As lasers have advanced, so has the detection abilities of fluorescent flow cytometry. Most modern fluorescent flow cytometers have multiple excitation lasers, enabling the detection of multiple fluorochromes within one sample. Due to advances in fluorochrome development, 18 or more colors can be differentiated in a single sample[179].

Fluidics are also fundamental to flow cytometry. Laser light can be focused to illuminate a single bacterial cell at a time, but this ability is of no consequence if the fluidics system is insufficient for proper sample measurement. With particles flowing past the excitation and detection sight, flow cytometry ensures that each particle is analyzed only once. One requirement of flow cytometry fluidics is that cells flow in suspension and form a single file line. This necessitates removal of extracellular matrix from cell colonies and tissues requiring disaggregation. Despite additional processing steps, large numbers of cells can be analyzed and populations characterized, with a sufficient flow rate. To achieve sufficiently fast and uniform flow rates, Crosland and Taylor developed a strategy for injecting sample flow into the center of a wider faster moving stream, named sheath stream[180]. Crosland-Taylor's technique results in a narrow stream of cells encapsulated by a wider sheath stream the minimizes turbulence and maximizes optical efficiency[178]. In this way, the flow rate of the cell suspension can be increased or decreased for rapid processing but also that ensure only one cell passes though the detection laser at a time.

Analysis of signals derived from cells is primarily dependent upon the signal detection method. The signal detection is where the most common type of flow cytometry differs from other

types. Fluorescent flow cytometry relies on the absorption of photons and detection of the fluorescence given off by a particle at a different wavelength. Fluorescence can be detected using dichroic mirrors to filter out unwanted wavelengths. Alternatively, filters can be used to ensure that only one wavelength of light is allowed to reach each photomultiplying tube (PMT). The photodetectors convert the photons hitting them into an electrical current that is proportional to the intensity of light. Photodetectors are usually used for forward scatter light from the detection laser. Photomultiplying tubes are used for side scatter light, or detection of fluorescence from a detected object. Photomultiplyers use high voltage to increase their gain in order to detect weaker signals. Signals from both photodetectors and photomultiplyers are then amplified which produces a voltage pulse proportional to the number of photons that reached each detector[178]. There are a multitude of signal processing systems and methods for fluorescent flow cytometry. Many of the recent advancements have been from the signal processing and computational methods used to analyze the detections[181].

Despite the many advancements in detection and signal processing of fluorescence there are some fundamental downsides. Photons are much easier to be blocked or scattered, especially in turbid environments.

3.4 Photoacoustic Flow Cytometry

3.4.1 In Vivo Photoacoustic Cytometry

In vivo photoacoustic flow cytometry setups have also been built and utilized particularly in small animal models. For *In vivo* models, there are different hurdles to overcome and factors

that can greatly influence the accuracy and reproducibility of the system. There are also many advantages to *in vivo* photoacoustic flow cytometry. Sample preparation time is eliminated using *in vivo* systems as well as any variability introduced by manual processing of samples. Sample processing for *in vitro* systems could possibly bias samples towards an extreme by eliminating potential targets or failing to eliminate off-target absorbers such as red blood cells. *In vivo* systems have no built in processing bias nor is time used in sample processing. Despite the processing advantage, *in vivo* systems require preparation of the tissue or vessel used as well as possess potential detection bias based on system configuration. *In vivo* systems have one large advantage in that the amount of blood or sample that can be surveyed is not limited and therefore much larger volumes can be used. For this reason, *In vivo* systems with sensitivities loves of 1-10 cells/ml can detect very early stage disease[182-184].

In vivo photoacoustic flow cytometry is non-invasive and usually label free, relying on natural pigmentation of cells for detection. Zharov *et al.* have described labeling systems using gold nanoparticles for *in vivo* labeling and even ablation of target cells[185]. In their system, they conjugate gold nanoparticles with monoclonal antibodies specific to *Staphylococcus aureus* and a multi-laser system to detect and produce laser-induced overheating of gold nanoparticles bound to *S. aureus* cells. To accomplish this, a dual Nd: YAG laser is used to produce both 532nm laser light from the second harmonic crystal and 355nm laser light produced from the third harmonic crystal. A Third He-Ne laser producing 633nm laser light was introduced to complete the thermal lysis of bacterial cells. The bound cells were ideally detected by the 355nm with a 0.1 s delay till irradiation with the 532nm and 633nm lasers light. Once detected, cells were irradiated with 532nm laser light for 8 ns which caused bubble formation and defocusing of intensity allowing the

addition of the 633nm laser light to finish the thermal lysis effect[185]. A schematic of this system is displayed below in figure 11.

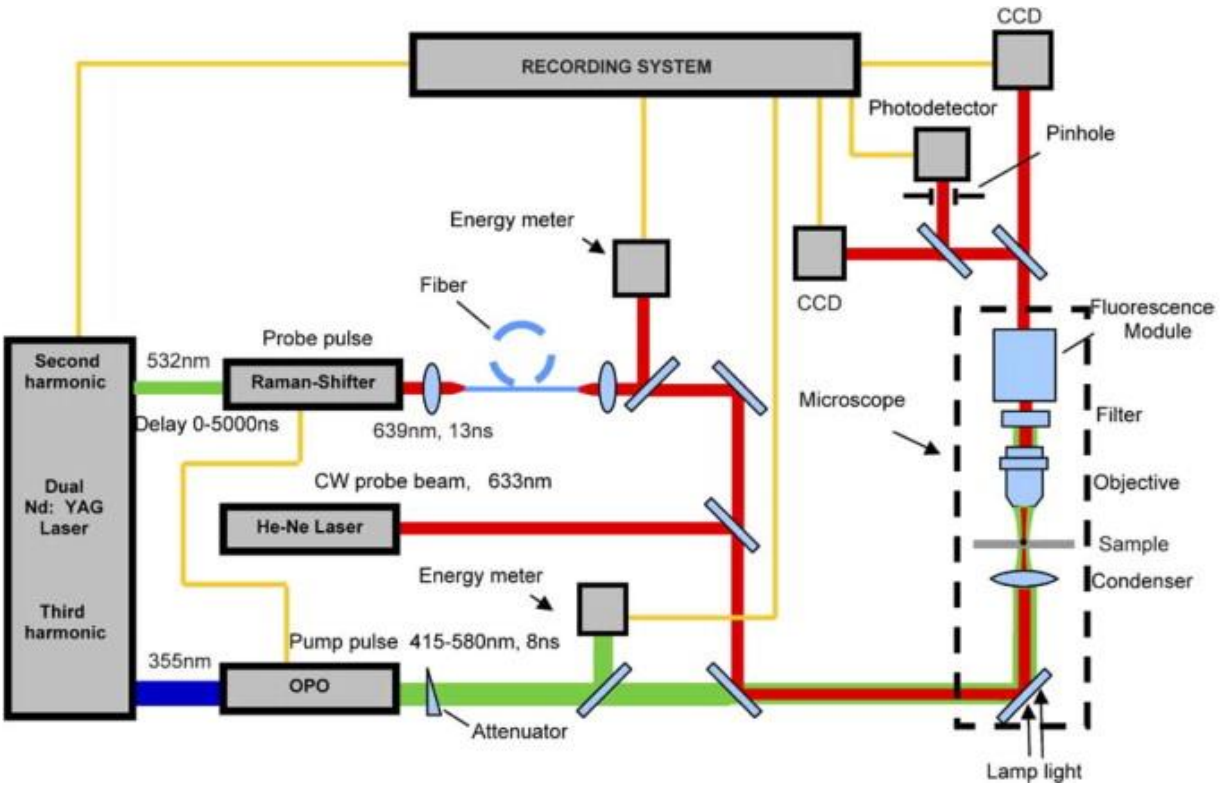

Figure 11 Schematic of in vitro flow cytometry setup described by Zharov et al.

In addition to the photoacoustic lasers, a CCD based Photothermal (PT) microscope visualizes and records the lysis even. Images were illuminated from the laser light and images recorded using the CCD camera to determine and record each as a lysis even.

This particular system, though designed for *in vivo* usage, is almost exclusively tested on *in vitro* samples as a proof of principle. One major drawback to using this system *in vivo* is the minimal depth that can be achieved before light scattering requires laser energies that will damage surrounding tissue. For this reason, only small vessels near the surface are suitable for this system. Large surface vessels are also unsuitable for this method due to their wide diameter, which allow

multi file flow. Multi file flow eliminates the ability to reliable enumerate and detect every cell with a narrowly focused laser beam. Widening the laser beam creates another problem of damaging unwanted cells as well as eliminating the ability to differentiate signals generated from multiple cells or single cells.

One of the largest drawbacks to *in vivo* Photoacoustic flow cytometry is light scattering. To minimize the effects of light scattering, Tuchin e*t al.* described a method of hyperosmotic cleaning of tissue[186]. By cleaning the surrounding tissue to the vessel being used for *in vivo* photoacoustic detection, they were able to achieve a 1.6-fold decrease in laser spot blurring in a mouse model[187]. In human trials they were able to achieve 2-fold increase and acquire signals from a 1.3mm-deep vein[186]. Despite the increase in signal and improvements, *In vivo* methods of photoacoustics are still only useful on small surface vessels. This limiting factor means, that despite the claim of being able to process an entire human's blood pool, the practical time limits render this method unusable.

One advancement of *in vivo* photoacoustics has been minimally invasive delivery of laser light. In this case, a laser is coupled to a 100 μm-diameter quartz fiber and inserted directly into a mouse abdominal skin vessel[188]. The laser light is delivered directly to the vessel and a focused transducer is directed towards the vessel from the skin surface. This method was used in a mouse model to detect circulating melanoma tumor cells at a very low concentration. Direct delivery of laser light lessens the drawback of optical scattering and partially lessens the burden of achieving high resolution. Direct laser light delivery can also only be used in sufficiently small vessels with appropriate flow volumes limiting its useful ness to small surface vessels.

There are advantages and disadvantages of every method. Many advantages of *in vivo* photoacoustics are listed above such as the detectable volume and lack of sample preparation.

Several disadvantages such as limitations of vessels used and vessel size. Also, inability to control flow dynamics and optical scattering are constant hurdles to overcome. Perhaps the largest hurdle to *in vivo* photoacoustics is the presence of multiple off target light absorbers, primarily red blood cells. Processing of blood samples to remove red blood cells is a standard part of *in vitro* photoacoustics. Without labeling and processing of blood samples, *in vivo* photoacoustics is dependent on methods of eliminating signals derived from red blood cells and any other of target optical absorbers present. Much work has been done to eliminate confounding signals from red blood cells. Changing the concentration of blood osmolarity as well as oxygenation level far outside of physiological norms was proposed and tested [189] but ultimately showed little useful improvement and proved impractical to integrate into an *in vivo* photoacoustic system. Target differentiation using two different laser wavelengths has been more successful[188]. Galanzha *et al.* describe a multi laser setup to detect circulating melanoma tumor cells in a mouse model using a small vessel of the mouse ear. Their system consists of a single 3.5 MHz unfocused ultrasound transducer or a focused 20 MHz transducer detecting signals. Laser light was delivered to the detection sight at a wavelength of 865 nm and 639nm employing a Raman shifter to induce a 10-μs delay. Laser pulse durations were limited to 5-10 μs each allowing the signals to be time resolved. The short pulse duration resulted in a compressed amplified and processed as well as estimation of flow velocity. Signals from red blood cells were detected using the 865 nm wavelength laser light were compared to signals generated from the 639 nm wavelength. Red blood cells showed weak acoustic signal from 865 nm wavelength and no signal from 639 nm wavelength. Spiked melanoma tumor cells showed strong signals at both wavelengths allowing for differentiation of classification of each detection[188].

Cytometry has had a long history and development from its beginning with Alexander Graham Bell to today's fluorescent flow cytometry and recent advancements in photoacoustic flow cytometry. Advancements in fluidics and lasers have been the primary technologies allowing advances in flow cytometry. Fluorescent flow cytometry, despite being ubiquitously used, has many drawbacks that are eliminated by photoacoustics. The photoacoustic effect is used for a variety of purposes from laser hair removal to detection of particles under flow. Fundamentally, sound is a more robust medium for detection. Photoacoustic flow cytometry is well adapted to find rare particles in complex environments. Both *in vivo* and *in vitro* photoacoustic flow cytometry systems have been used for detection and isolation of circulating tumor cells as well as detection of bacteria. There is much room for innovation and development to advance the capabilities of photoacoustic flow cytometry.

3.4.2 In Vitro Photoacoustic Flow Cytometry

Photoacoustic flow cytometry is particularly good at finding rare particles in dilute samples. *In vitro* setups have the added benefit that detected cells can be isolated for further study. Additionally, blood samples can be preprocessed to increase specificity by removing red blood cells. Blood separation is often accomplished using a Ficoll separation technique commonly used in many hospital laboratories. A typical *in vitro* photoacoustics setup has been described earlier by Viator[190], O'Brien[191], and Edgar[192]. Each setup includes a laser source, flow cell, transducer and recording computer.

Aa a laser source a 532 nm Nd:YAG laser (Litron Nano, Bozeman, Montana). We chose 532nm due to the low cost and high energy output. A 1000 μm diameter, 0.39 numerical aperture, optical fiber (Thorlabs, Newton, New Jersey) is coupled to the laser in order to allow focused

energy to be deposited on our sample. The laser beam energy coupled through the optical fiber was maintained and measured from 0.8 - 4.6 mJ, depending on the experiment. Energies above 6 mJ caused burning of the optical fiber. The laser repetition rate is set at 5 nanosecond pulses and the trigger was connected to our amplifier for signal recording. Laser light was directed to a quartz tube with 10-micron thick walls passing through a 3D-printed flow chamber. The 10-micron thick quartz allows the propagation of ultrasonic waves as well as providing a chamber for the sample to flow through which provides no optical contrast.

A 2.25 MHz transducer (Olympus, Waltham, Massachusetts) focused on the quartz sample tube was fitted to the base of the 3D-printed flow chamber. Signals are then transferred along standard coaxial cables to an amplifier (National Instruments, Austin, Texas) with a gain of 50. Amplified signals are subsequently transferred to a recording computer running a customized LabView program. This can be seen in Figure 13.

The internal volume of the chamber was filled with Sonotech LithoClear acoustic gel to provide a medium for propagation of acoustic waves. This flow chamber set up served as the excitation and acoustic wave collection device and is illustrated in Figure 12.

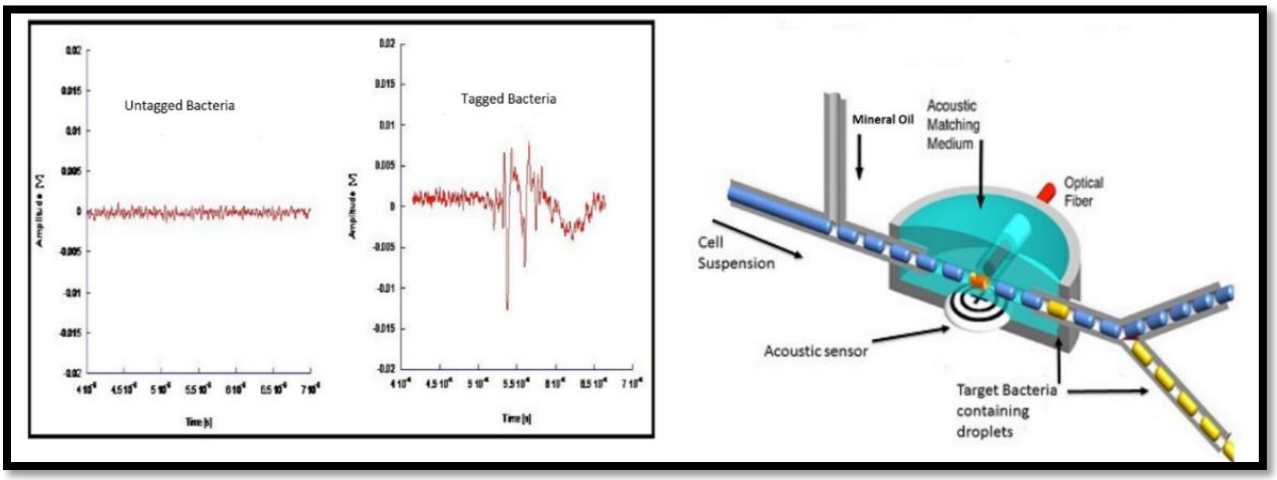

Figure 12 Left picture: Representative signal produced from a positive detection of a tagged bacterial cell. Right picture: Schematic of photoacoustic flow chamber with parts labeled for identification.

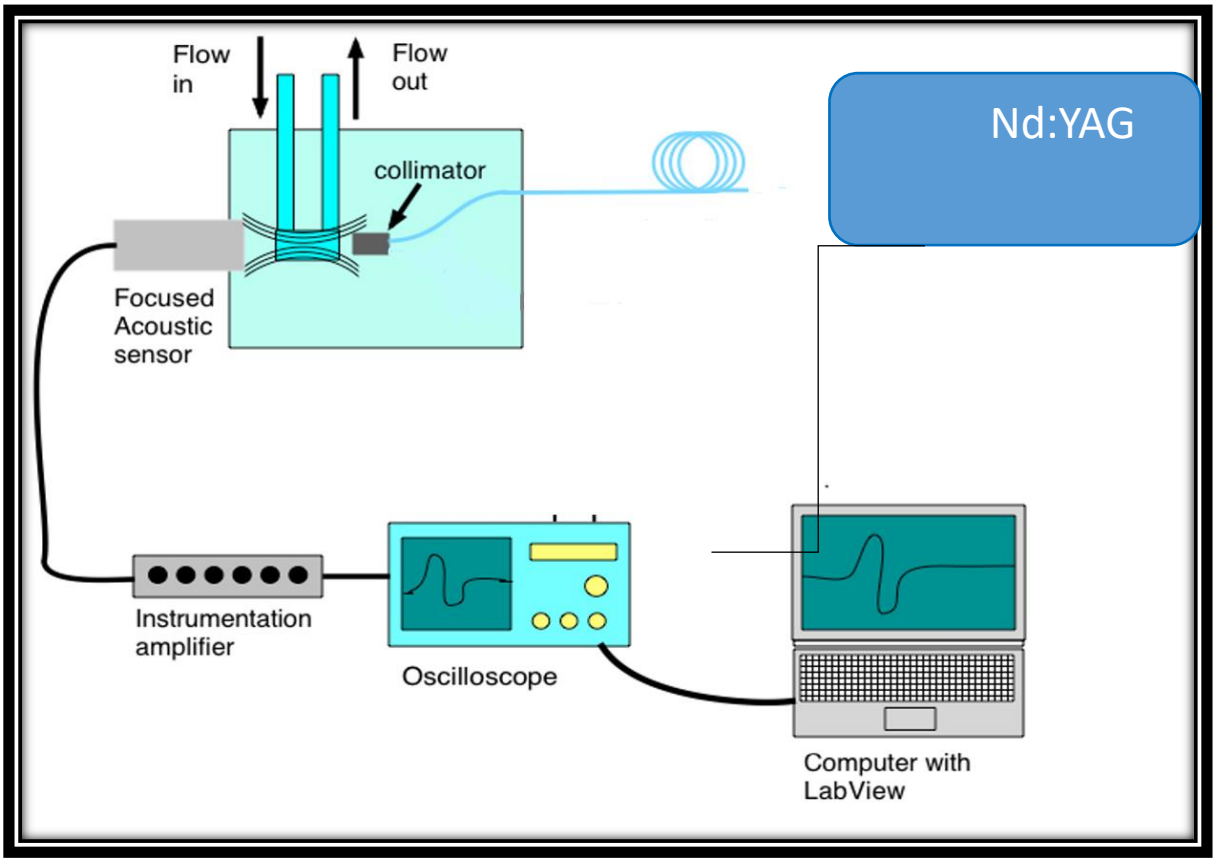

Figure 13 Schematic of our photoacoustic setup with parts labeled for identification. Nd:YAG laser emits 532nm laser light which is collimated into optical fiber. Samples flow through excitation chamber and are irradiated by laser light.

Our assay combines the specific tagging of bacteria using bacteriophage and the ability to rapidly detect individual small tagged bacterial cells with PAFC. By exploiting the different host ranges of bacteriophage, we are able to further specifically discriminate pathogenic bacterial

strains from non-pathogenic strains. Bacteriophage present many advantages over antibodies or other types of tags.

4.0 Bacteriophage Mediated Identification of Bacteria Using Photoacoustic Flow Cytometry

Robert H. Edgar[a], Justin Cook[b], Cierra Noel[b], Austin Minard[b], Andrea Sajewski[b], Matthew Fitzpatrick[b], Rachel Fernandez[b], John D. Hempel[b], John A. Kellum[c], John A. Viator[a,b,*]

[a]University of Pittsburgh, Swanson School of Engineering: Bioengineering, 3700 O'Hara Street, Pittsburgh, PA, United States, 15261

[b]Duquesne University, 600 Forbes Ave, Pittsburgh, PA, United States, 15282

[c]Center for Critical Care Nephrology, Department of Critical Care Medicine, University of Pittsburgh, 3347 Forbes Ave, Suite 220, Pittsburgh, PA, United States, 15213

Chapter Abstract. Infection with resistant bacteria has become an ever increasing problem in modern medical practice. Currently, broad spectrum antibiotics are prescribed until bacteria can be identified through blood cultures, a process that can take two to three days and is unable to provide quantitative information. In order to detect and quantify bacteria rapidly in blood samples, we designed a method using labeled bacteriophage in conjunction with photoacoustic flow cytometry. Photoacoustic flow cytometry is the generation of ultrasonic waves created by the absorption of laser light in particles under flow. Bacteriophage are viruses that infect bacteria and possess the ability to discriminate bacterial surface antigens, allowing the bacteriophage to bind only to their target bacteria. Bacteria can be tagged with dyed phage and processed through a photoacoustic flow cytometer where they are detected by the acoustic response. Here we demonstrate that *E. coli* can be detected and discriminated from *Salmonella* using this method. Our goal is to develop a method to determine bacterial content in blood

samples. We hope to develop this technology into future clinical use and decrease the time required to identify bacterial species from 3-4 days to under 1 hour.

Keywords: diagnostics, optoacoustics, Bacteriophage

*Dr. John A. Viator, viatorj@duq.edu

4.1 Chapter Introduction

Bacterial infections that may lead to sepsis in patients is a major problem in many aspects of hospital care, including emergency medicine, transplant surgery, and intensive care[193]. To combat these infections, current medical practice calls for the use of broad spectrum antibiotics until bacterial cultures can identify specific pathogens. Because of the doubling time of bacteria, this process may take 48 to 96 hours. There are also well known drawbacks to broad spectrum antibiotic use, such as increased antibiotic resistance, costs, and toxicity [194]. Furthermore, some outbreaks involve bacteria that are resistant to standard broad spectrum coverage and delays in diagnosis may result in more advanced disease.

Bacterial cultures are still the gold standard for identification of blood stream infections [195], though there is a critical need to develop early detection and identification methods for bacterial pathogens that avoid the requirement of bacterial culture, obviate the need for broad spectrum antibiotics, and improve patient outcomes [196].

As an early diagnostic tool, Gram staining, developed in the 19th century, is employed to narrow the types of possible bacteria before culture results can be obtained. Gram staining allows doctors to group bacteria into classes correlated with likely antibiotic sensitivity 24 hours before bacteria can be identified from plate cultures [197]. However, this method classifies thousands of

bacterial strains, pathologic or not, into four large groups and is incapable of providing further resolution. Thus, a variety of newer assays have been developed in an effort to obtain faster bacterial identification. Many of these assays detect bacterial DNA and require polymerase chain reaction (PCR)[24, 198, 199]. Clinical PCR assays, unlike in research laboratory settings, have to deal with secondary and tertiary DNA structures, unknown salt content, and additional polymerase inhibitors such as EDTA and immunoglobulins [15]. FDA cleared Pnuemonia pathogen test by Unyvero is a qualitative multiplex PCR that has been widely used but has a higher limit of detection ($1x10^4$ to $1x10^5$ CFU/ml) thank traditional respiratory culture ($1x10^3$ CFU/ml)[17]. The most widely adopted rapid diagnostic test, Verigene and FilmArray, as well as the majority of available rapid diagnostic tests require amplification of the organism from inoculated blood culture broth [17]. Microarrays and real-time PCR have been developed, and produce more consistent results but can be cost prohibitive [200]. Furthermore, because of the amplification, the techniques are only semi-quantitative. Approaches that obviate the need for DNA amplification such as smudge plate in conjunction with matrix-assisted laser desorption ionization time-of-flight (MALDI ToF) identification still require 19 hours of culture and growth time before identification [8]. Implementation of MALDI-TOF systems nearly halved the amount of time to optimal antibiotic therapy (63h vs 32h) but still required more than the desired time to optimal therapy [201]. T2 Biosystems tests, based on magnetic resonance, do not require positive cultures, but do require expensive and sensitive machinery and deliver results in 3-6 hours [19]. Using in-situ hybridization the PhenoTest BC can deliver results in 90 minutes and produce antimicrobial susceptibility testing in 7 hours. The PhenoTest BC has sensitivity of 94.6 percent and a Very Major Error rate of 1 percent when tested in a multicenter evaluation [18]. Each of these rapid

diagnostic systems have advanced therapeutic care and decreased the time to prescription of targeted antibiotics.

A promising candidate technology for advancing therapeutic care when dealing with bacterial identification is photoacoustic flow cytometry, that can find rare particles in fluids using the photoacoustic effect[202]. Photoacoustic flow cytometry (PAFC) is not a new technology and has been utilized by several groups. Zharov *et al.* have detected particles under flow in mouse blood vessels by labeling with carbon nanotubes or gold nanorods [203]. PAFC systems have been used to target *Staphylococcus aureus* cells labeled using antibody fused gold nanoparticles[204] . Other groups expanded on this work to develop photoacoustic detection coupled with photothermal eradication of bacteria *in vivo* model [205]. More recently *in vivo* photoacoustics have been used with magnetotactic bacteria as well as the detection of infected phagocytic macrophage cells through a novel interaction and self assembly [206, 207]. In contrast, our method uses a novel bacterial tag, bacteriophage, that bind irreversibly and specifically and does not require a bacterial culture step or DNA amplification like many clinical diagnostics. Accuracy can be achieved by leveraging bacteriophage that bind to bacteria irreversibly and with specificity [208], including to subspecies, often correlating with antibiotic sensitivity patterns. Bacteriophage can be modified to create optically absorbing bacterial tags. By exploiting the different host ranges of bacteriophage, we are able to further discriminate pathogenic bacterial strains from non-pathogenic strains. Bacteriophage present many advantages over antibodies or other types of tags. Bacteriophage have greater specificity than antibodies, are easier to produce, bind irreversibly, and are more stable [209-212] . Bacteriophage are able to identify and discriminate target bacteria within a matter of seconds, even in complex environments such as blood [213]. Bacteriophage host attachment is determined by tailspike, or long tail fiber, proteins attached to the distal end of their

tail structure [56]. These specialized bacteriophage proteins have evolved to bind to bacterial surface antigens that are essential to the bacteria, and thus are not easily changed. Additionally, the majority of bacteriophage have multiple tailspike trimers or long tailfibers, all of which allow the bacteriophage binding to be fast, specific and irreversible [209]. Tailfiber and tailspike proteins, essential to the survival and fitness of bacteriophage, have developed to be the most stable protein structures yet to be discovered. As bacteria have continued to evolve and diverge, bacteriophage have co-evolved and adapted to infect new and different subspecies of bacteria, even those bacteria that have acquired antibiotic resistance. Bacterial virulence is always accompanied by changes in cell surface antigens and bacteriophage often take advantage of this fitness cost by target virulence factors and essential genes[214]. The ability of bacteriophage to discriminately and irreversibly bind to their target bacteria is central to their evolutionary fitness and survival.

In this study, we use bacteriophage Det7and bacterial strains LT2 *Salmonella* and K12 *E. coli*. The genome of bacteriophage Det7, the particle structure, and the host range have previously been characterized[56, 215]. Det7 bacteriophage binds specifically to the O-antigen of many *Salmonella* strains but does not bind to any *E. coli* strains. *Salmonella* and *E. coli* were used because of their physical similarities, the diversity of surface antigens, and the host of literature using them as model organisms for bacterial identification[216].

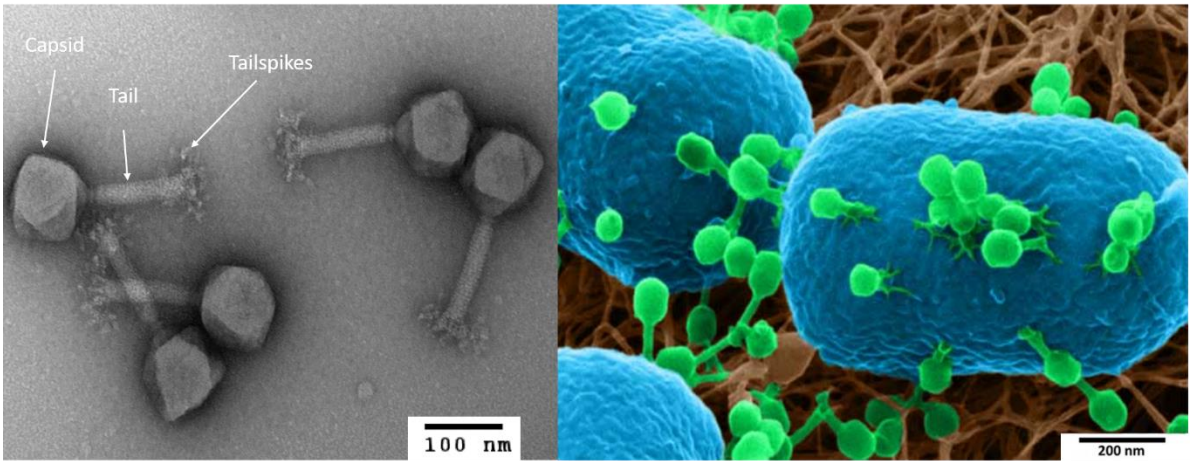

Figure 14 Left: Electron micrographs of bacteriophage Det7 showing the major structural components of all bacteriophage. TEM by R. Edgar. Right: Multiple bacteriophage particles attached to a single E. coli cell imaged using Helium Ion microscopy by Leppänen et al.

4.2 Materials and Methods

Photoacoustic flow cytometry generates ultrasonic waves resulting from absorption of light in particles under flow[217]. These ultrasonic waves are often created by thermoelastic expansion and contraction of an object that absorbed laser light[218, 219]. In our photoacoustic flow cytometry setup, a nanosecond laser operating at 532 nm is used to irradiate a sample under flow. The ultrasonic waves are detected by a piezoelectric transducer and recorded onto a computer. Our photoacoustic sensing setup is directly based on our system used to detect circulating melanoma cells in blood [191, 220, 221].

Bacteriophage have low optical absorbance at 532 nm wavelength. In order to provide optical contrast to bacteriophage Det7, Direct Red 81 dye, a polysulfated photostable protein dye capable of generating photoacoustic waves after laser irradiation, was attached. Absorption spectra

of dyed and undyed bacteriophage Det7 were measured using a Nanodrop 2300. Bacteriophage remain permanently dyed by Direct Red 81, which contains two sulfonic acid groups with pKa values in the negative range, allowing salt bridges to form with basic groups such as lysine and arginine side chains. These salt bridges are more tenacious than some covalent bonds at relatively neutral pH values, and therefore, these bonds are only broken at an elevated pH in high salt concentrations.

4.2.1 Photoacoustic Flow Cytometry

A Nd:YAG laser (Litron Nano, Bozeman, Montana) coupled into a 1000 µm, 0.39 numerical aperture, optical fiber (Thorlabs, Newton, New Jersey) was used to produce 532 nm laser light with 5 nanosecond pulses. The laser beam energy coupled through the optical fiber was maintained and measured from 1.9 - 2.1 mJ for most detection experiments. Laser energy was increased to 4 mJ for single cell detection experiment. Laser light was directed to a quartz tube (Quartz 10 QZ, Charles Supper, Natick, Massachussetts) with 10 µm thick walls passing through a 3D-printed flow chamber. The 10 µm thick walls allow the propagation of ultrasonic waves, as well as providing an optically transparent pathway for the sample to flow through. Optical fiber was placed 5 mm from the quartz tube to create a detection volume of 0.04 µl. Laser beam shape was Gaussian and fluence was calculated to be 0.014 mJ/cm^2

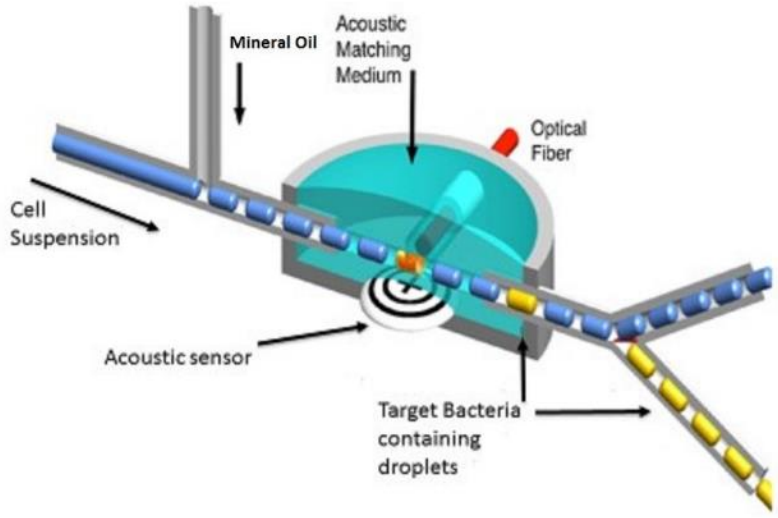

Figure 15 Schematic of photoacoustic flow chamber with parts labeled for identification

A 2.25 MHz transducer focused on the quartz sample tube was fitted to the base of the 3D-printed flow chamber. The internal volume of the chamber was filled with Sonotech LithoClear acoustic gel (NeXT Medical Products Company, Branchburg, New Jersey) to provide a medium for the propagation of acoustic waves. Syringe pumps were used to create an alternating flow of sample and mineral oil equal to 60 µl/min flow rate. The introduction of sample and the immiscible mineral oil induced two-phase flow [191]. Two-phase flow was employed to allow for future collection of the samples for further analysis, while eliminating the possibility of samples becoming stuck or delayed inside the tubing. Signals were amplified with a gain of 50 using a Tegam 4040B amplifier (Tegam, Inc., Geneva, Ohio) and sent to a desktop computer running a customized LabView program. This computer also served for system control and data collection. This flow chamber set up served as the excitation and acoustic wave collection device.

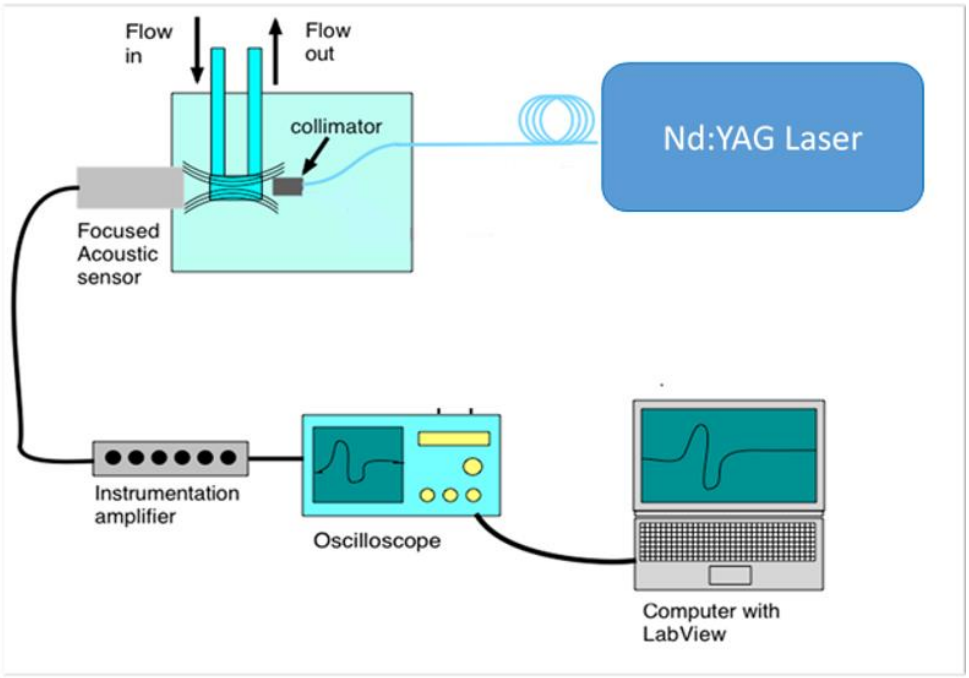

Figure 16 Schematic of photoacoustic flow setup with parts labeled for identification

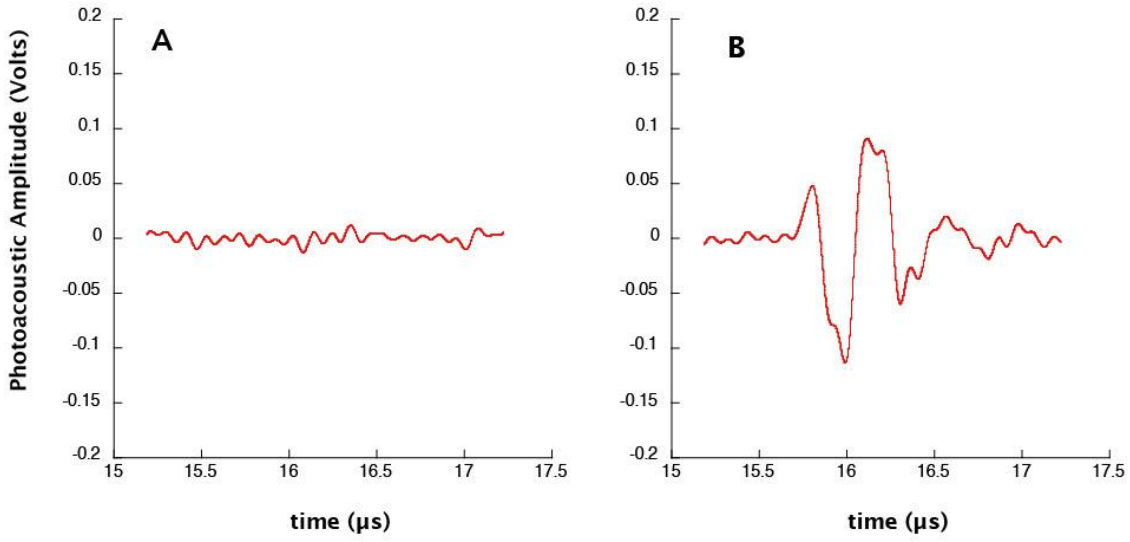

Figure 17 (A) Signal from irradiating PBS, resulting in background noise. (B) Signal generated from irradiating bacteriophage bound to target bacteria. A detection is defined as any single waveform with 1.5 times or greater amplitude than the root mean square noise value

Detections were determined by two methods. Primary detection was through amplitude detection above a given threshold. Threshold was empirically set at 1.5 times the root mean square noise value. A scoring function derived from known positive detections was derived to score each waveform based on its key aspects. Each detection above threshold was scored using the scoring function and given a confidence value.

4.2.2 Bacteriophage Preparation

Det7 Bacteriophage lysates were concentrated using polyethylene glycol 8000 (PEG) precipitation described by Nielson *et al.*[222] and initially described by Yamamoto *et al.*[223]. Differential centrifugation and cesium chloride gradients were used to further purify and concentrate bacteriophage Det7 stocks[224]. Stock concentrations of $5x10^{11}$ plaque forming units per milliliter (PFU/mL) or greater were produced. Pure stocks of bacteriophage were then diluted into a saturated solution of Direct Red 81 dye (Sigma Aldrich, Saint Louis, Missouri). Bacteriophage Det7 virion particles were then pelleted and resuspended in 10 mM Tris, pH 7.5, 10 mM $MgCl_2$, 68 mM NaCl (bacteriophage buffer) to remove any unbound dye. A Nanodrop 2300 spectrophotometer was used to record the absorbance spectrum and to verify an increase in dyed bacteriophage absorbance at 532 nm wavelength. An increase of absorbance at 532 nm was identified for dyed bacteriophage Det7 when compared to the absorbance of undyed Det7 bacteriophage. Dyed Det7 bacteriophage were retested for their ability to infect their target bacteria and stocks were titered to determine the total number of dyed infectious particles. Titers before

and after dyeing protocol are expected to be within 3-5%, as this is the expected variation derived from multiple titers. Any decrease in titer would suggest that the dye modification is inactivating bacteriophage particles. No difference in titer was determined even when Det7 bacteriophage were kept in an excess of dye for 60 days, demonstrating that the bacteriophage are robust and unaffected by the attachment of the Direct Red 81 dye.

Table 2 Detection of Bacteria, Bacteriophage, and Dyed Bacteriophage

	Concentration	*Detections*
Salmonella LT2	$10^1 – 10^8$	0
E coli K12	$10^1 – 10^8$	0
Undyed bacteriophage	$10^1 – 10^{12}$	0
Dyed bacteriophage	$10^1 – 10^{10}$	0
Dyed bacteriophage	$10^{11} – 10^{12}$	873-915

4.3 Results

4.3.1 Bacteriophage Detection

Bacteriophage buffer was run through the photoacoustic flow cytometry system to demonstrate a level of background detection and any variability with PBS. Purified bacteriophage were next titered through the photoacoustic flow cytometry system; 0.5 mL of each concentration ranging from $1x10^1$ PFU/mL to $1x10^{12}$ PFU/mL were tested. No detections were observed for

either undyed bacteriophage or phage buffer demonstrating their inability to absorb laser light and produce a photoacoustic response using 2 mJ laser energy.

Next, purified dyed bacteriophage were tested with a laser energy of 2 mJ; 0.5 mL of each concentration ranging from $1x10^{1}$ PFU/mL to $1x10^{12}$ PFU/mL were tested. As can be seen in Table 1, no detections were recorded until bacteriophage reached a concentration of $1x10^{11}$ PFU/mL. At a concentration of $1x10^{11}$ PFU/mL there are approximately $1x10^{5}$ dyed bacteriophage in the detection volume of 0.04 µl. Using 2 mJ of laser energy $1x10^{5}$ dyed bacteriophage per detection volume produce a signal that crosses our threshold of 1.5 times the root mean square noise value. All concentrations below $1x10^{10}$ PFU/mL bacteriophage were assumed to be free-floating and evenly dispersed throughout the sample.

4.3.2 Bacterial Detection

The photoacoustic response of free-floating bacteria was determined next. Overnight cultures of *Salmonella* LT2 and *E. coli* K12 were grown and diluted into fresh LB media. Cultures were grown at 37˚ C for 3 hours to ensure bacteria were in exponential growth phase. Dilutions of each exponential culture were made and concentrations from $1x10^{8}$ CFU/mL through $1x10^{1}$ CFU/mL were tested for their photoacoustic response. Neither *Salmonella* LT2 nor *E. coli* K12 produced a photoacoustic response and no detections were recorded.

After determining background and baseline detection thresholds, we turned our attention towards our goal of detecting bacteria. When bacteriophage bind to their target bacteria, they are localized on the cell surface. This localization of bacteriophage, even when total concentration is well below detectable concentrations, creates a local increase in concentration that is then above

the detection threshold. It is this localization of bacteriophage that results in the production of signals above our detection threshold.

Bacteriophage Det7 dyed with Direct Red 81 was incubated with *Salmonella* LT2 or *E. coli* K12 and allowed to bind to the bacterial cell surface. The host range of Det7 has previously been tested and described in detail[56]. Det7 infects a wide variety of *Salmonella* serovars but does not infect any *E. coli* strains. *Salmonella* LT2 bacteria were incubated with dyed Det7 bacteriophage in increasing ratios from 1:1 (bacteria: bacteriophage) increasing by order of magnitude to 1:1000. Mixed cultures were held at room temperature for 10 minutes to allow the bacteriophage time to adsorb to the surface of the *Salmonella* cells. Tests were run with bacterial cell concentrations ranging from $1x10^4$ CFU/mL to $1x10^8$ CFU/mL. Each test was repeated using target bacteria, *Salmonella* LT2 and non-target bacteria *E. coli* K12. Table 2 demonstrates that in the presence of target bacteria, *Salmonella* LT2, and below threshold concentrations of dyed bacteriophage Det7, multiple detections were recorded. Detections were limited with a built-in delay between signals to allow recording of each waveform. This delay limited the total number of signals that could be detected to 660 signals per test. Both the $1x10^4$ CFU/mL and $1x10^8$ CFU/mL were near constant detections, while the $1x10^5$ CFU/mL and $1x10^6$ CFU/mL showed a much lower number of detections. Table 4 shows that for non-target *E. coli* K12, no detections were recorded when mixed with dyed Det7 bacteriophage, except at a concentration of dyed bacteriophage of $1x10^{11}$ PFU/mL. At a concentration of $1x10^{11}$ PFU/mL, there are $1x10^6$ bacteriophage per detection volume of 0.04 µL.

Table 3 Detection of Target Bacteria

Bacteria	Dyed Bacteriophage	Ratio	Detections
Salmonella LT2 10^5 CFU/mL	Det7 10^5 PFU/mL	1:1	0
Salmonella LT2 10^5 CFU/mL	Det7 10^6 PFU/mL	1:10	0
Salmonella LT2 10^5 CFU/mL	Det7 10^7 PFU/mL	1:100	2
Salmonella LT2 10^5 CFU/mL	Det7 10^7 PFU/mL	1:1000	496
Salmonella LT2 10^6 CFU/mL	Det7 10^8 PFU/mL	1:1000	55
Salmonella LT2 10^7 CFU/mL	Det7 10^9 PFU/mL	1:1000	83
Salmonella LT2 10^8 CFU/mL	Det7 10^{11} PFU/mL	1:1000	502

Table 4 Detection of Non-Target Bacteria

Bacteria	Dyed Bacteriophage	Ratio	Detections
E.coli K12 10^8 CFU/mL	Det7 10^{11} PFU/mL	1:1000	3
E.coli K12 10^7 CFU/mL	Det7 10^{10} PFU/mL	1:1000	0
E.coli K12 10^6 CFU/mL	Det7 10^9 PFU/mL	1:1000	0
E.coli K12 10^8 CFU/mL	Det7 10^8 PFU/mL	1:1000	0
E.coli K12 10^4 CFU/mL	Det7 10^7 PFU/mL	1:1000	0

We next directed our attention towards our goal of detecting single bacterial cells tagged with labeled bacteriophage. LT2 *Salmonella* was mixed with dyed Det7 bacteriophage in a 1:1000 ratio. The cell/bacteriophage mixtures were serially diluted to produce 100 cells per test volume of 0.5 mL and laser energy was increased to 4 mJ. The experiment was replicated 5 times with new serial dilutions of bacterial cells and bacteriophage to ensure the significance of detection numbers. As seen in Table 4, we detected an average of 43.4 out of every one hundred cells.

Table 5 Single cell detection

Laser Energy	LT2: Det7 Ratio	Expected	Detected
4mJ	1:1000	100	58
4mJ	1:1000	100	32
4mJ	1:1000	100	31
4mJ	1:1000	100	41
4mJ	1:1000	100	55

4.4 Chapter Discussion

4.4.1 Bacteriophage Detection

Undyed bacteriophage showed no photoacoustic response when run through our detection system. When Direct Red 81 dye was added to the phage particles, detections were only observed when concentrations of phage reached $1x10^{11}$ PFU/mL. At a concentration of $1x10^{11}$ PFU/mL, there will be approximately $4x10^{5}$ dyed bacteriophage per detection volume of 0.04 µL, resulting in a signal. At a concentration of $1x10^{10}$ PFU/mL, bacteriophage are present at about the level of one bacteriophage per 0.6 μm^3, which is about the volume of a bacterial cell. We hypothesize that at $1x10^{11}$ PFU/mL concentration, bacteriophage start to clump together and form multi-phage complexes, as has previously been seen by electron microscopy. Multiphage complexes can form for a variety of reasons, chief among them would likely be entanglement of tail fibers or low pH as described by Goldwasser and Putnam[225]. All concentrations of bacteriophage below $1x10^{11}$

PFU/mL are assumed to be free-floating and evenly distributed. Free-floating bacteriophage less than approximately $4x10^5$ per detection volume are below the detection threshold for our system. A signal is produced when target bacteria are present that allow bacteriophage binding. Binding of multiple bacteriophage to a bacterial cell surface will increase the local concentration of dyed bacteriophage. We hypothesize that this increase in local concentration of bacteriophage is what leads to a positive signal above our detection threshold.

4.4.2 Bacterial Detection

Table 2 and Table 3 demonstrate that our bacteriophage are specific to their target bacteria and that we do not get a signal from unattached bacteriophage except when in extremely high concentrations. Table 2 shows our ability to detect bacterial cells when tagged with dyed bacteriophage. When cells are tagged with 1, 10, or 100 bacteriophage they are below our detection threshold. Some cells were missed due to our built-in delay for recording of signals, while others were simply missed due to our testing of only a single laser energy. In Table 2, the concentrations of bacteria with 1000 bacteriophage per cell showed detections. Due to our built in delay, $1x10^5$ CFU/mL and $1x10^8$ CFU/mL showed saturated detections. Laser energies of 4 mJ have previously been shown to increase detection sensitivity of the system. In future trials, increasing laser energies will be tested until our background noise increases or we reach 100 percent cell detections. The variation between the number of detections between the $1x10^4$ CFU/mL and $1x10^8$ CFU/mL and the $1x10^5$ CFU/mL and $1x10^6$ CFU/mL could be due in part to non-homogeneous mixing of our bacteria and phage. Additionally, there could have been imperfections or bubbles in our acoustic gel that led to decreased signal propagation. Additional work is being done to remove bubbles from acoustic gel and develop better and more permanent ways of producing flow

chambers and ensuring acoustic coupling in our system. Currently, repeated measurements in alternating orders are used to rectify this inconsistency. This represents an area of refinement and future work in preparing this system for more diagnostic purposes. Table 4 demonstrates our system's ability to detect individual cells when tagged with modified bacteriophage. Cells were serially diluted to produce roughly 100 cells per test volume. Chase and Hoel first described and modeled the error associated with serial dilutions of bacteria and bacteriophage[226]. We therefore expect some variation and loss of cells from manual pipetting and serial dilutions. Despite this loss, we detected nearly 50 percent of estimated cells. Future work to resolve this challenge and produce 100 percent detection rate will come from using higher concentrations of cells with less chance of loss as well as optimizing our flow system. Using higher concentrations of bacteria will reduce the error from pipetting and serial dilutions. In future trials, bacteria can be collected after exiting our flow system and plated to determine relative number of bacteria present and calculate loss. Additionally, larger sample sizes will provide more robust measurements and greater accuracy in number of bacteria present. Moreover, the ability to detect about half of all single cells is probably much more sensitive than needed clinically, as the concentration of bacteria in blood would need to be much higher to cause illness in a human being.

4.4.3 Chapter Conclusion

Bacteriophage have evolved to identify and bind to their target bacteria with high specificity. Bacteriophage host attachment is mediated solely by tail fibers [56]. Tail fibers are differentiated into long tail fibers like that of Bacteriophage T4 and tail spike proteins such as P22 TSP. Bacteriophage host attachment has many advantages over antibodies. Antigens used by antibodies are often the most abundant surface molecules or those that cause the greatest immune

response [227]. These surface molecules can often change to avoid antibody detection [228]. Conversely, bacteriophage have evolved to use surface epitopes that are essential and difficult to change [229]. Bacteriophage have even been shown to target cell surface pumps used in bacterial antibiotic resistance. Though bacteriophage resistance can evolve, it happens at a much lower rate than antibody avoidance and always has a negative fitness effect on the bacteria [230]. Bacteriophage attachment proteins are also among the most stable protein structures to be discovered and bind the phage irreversibly to the bacterial cell [231]. Antibodies are more expensive to produce [232], are less stable [167], and bind less strongly than bacteriophage. Antibodies have a binding constant, kD, in the range of 1—10 nM, while bacteriophage have a binding constant closer to 10—50 nM[233, 234].

Photoacoustic flow cytometry presents a rapid way to detect microscopic particles under flow based on their ability to absorb laser light. These initial experiments demonstrate our ability to use readily available protein dyes on bacteriophage without affecting their ability to attach to target bacteria. This research presents an innovative way of identifying and differentiating bacterial strains. This method can be further developed for use with other bacterial pathogens in blood cultures representing a major step forward in clinical practice. The time and money saving potential of rapid detection and identification of bacterial infection are overshadowed only by the number of potential lives saved. Often the limiting factors for treatment of patients is the time spent waiting for results. It is our hope that the work presented above can be a foundation for future work and an ability to detect bacterial pathogens in blood cultures. Bacterial plate cultures and Gram staining are 19^{th} century technologies that have been the gold standard for decades, but current trends in resistant bacteria have necessitated a move towards more rapid and quantifiable diagnostic tools.

4.5 Disclosures

R.H. Edgar, J.D. Hempel, J.A. Kellum, and J.A. Viator have interest in PhotoPhage Systems, LLC, a company formed to commercialize photoacoustic technologies.

4.6 Acknowledgments

Research reported in this article was supported by the National Cancer Institute of the National Institutes of Health under award number 1R01CA161367-01.

5.0 Photoacoustic Flow Cytometry Using Functionalized Microspheres For The Selective Detection of Bacteria.

5.1 Chapter Introduction

Bacterial contamination is part of all medical and industrial services. Detection of bacterial contamination early and accurately is imperative to reduce negative impacts on patient outcomes and production. The two main areas of bacterial diagnostics occur in the manufacturing and food industries and in the medical field. In these sectors, rapid determination of bacterial type and species as well as antibiotic sensitives are required. Many of the current methods have been developed to speed up the process of identification.

Culturing bacteria directly from a patient or sample is the gold standard whereby all other detection methods are judged. Culturing of bacteria stems from at least 7000 B.C. with the production of cheese[4] and other fermented foods. As humans developed various methods of food fermentation and preservation, so did their understanding of the effects of bacteria upon food production and preventing spoilage. Although the people producing cheese and yogurt did not have the technical ability to recognize and fully understand the microorganisms responsible for these activities, they were able to understand the effects that bacteria can have upon food in terms of spoilage and fermentation. It is this understanding of bacteria's effects that have led to some of our modern detection techniques.

Two main advantages of using bacterial cultures are reproducibility and the ability to separate bacteria for further cultures or testing. A bacterial culture consists of millions of individual bacterial cells that can be subdivided for future tests, including antibiotic sensitivity.

Culturing of bacteria in a clinical diagnostic laboratory consists of inoculating a patient sample into liquid or solid media. If bacteria are present in the sample, they will grow and divide rapidly until a suitable number are present for visual or biochemical identification. Once a culture grows to appropriate density, a smear can be prepared and examined using light microscopy and staining procedures to identify bacterial shape and arrangement. In the clinical microbiology lab, Gram staining is one of the first steps in the culture-based bacterial identification process. This process, developed by Hans Christian Gram in 1884, was the first advancement in bacterial identification[5]. Gram staining involves staining a bacterial smear with crystal violet-iodine complex, rinsing with alcohol, and applying safranin counter stain. This method classifies bacteria based on cell shape, cell arrangement, and the biochemical nature of the bacterial cell wall. Gram-negative microorganisms have a high lipid content and low peptidoglycan content compared to Gram-positive bacteria. The differential nature of the Gram stain method results in Gram positive bacteria retaining the crystal violet-iodine complex within their cell walls while Gram negative bacteria fail to retain the stain during alcohol rinse. Gram-negative bacteria will appear red/pink under the light microscope due to the safranin counter stain while Gram-positive bacteria will appear purple. Because antibiotic therapy often depends on the biochemical nature of the bacterial cell wall, determining the Gram reaction of clinical samples is very critical for medical diagnosis.

Bacteriophage also use the biochemical nature of the cell wall to discriminate bacterial targets. Bacteriophage have evolved to rapidly and specifically discriminate bacteria using tailspikes and tailfibers. As different subspecies of bacteria have emerged, some with variations in antibiotic susceptibility, bacteriophages have adapted. Importantly, bacteriophages will continue to evolve along with bacteria and these naturally occurring probes provide an innovative solution to the shifting sands of bacterial epidemiology. By attaching bacteriophage tails to uniformly

produced microspheres, we leverage the specificity of bacteriophage with the reproducibility and uniformity of commercially produced dyed microspheres. Dyed microspheres allow us to easily modulate color and signal strength as well as capture bound microspheres for further analysis.

5.2 Materials and Methods:

5.2.1 Photoacoustic Flow Cytometry

Photoacoustic flow cytometry has been used by several groups to detect circulating tumor cells both *in vitro[187, 190, 192, 235]* and *in vivo[184, 188]*. Additionally, we have previously used photoacoustic flow cytometry for the detection of bacterial contamination using bacteriophage[202]. Our photoacoustic testing set up is based on our previously developed system for detection of circulating melanoma and bacterial cells. A schematic of the flow system is displayed below. Laser light at a wavelength of 532 nm was coupled into a 1000 µm optical fiber with numerical aperture 0.39 (Thorlabs, Newton, New Jersey) and used that to deliver 5 ns laser pulses directly to our sample. For sample handling, a syringe pump system maintained a constant flow rate of the sample through the acoustic excitation chamber. The excitation chamber consists of a quartz tube with 10 µm thick walls (Quartz 10 QZ, Charles Supper, Natick, Massachusetts) submerged in Sonotech LithoClear acoustic gel (Next Medical Products Company, New Jersey). The optical fiber was placed 5 mm from the quartz tube with a 2.25 MHz focused transducer (Olympus, Waltham, Massachusetts) positioned below quartz tube. A 3D printed polylactic acid (PLA) was used to hold the quartz tube, optical fiber, and transducer with acoustic gel filling the internal volume.

To allow for microfluidic capture of detected cells we introduced two phase flow. An immiscible liquid, mineral oil, was introduced into our sample flow to create alternating droplets of oil and sample. These alternating droplets ensured cells could not be retained in the flow system and allowed for localized detection and isolation of acoustic events. The detection of acoustic events was accomplished using the focused transducer coupled to a amplifier (National Instruments, Austin, Texas) connected to a desktop computer (Dell, Round Rock, Texas) running our LabVIEW (National Instruments, Austin, Texas) program built for recording and quantifying acoustic events.

To determine background noise the photoacoustic flow cytometry (PAFC) system was tested using phosphate buffered saline (PBS) and Phage Buffer (10 mM Tris, pH 7.5, 10 mM $MgCl_2$, 68 mM NaCl). As a positive system control, 10 µm polystyrene microsphere (Polybead, Warrington, PA) were tested and tittered through the PAFC system. Bacterial cultures of LT2 *Salmonella* and K12 *E. coli* were diluted into PBS and tittered through the PAFC system. Additionally, 0.2 µm streptavidin coated dyed microspheres were tittered through the system and concentration of microspheres was increased until microspheres were able to be detected.

5.2.2 Production of Bacteriophage Tails

Bacteriophage were purified using cesium chloride (CsCl) gradient purification. Osmotic shock was used to removed phage capsids from tails as described earlier[56]. Bacteriophage were produced and concentrated to be $1x10^{12}$ pfu/ml and CsCl was added to increase the density of the solution to 1.5 g/ml. Bacteriophage were incubated in CsCl overnight allowing the CsCl to infuse into the bacteriophage DNA that is tightly packaged in the capsid. CsCl infused bacteriophage were then rapidly diluted into phage buffer, causing the rapid diffusion of CsCl out of the

bacteriophage. This rapid diffusion resulted in the separation of bacteriophage capsid and tails at the neck connecter. This process of separating intact capsids and tails has been used by phage biologists for many years [56, 236].

Phage tails were further purified using Bio-Rad HPLC (Hercules, California) and purity was determined by spectrophotometry as well as electron microscopy. Protein purity and concentration was calculated from optical absorbance using a BioTek Synergy H1 (Winooski, Vermont). A 96 well plate was used with the BioTek Synergy H1 to obtain multiple optical absorbance measurements at 280 nm. The Beer-Lambert law was then used to estimate the protein concentration. The absorbance ration between 260 nm and 280 nm was then used to estimate the purity of our protein and any possible DNA contamination.

Electron micrographs were taken by Dr. James Conway (Department of Structural Biology, University of Pittsburgh). Micrographs were taken on a THermo Fisher/FEI T12 Spirit using a Gatan US 1000 and Orius CCD camera (Hillsboro, Oregon). Micrographs were examined to for the presence of contaminating DNA or groEL, both of which commonly purify with bacteriophage. Tail preparations were found to be of high quality and purity with no observation of contaminating DNA or groEL. Following confirmation of purity, tail preparations were used in later procedures for attachment to microspheres.

5.2.3 Attachment of Phage Tails to Streptavidin Coated Microspheres

Streptavidin coated dyed polystyrene microspheres with nominal diameter of 0.19 μm were obtained from Bangs Laboratories (Fishers, Indiana). Streptavidin coated microspheres were washed four times in PBS to remove stabilizer and antimicrobial agents used by the manufacturer. Microspheres were washed using PBS and using Spin-X concentrator columns three times. Biotin

(Thermo Scientific EZ-Link Sulfo-NHS-Biotin) was prepared separately and resuspended in PBS at a concentration of at least 20 fold excess to the phage tail protein binding. Biotin and purified tails were combined and incubated on ice for two hours. After incubation, excess biotin was removed by dialysis using 2kD molecular weight cut off dialysis cassettes (Slide-A-Lyzer, Thermo Scientific). Biotinilated tails were incubated with washed streptavidin coated microspheres at room temperature for 30 minutes with gentle mixing. Microspheres were washed ten times to remove any unbound biotinylated phage tails. Microspheres with bound phage tails were then concentrated using slow speed centrifugation.

5.2.4 Verification of Functionalized Probes

We examined microspheres with attached tails using electron microscopy. Samples were negatively stained and multiple dilutions of microsphere with bound tails were examined. Uniform attachment of tails was observed. No microspheres were identified that did not have a full compliment of unbound phage tails. Very few free floating unbound phage tails were identified in each preparation suggesting that both our tail binding and washing procedures were effective. Additionaly, signs of contamination by DNA or groEL investigated. No presence of either was observed in any prepared samples suggesting a high level of purity. Examples of functionalized microspheres can be seen in Figure 18:

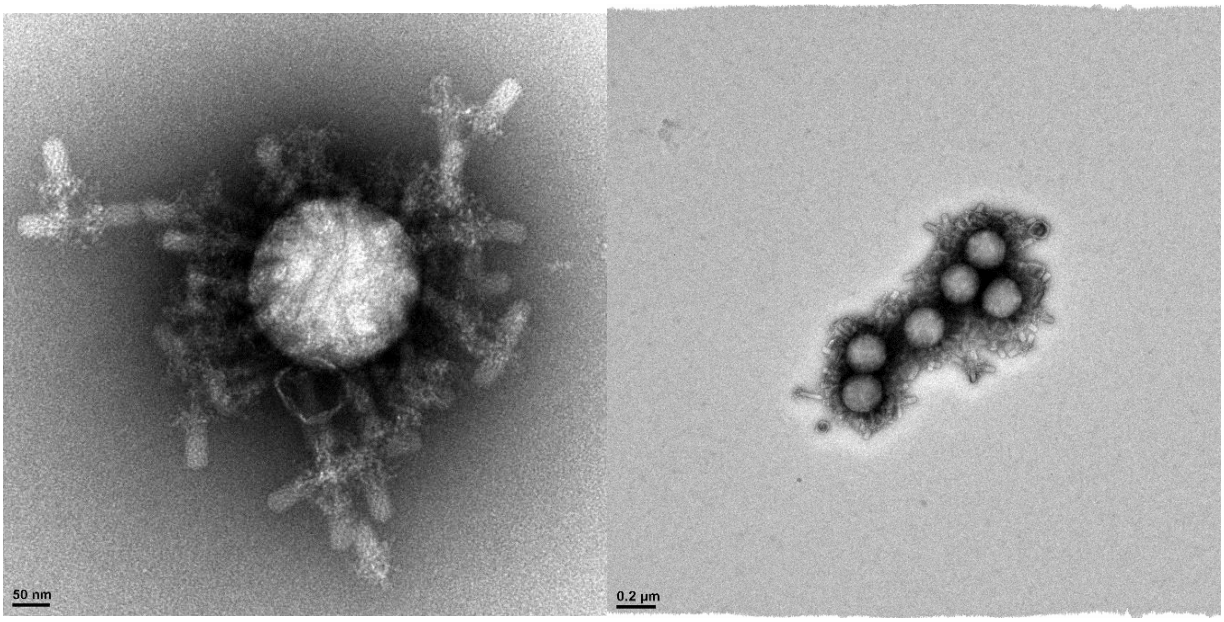

Figure 18: Left panel shows single functionalized microsphere with multiple bound phage tails in random orientations. Right panel shows multiple functionalized microspheres with attached phage tails. Micrographs take by Dr. James Conway, University of Pittsburgh

5.2.5 Photoacoustic Flow Cytometry using Functionalized Microspheres

Overnight cultures of each *Staph aureus* strain were prepared in Mannitol Salt Phenol Broth (MSB) media (Millipore Sigma, Burlington, MA). Overnight cultures were diluted 1/20 and regrown in LB media for two hours to ensure synchronous cultures in exponential growth phase. After re-growth cultures were pelleted and diluted to desired concentration for PAFC. Each sample was diluted to contain roughly 100 bacterial cells per test. Functionalized microspheres were added to diluted bacterial cultures and incubated at room temperature for 10 minutes to allow binding to bacterial surfaces. An excess of functionalized microspheres was added to each bacterial culture so that there were approximately 500 functionalized microspheres per bacterial cell. Combined

samples were run on PAFC system using two-phase flow at a combined rate of 60 µl/min as previously described [190, 202, 235].

In order to test our functionalized microspheres for binding and signal generation we used two bacterial strains. *Salmonella* LT2 is the target host for bacteriophage Det7 from which the tails were produced. Specificity of binding and host range of bacteriophage Det7 has previously been established[56]. As a negative binding control we used E.*coli* strain K12 to which bacteriophage Det7 does not bind. Black 1µm polystyrene microspheres were tested in the PAFC system as a positive control and to give high detection signals. As a negative control, we first demonstrated zero signals were produced from our resuspension buffer PBS. Subsequently, both bacterial strains were run at concentrations equal to our testing concentrations demonstrating zero signals. For this series of experiments we used streptavidin coated red and blue dyed 0.2 µm polystyrene microspheres. Each color microsphere was tested at 1x and 10x concentrations. Zero detections were registered for either color regardless or concentration.

5.3 Chapter Results:

Results from control experiments are displayed in table 6.

Table 6 Control experiments demonstrating positive signals from black microspheres while obtaining zero signals from PBS, target and non-target bacteria, and read and blue microspheres

Control Type	Sample	Detections
Positive	Black 1µM Microsphere	967
Negative	PBS	0
Negative	LT2 bacteria alone	0
Negative	K12 bacteria alone	0
Negative	1X Red streptavidin 0.2µM Microsphere	0
Negative	1X Blue streptavidin 0.2µM Microsphere	0
Negative	10x Red streptavidin 0.2µM Microsphere	0
Negative	10x Blue streptavidin 0.2µM Microsphere	0

To test the binding and detection of our functionalized microsphere we tested each combination of target and non-target bacteria with red and blue functionalized microspheres. Bacterial strains were grown as described earlier and cultures diluted to roughly 100 cells per test. Microspheres were added to approximately 500 functionalized microsphere per bacterial cell or 50,000 per test. The results are listed in table 7 below. In order to demonstrate a similar level of detection between red functionalized microspheres and blue functionalized microspheres a Kruskal-Walls statistical test was performed. The goal of this analysis is to demonstrate that both red and blue functionalized microspheres discriminate the same. The results of this test show that

the medians are unequal therefore both functionalized microspheres discriminate similarly. Any differences in detections can be assumed to be due to absorbance. To test this we determined the absorbance spectrum of each colored microsphere and results are shown in Figure 19.

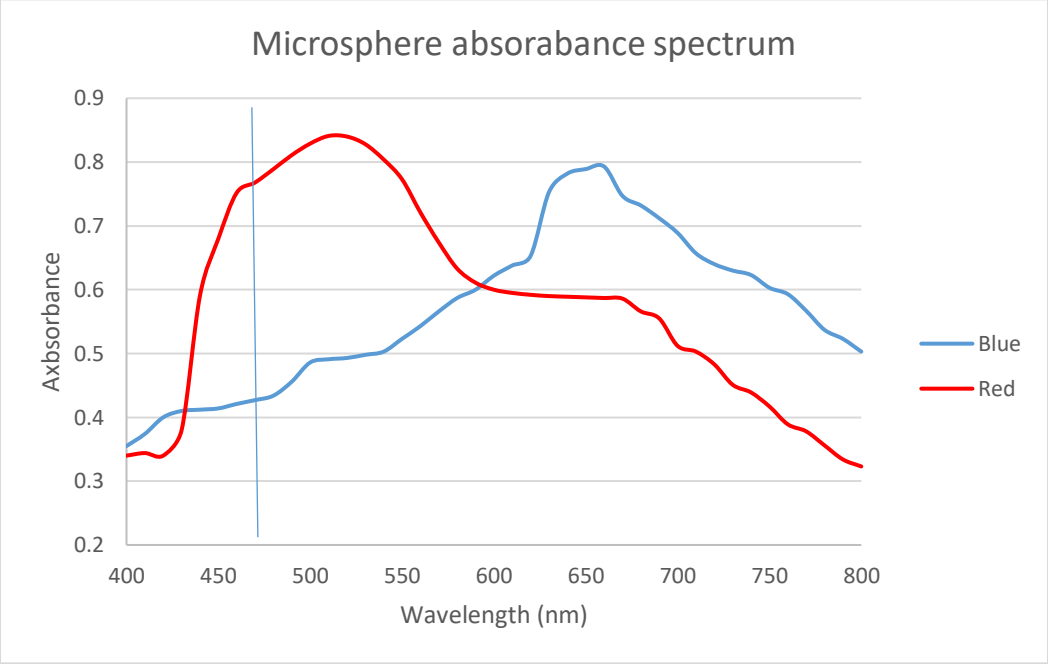

Figure 19 Absorbance spectrum of Red and Blue 0.19 µm microspheres with vertical line marking 532nm.

Table 7 Red functionalized microspheres (RFM) tested with target bacteria (Salmonella LT2) and non-target bacteria (E.coli K12). Blue functionalized microspheres tested with target bacteria (Salmonella LT2) and non-target bacteria (E.coli K12)

Microsphere	Bacterial strain	Trial #1	Trial #2	Trial #3
RFM	LT2	115	114	99
RFM	K12	3	3	0
BFM	LT2	75	84	101
BFM	K12	0	0	1

5.4 Chapter Discussions:

Detection of bacterial contamination and blood stream infections is a routine, but time-consuming procedure. Early identification of contamination can save Billions of dollars of produce each year[237, 238]. More importantly, early detection of blood stream infections can save countless lives each year. The CDC estimates nearly 2.8 million antibiotic resistant infections occur in the United States, with over 35,000 deaths annually[239]. Early and rapid detection has been a goal for hospitals and governments alike. Using functionalized microspheres and photoacoustic flow cytometry we have expanded our detection capabilities of bacterial contaminants.

Functionalized microspheres were produced by attaching bacteriophage tails directly to streptavidin coated colored photo absorbing microspheres. Bacteriophage tails contain the host attachment proteins responsible to selectivity and specificity of bacteriophage binding. By attaching them to commercially available microspheres we leveraged the high signal produced from microspheres with the attachment and irreversible binding obtained from bacteriophage tails. The uniform size and color of the microspheres allows for a uniformity of signal. Uniform signal size allows us to accurately determine peak thresholds for detections. Additionally, the robust and consistent signal obtained from microspheres allows us to increase our signal to noise ratio. Additionally, the elimination of phage capsids and DNA allow us to remove the potential for lysis of bacterial cells. This inhibition of lysis enables the downstream capture and testing of detected bacterial cells. Captured cells can then be sequenced or potentially clonal colonies could be grown from them to further analysis.

Here were tested two colors of microspheres and binding to two different bacterial hosts. Tails from bacteriophage Det7 were used to produce both red and blue functionalized microspheres. Det7 is a bacteriophage that exclusively binds to *Salmonella* bacterial species. As a non-target host we use E.*coli* K12, which Det7 does not bind to or infect. Red and blue functionalized microspheres were tested in triplicate in our PAFC system with *Salmonella* strain LT2. Red microspheres showed roughly 20% more detections with an average number of detections of 109.3 for red and 86.7 for blue microspheres. There are several possible reasons for this discrepancy in number of detections. Firstly, the red microspheres absorb the green laser light slightly better than the blue microspheres of the same size. It is very likely that the difference in absorbance accounts for the roughly 20% difference in detections. It is also possible, though unlikely, that the dilutions of each bacterial culture were slightly skewed. Despite these differences

in detections for target bacteria, the number of detections for non-target bacteria are consistently zero indicating very good discrimination between bacterial strains and specificity of binding.

Electron micrographs confirm complete coverage by bacteriophage tails to the surface of each microsphere. Bacteriophage tails were randomly oriented on the microsphere surface as confirmed by electron microscopy. Several other groups have shown that randomly oriented phage tails bind at nearly the same efficiency as oriented phage tails [240-242]. Therefore, we do not expect any significant reduction in binding capacity from the random orientation of tails as each microsphere has multiple tails attached allowing for multiple attachment points. While confirming the tail orientation a slight overabundance of tails was noticed. In future experiments we will try producing microspheres with a smaller number of attached tails to maximize the use of purified tails and any overcrowding issues.

5.5 Chapter Conclusions:

Combining the host attachment specificity of bacteriophage tails and the uniform production and absorption of dyed polystyrene microspheres allows us to quantitate specific bacterial contaminants. This technique allows for the potential producing multi target microspheres with any combination of binging produced by bacteriophage. The binding of bacteriophage is often to essential cell surface proteins making them far superior to antibody detection[228]. Additionally, Phage attachment proteins have been shown to be some of the most stable protein structures discovered allowing ease of storage and long-term viability of functionalized microspheres as bacterial probes [210, 243].

Photoacoustic flow cytometry in conjunction with functionalized microspheres presents a method of rapid bacterial detection and quantification with the added benefits of uniform signals and potential recovery of each detected bacterial cell. Further development of this methods and combining this technique with our previous work on antibiotic sensitivities shows the potential for clinical applications and point of care use. Rapid detection and identification of bacterial infection are not only a cost saving, but also more importantly potential lifesaving technology. Frequently the limiting factors for patient treatment is the time spent waiting for results. It is our hope that this technology can become the new golf standard and replace the 19th century technology of plate cultures and Gram staining.

5.6 Future Work:

Our future work centers on a more robust statistical validation of this method using a larger bank of target and non-target bacteria. Bacteriophage host range differs dramatically between types of bacteria. *Salmonella* has over 2600 serovars, all with different antigens for bacteriophage attachment and therefore very few bacteriophage have broad host ranges of Salmonella. Staph *aureus* has several bacteriophage with extremely broad host range due to the similarity of binding sites of the teichoic acids[244].

Additionally, we will also produce multi-host functionalized microspheres with wide target host ranges allowing for even more rapid identification of bacterial contamination. Initial multi-host microspheres will be focused on pathogenic versus non-pathogenic enteric bacteria. The ability to rapidly differentiate between non-pathogenic E.*coli* strains and pathogenic *E.coli* such as o157:H7 will be invaluable to the food industry. Real time monitoring of food processing

facilities or water purification facilities for pathogenic enteric bacteria would have substantial impacts particularly in third-world countries. Another target for development will be opportunistic blood-borne pathogens such as ESKAPE pathogens. Rapid identification of the presence of any of the ESKAPE pathogens allows for further testing to determine which specific one and initiate rapid antibiotic sensitivity testing.

6.0 Photoacoustic Discrimination of Antibiotic Resistant and Sensitive Staph. aureus Isolates

R. H. Edgar[2], A.P. Samson[1], J. Cook[1], M. Douglas[1], K. Urish[2,3], J. Kellum[2,4], J. Hempel[1], J. A. Viator[1,2]

[1]Department of Engineering, Duquesne University, 600 Forbes Avenue Pittsburgh, Pennsylvania, 15282

[2]Department of Bioengineering, University of Pittsburgh, 300 Technology Dr, Pittsburgh, Pennsylvania 15213

[3]Department of Orthopaedic Surgery, University of Pittsburgh Medical Center,3471 Fifth Avenue, Pittsburgh, Pennsylvania 15213

[4]Department of Critical Care Medicine, University of Pittsburgh Medical Center, 5115 Centre Ave, Pittsburgh, Pennsylvania 15232

6.1 Chapter Abstract

6.1.1 Abstract Objectives

Bacteremia is a serious and potentially lethal condition. *Staph. aureus* is a leading cause of bacteremia and methicillin resistant *Staph. aureus* (MRSA) accounts for more than a third of the cases. Compared to methicillin sensitive *Staph. aureus*, MRSA is more than twice as likely to be

fatal [2, 3]. Furthermore, sub-populations of seemingly isogenic bacteria may exhibit a range of susceptibilities, often called heterogenous resistance.

These heterogeneous antibiotic resistant infections are often misdiagnosed as hospital acquired secondary infections because there are no clinically used tests that can differentiate between homogeneous and heterogeneous antibiotic resistance.

We describe the development and proof of concept of rapid bacterial identification using photoacoustic flow cytometry and labeled bacteriophages with the characterization and differentiation of heterogeneous antibiotic resistant bacterial infections.

6.1.2 Abstract Methods

In photoacoustic flow cytometry, pulsed laser light is delivered to a sample flowing past a focused transducer and particles that absorb laser light create an acoustic response. Optically labeled bacteriophage are added to a bacterial mixture that flows through the photoacoustic chamber. The presence of target bacteria is determined by bound labeled phage which are detected photoacoustically. Incubation of bacterial samples in the presence and absence of the antibiotic daptomycin creates a difference in bacterial cell numbers that is quantified using photoacoustic flow cytometry.

6.1.3 Abstract Results

Four clinical isolates were tested in the presence and absence of daptomycin. Photoacoustic events for each isolate were recorded and compared to growth curves. Samples treated with daptomycin fell into three categories: resistant, susceptible, and heterogeneous resistant.

6.1.4 Abstract Conclusions

Here we show a method to determine the presence of bacteria as a marker for blood stream infection level and antibiotic sensitivity in less than 4 hours. Additionally, these results show an ability to identify heterogeneous resistant strains that are often misidentified.

Key Words: Bacterial resistance; early detection; lasers; optics; optoacoustics

Grant sponsor: NCI; Grant number: 1R01CA161367-01

*Correspondence to: J. A. Viator Tel.: 412-396-2661. E-mail: viatorj@duq.edu

6.2 Chapter Introduction

Antimicrobial resistance has become one of the most pressing concerns for global health and therefore has become an ever increasing focus of research and product development. Antibiotic resistance arises most often when bacteria gain and express gene cassettes that confer the ability to outmaneuver the action of an antibiotic. Bacteria employ two main strategies to gain resistance to antibiotics; pumps and enzymes[245]. Pumps work to evacuate the antibiotic from cell cytoplasm before they can reach a critical level. Enzymes work to degrade antibiotic molecules before they can have an effect. Non-genetic antibiotic resistance also occurs, though in a minority of cases, and is often mediated by small molecule communication between cell populations or general impermeability of the cell wall[246]. Resistance to antibiotics is an inevitable outcome of their use. The first cases of penicillin resistance was reported only 2 years after its widespread

use[247]. There are multiple pathways of acquiring antibiotic resistance in each type of bacteria. Horizontal gene transfer is the dominant method of acquiring antibiotic resistance[248].

The most rapid test for antibiotic resistance in *Staph. aureus* is a polymerase chain reaction (PCR) based test for the *mecA* gene. PCR is much faster than the standard antibiotic disc method[43], but is used in only a minority of cases. The antibiotic disc method requires an antibiotic disc placed on a lawn of bacteria and measuring the zone of inhibition caused by the antibiotic. This method requires an additional 24 hours after initial bacterial identification. PCR methods can be completed in 3-4 hours but can suffer from failure due to unknown sample conditions and concentrations or amplification of sub-populations that mask clinically relevant genetic traits or markers. Most problematic for clinicians are the false negatives when a resistant strain is misidentified as a susceptible strain. This delay in appropriate antimicrobial treatment can be detrimental to patients.

Occasionally, these tests give intermediary or conflicting results regarding a strain's resistance.

Isolates that are heterogeneous in their expression of a resistance gene can lead to serious problems for patient treatment. A low expressing strain will appear to be susceptible when using the antibiotic disc method and when treated with first line antibiotic such as oxacillin. In some cases, the majority of bacteria are killed and the small remaining percentage are dealt with by the immune system. In other cases, the infection appears to be cleared only to reemerge a few days later. Despite the infection still being the original bacterial strain that the patient presented with, it will be treated by the clinician as an unresolved infection or a new infection, depending on the time taken for the infection to reemerge. The reemergence of infection will likely be classified as a hospital acquired infection. Hospital acquired infections are no longer reimbursed by the Centers

for Medicare and Medicaid Services. Additionally, increased hospital acquired infections negatively impact each institutions Hospital-Acquired Condition score resulting in overall reduction of funding and reimbursement rates from Medicare and Medicaid Services[249]. For healthcare institutions, this is a costly mistake since they can no longer charge for the initial community acquired infection.

In order to develop a system of determining antibiotic resistance, we used the antibiotic daptomycin in conjunction with photoacoustic flow cytomtery (PAFC) and bacteriophage as molecular tags. Daptomycin has shown a lack of cross resistance with other antibiotic classes[250] as well as being broadly active against MRSA isolates[251]. Flow cytometry has been effectively used to analyze large heterogeneous cell populations since Wolfgang Göhde first developed it in 1968. Fluorescent flow cytometry relies on the absorption of laser light by an object and the detection of the fluorescence from that object at an alternative wavelength. Fluorescence flow cytometry has a few disadvantages that can limit its usefulness for bacterial identification. Light, though very powerful, is easily quenched or blocked in a turbid environment such as blood. Additionally, small amounts of light from single cells can be hard to detect in dilute samples. Fluorescent flow cytometry works best with large numbers of cells and clear non turbid environments. As an alternative, PAFC relies on the absorption of laser light and the detection of ultrasound waves created by the photoacoustic effect[217].

The photoacoustic effect has been used in many ways. Depth profiling in human tissues for the treatment of port wine stains[252] has been done as well as photoacoustic imaging of blood vessels[153]. PAFC has successfully been used to enumerate circulating tumor cells and has been shown to be a robust predictor of metastasis in melanoma [221, 235]. Additionally, PAFC has been used successfully for the isolation of circulating tumor cells by several groups[187, 253].

PAFC was invented to find rare, individual particles in complex environments[254]. The ultrasonic waves created by the photoacoustic affect are robust and not quenched in turbid media, such as cell suspensions or blood samples. Recently, PAFC has been used on blood samples, *in vitro*, to detect bacteria using modified bacteriophage as optical tags[202].

Bacteriophage, viruses that infect bacteria in a specific manner, have been used for many years as a way of classifying bacterial strains[255]. A bacteriophage's ability to discriminate and bind tightly to their host bacteria is vital to their fitness and evolutionary survival. Even in complex environments, bacteriophage are able to identify and bind target bacteria within seconds[213]. Bacteriophage-host attachment is achieved via protein-protein interactions with the long tail fibers or tail spike proteins[56].

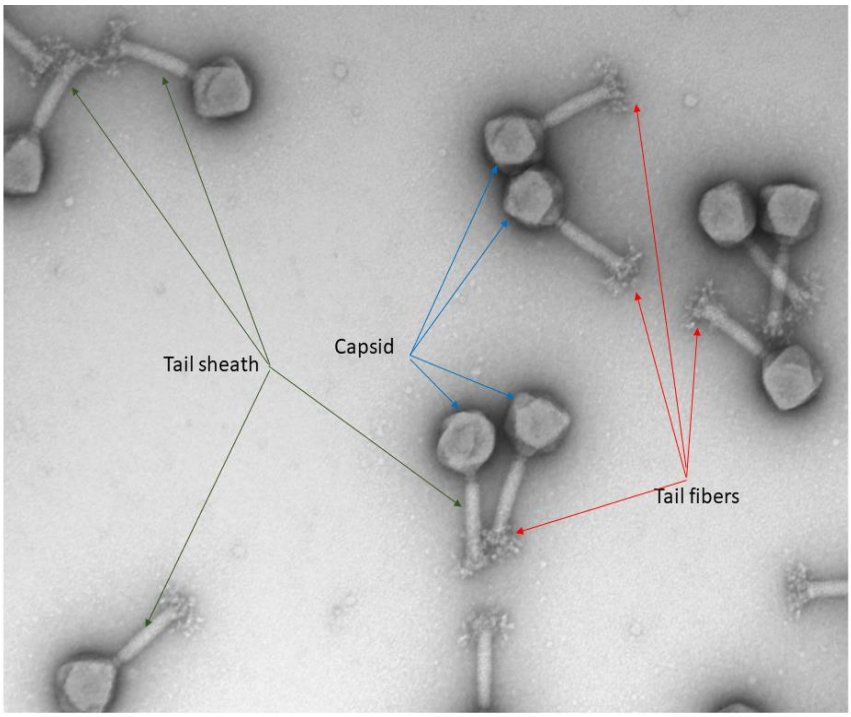

Figure 20 Bacteriophage Det7 virion particles with Tails sheath, Capsid, and Tail fibers labeled. Picture take by Robert H. Edgar at a magnification of 52,000x using a Leica TEM with uranyl acetate stain

These proteins have developed to be among the most stable protein complexes found in nature[210]. As bacterial probes, tail fiber proteins have many advantages over antibodies. Tail fibers are produced as part of bacteriophages that are self-replicating within a bacterial host, making them cheaper to produce than antibodies. An electron micrograph of bacteriophage tail fibers is shown in Figure 19. Additionally, tail fibers are more stable than antibodies[209, 211]. Bacteriophage tail fibers also have greater specificity than antibodies and have evolved to bind to essential surface antigens of the bacteria and are therefore hard for the bacteria to change.

Bacteriophage have evolved alongside bacteria as they have differentiated into new subspecies of bacteria, even those that have acquired antibiotic resistance. Bacteriophage attaching to bacterial surface antigens are displayed in Figure 20 [256].

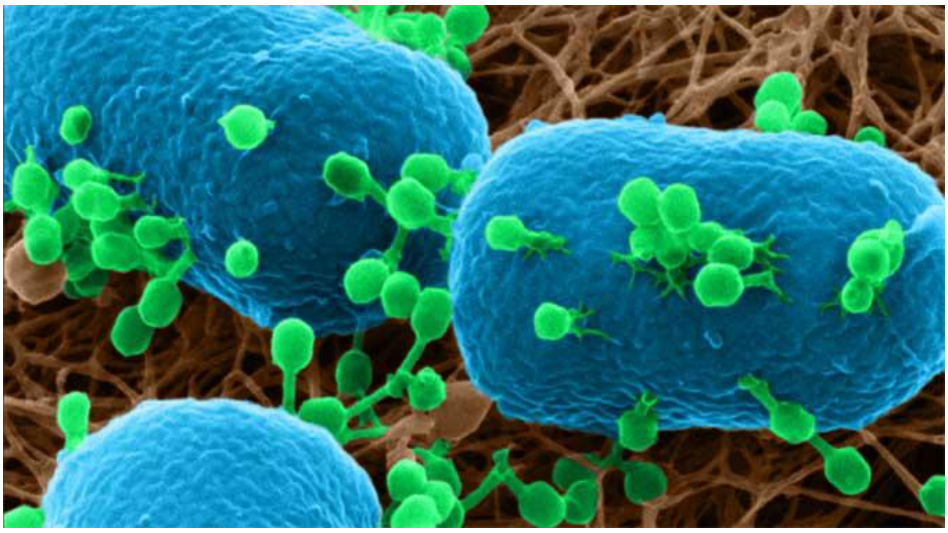

Figure 21 Multiple bacteriophage particles attached to a single E. coli cell imaged using Helium Ion microscopy by Leppnen [202]

6.3 Materials and Methods

Our photoacoustic setup is based on our system used to detect circulating melanoma cells in blood [190, 235] PAFC has been described previously and was shown to be a robust method of detecting rare particles in dilute samples.

The PAFC system was tested with phosphate buffered saline (PBS) to demonstrate a level of background noise or variability. As a positive control for system function we used 10 μm polystyrene spheres obtained from Polybead (Warrington, PA) and titered them through the PAFC system. *Staph. aureus* strain SA113 (ATCC 35556, Manassas, Virginia) was obtained from American Type Culture Collection and we used *E.coli* K12 as a control bacterial cell type. Dyed SP1 bacteriophage were added to resuspended cultures at a ratio of 1000 phage per bacterial cell. Phage/bacteria mixtures were incubated on the bench top for 10 minutes to allow phage attachment, then processed thought PAFC system.

6.3.1 Sample Preparation

Clinical isolates of *Staph. aureus* were obtained from the Urisch laboratory at the UPMC Department of Othopaedic Surgery. Isolates were de-identified according to IRB protocol and were stored in 50% glycerol solution at -80˚C. Isolates were streaked for single colonies on mannitol salt agar (MSA) plates and cultures were grown in mannitol salt broth, shaking at 36.5˚C. Overnight cultures were then diluted into fresh media and regrown for 2 hours to ensure that bacteria were entering exponential growth phase. Exponentially growing cultures were mixed with media or daptomycin in a 1:1 ratio. Daptomycin was added to 0.5 ml of culture to a final concentration of 0.25 μg\ml. Identical cultures were used in all experiments using PAFC and

BioTek H1 plate reader. For photoacoustic testing, bacteriophage SP1 was added to a concentration of 1000 phage per bacterial cell. Growth curves were performed for 16 hours with measurements taken once every minute. Growth curves for each strain and corresponding PAFC results are displayed in Figure 4.

Treated and control cultures were placed in a round bottom 96 well culture plate (Falcon microtest 96 well plate 35077, ThermoFisher, Waltham, Massachussetts) and were placed into the BioTek H1 plate reader. Optical density (OD) measurements were taken every minute at 600 nm wavelength. Between measurements, the plate was shaken at 100 rpm and maintained at 36.5˚C allowing for bacterial growth. The two hour time point was determined to be sufficient to differentiate the growth rates. Additionally, multiple replicates of each bacterial strain was grown at 36.5˚C in the BioTek H1 plate reader and 100 µl was removed and plated on MSA plates every 10 minutes. Growth curves were made directly from these titers for each strain to give a quantifiable number of bacterial cells for each OD. Each strain was found to consistently correlated between cell titer and OD.

6.3.2 Photoacoustic Flow Cytometry

The photoacoustic flow chamber is shown in Figure21.

A 1000 µm optical fiber with numerical aperture of 0.39 (Thorlabs, Newton, New Jersey) was used to deliver laser light at 532 nm with a 5 ns pulse duration from a Nd:YAG laser(Litron Nano, Boseman, Montana). Laser beam energy was maintained and measured between 1.9 and 2.1 mJ for all PAFC experiments. The optical fiber was placed 5 mm away from a quartz tube (Quartz 10 QZ, Charles Supper, Natick, Massachussetts) with 10 µm thick walls. Samples were pumped through the quartz tube inside a 3D printed flow chamber. The laser beam was assumed

Gaussian in shape and fluence was calculated to be 0.014 mJ/cm^2 and detection volume was determined to be 0.04 µl.

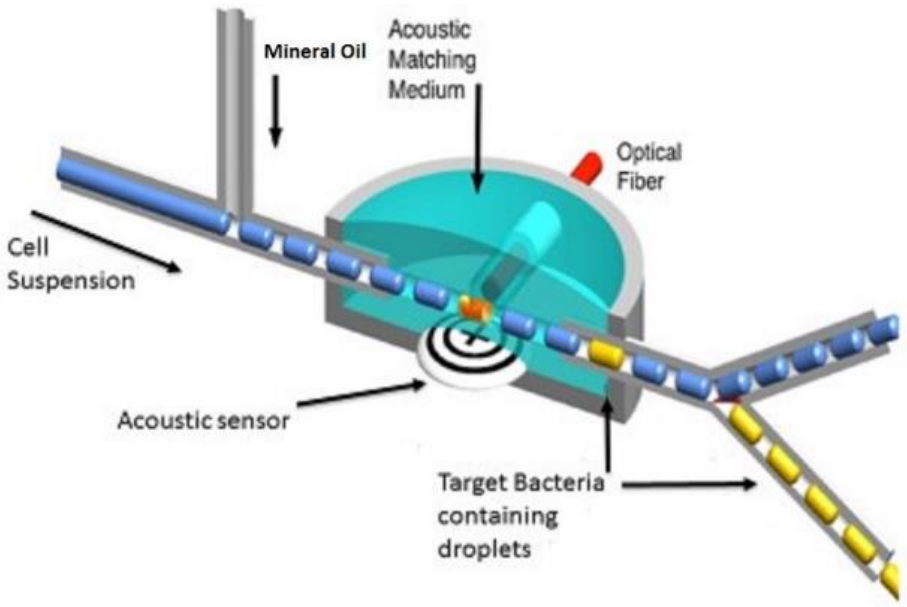

Figure 22 Schematic of photoacoustic flow chamber with parts labeled for identification

Sonotech LithoClear acoustic gel (Next Medical Products Company, Branchburg, New Jersey) filled the internal space of the 3D printed flow chamber and a 2.25 MHz transducer was focused on the quartz sample tube. The acoustic gel provided acoustic coupling between the quartz tube and the transducer along the propagation of acoustic waves generated from thermoelastic expansion. A Tegam 4040B amplifier (Tegam, Inc., Geneva, Ohio) amplified signals with a gain of 50. A computer running a LabView program recorded signal waveforms[257].

6.3.3 Bacteriophage Preparation

SP1 bacteriophage were grown using *Staph. aureus* strain SA113 (ATCC, Old Town Manassas, Virginia) and concentrated using methods described previously[202]. Purified phage of $1x10^{12}$ plaque forming units per milliliter (PFU/ml) were added to a saturated solution of Direct Red 81 dye (Sigma Aldrich, Saint Louis, Missouri). Virion particles were then pelleted and resuspended in buffer (10 mM Tris, pH 7.5, 10 mM $MgCl_2$, 68 mM NaCl). This process was repeated to ensure the removal of unbound dye. The absorbance spectrum of dyed phage was determined using the BioTek H1 and compared to that of undyed phage particles. Dyed phage were titered to ensure no detrimental effects were observed from the dying process. Dyed phage were retested for their ability to infect after 150 days and no difference in titer was observed.

All strains were tested in the presence and absence of daptomycin. Cultures were diluted into fresh media and regrown for 2 hours in the presence and absence of 25 μg/ml of daptomycin. Each sample was then incubated at room temperature for 10 minutes with multiple dyed phage per bacterial cell. Incubated samples were then processed through the PAFC system and number of detected cells recorded. Isolates were tested in triplicate for both the plate reader and PAFC system.

6.4 Chapter Results

Differential growth rates were identifiable after two hours of the sixteen hour growth curve. Two hour differentiation was confirmed by Newton-Raphson root finding method. Samples treated with daptomycin fell into three categories: resistant, susceptible, and heterogeneous resistant.

Resistant strains are those where no inhibition of growth was observed in the treated sample versus the untreated control. In resistant strains, the rate of exponential growth was identical between treated and untreated samples as well as nearly identical carrying capacity. Susceptible strains showed near complete inhibition of growth in treated sample versus untreated control.

Heterogeneous resistant strains were those where clonal isolates (genetically identical) growth curves where intermediary to susceptible and resistant growth curves. Heterogeneous samples displayed either a delay in reaching exponential growth phase or a complete retardation in achieving exponential growth. We tested all samples using the PAFC system in parallel to measuring growth rates. Growth curves for each of the bacterial strains were matched with their reported genotype. Strains that showed susceptibility at 0.25 μg/ml of daptomycin matched genotypically with MRSA strains where the *mecA* gene was not present in the genome.

Number of cells detected are displayed with corresponding growth curves in Figure 22. Untreated culture are shown in red and treated cultures shown in blue. Left hand panel shows 2 hours growth differentiation. Right hand panel shows full 16 hours of growth. Tables shows photoacoustic detection's of each sample tested at two hour time point. Homogeneous susceptible (1) strain shows a complete inhibition of growth and zero detection in treated samples. Heterogeneous resistant (3) strain A shows a delay of exponential growth. Homogeneous resistant (2) strains show no delay or inhibition of growth and both treated and untreated samples reach exponential growth simultaneously. Heterogeneous resistant (4) strain B shows no delay in initial growth but sever retardation of growth starting at 1.5 hours and continuing until the end of the test.

Homogeneous Susceptible

1

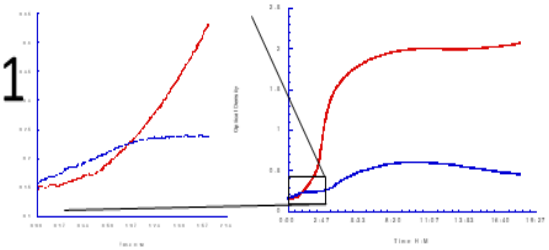

Untreated	Treated
101	0
117	0
110	0

Homogeneous Resistant

2

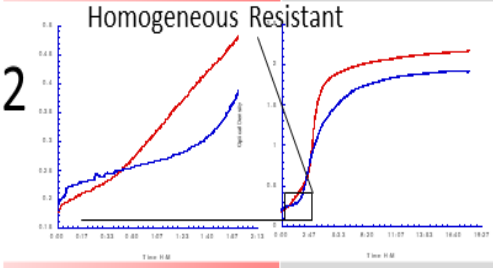

Untreated	Treated
24	25
40	67
73	33

Heterogeneous resistant A

3

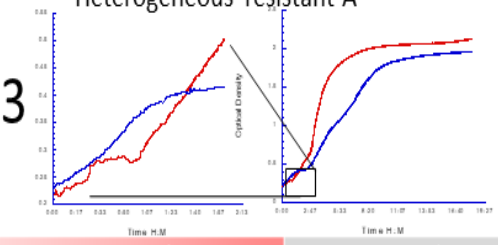

Untreated	Treated
200	44
45	29
52	39

Heterogeneous resistant B

4

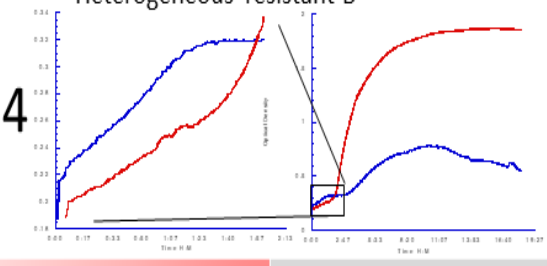

Untreated	Treated
234	97
223	67
134	101

Figure 23 Untreated culture are shown in red and treated cultures shown in blue. Left hand panel shows 2 hours growth differentiation. Right hand panel shows 16 hours of growth. Tables shows photoacoustic detection's of each sample tested at two hour time point

6.5 Chapter Discussion

Bacterial resistance continues to be a growing problem worldwide. The 2019 antibiotic resistance threat report[239] from the CDC estimates over 2.3 million antibiotic resistant infections occur in the United States each year[239]. MRSA is one of the best known resistant bacteria and is also the most common. Using PAFC we have shown a way to rapidly identify antibiotic resistance and to quantify the level of resistance expression using a short treatment of antibiotics.

Growth curves for each bacterial strain were performed over 16 hours using a BioTek H1 plate reader. This technique allowed us to confirm reliable differentiation between strains growth at 2 hours. Daptomycin was used to test for antibiotic resistance. Daptomycin has been found to be more broadly active against MRSA isolates than the standard oxacillin[251]. Additionally, daptomycin has shown a lack of cross resistance with other antibiotic classes[250]. Sensitivity to daptomycin is dosage dependant for both MRSA (MIC 0.25-1 µg/ml) and VRSA (MIC >4 µg/ml)[251]. Daptomycin was used at a concentration of 0.25 µg/ml as has been used by several other groups and been widely effective against antibiotic resistant *Staph. aureus* strains tested throughout Europe[258].

Growth curves for each of the bacterial strains were matched with their reported genotype. Strains that showed susceptibility at 0.25 µg/ml of daptomycin matched genotypically with MRSA

strains where the *mecA* gene was not present in the genome. Susceptible strains were tested in the presence and absence of daptomycin. In the presence of daptomycin, little or no growth was observed at either the 2 hour or 16 hour time point as can be seen in Figure 22 panel 1. To correlate the OD growth curves with photoacoustics, we tested multiple strains in our PAFC system in the presence and absence of daptomycin. Dyed bacteriophage SP1 was added to resuspended cultures to add optical absorption to the bacterial cells for photoacoustic detection. For homogeneous susceptible strains, no bacteria were detected in the treated bacterial cultures demonstrating a complete inhibition of growth as seen in Figure 22, panel 1. Our PAFC system results are corroborated by the 16 hour growth curves demonstrating our ability to identify antibiotic sensitivity in under 4 hours.

MRSA strains were tested using PAFC and OD growth curves. Resistant strains fell into two distinct categories. What we defined as homogeneous resistance were strains in which the growth in the presence and absence of daptomycin was indistinguishable, examples are shown in Figure 22 panel 2. Homogeneous resistance could also be described as having complete penetrance of *mecA* gene expression. When tested with PAFC, we see identical numbers of cell detected between the treated and untreated cultures. In contrast, heterogeneous strains were ones where a slight retardation in growth was observed, Figure 22 panel 3 and 4. Many genotypically resistant strains displayed an intermediary growth in the presence of daptomycin. The level of growth inhibition is correlated to the amount of penetrance of *mecA* gene expression in that population. Heterogeneous resistant A and B (Figure 22, panel 3 and 4) are representative examples of strains where growth curves showed an intermediary inhibition in the presence of daptomycin. When these strains are tested in our PAFC system, we again see corroboration with the growth curves

and the intermediary number of cells detected. Heterogeneous Resistant B in Figure 22, panel 4 demonstrates both a delay in growth and large, but not complete, inhibition of growth.

In our current study, production and purification of phage was the limiting factor for how many samples we could test. Though the production and purification is relatively cheap, even on a laboratory scale, it is time consuming and requires specialized skills. With advancements in phage therapy several companies such as Advanced Phage Therapeutics (Gaithersburg, MD) and ARMATA pharmaceuticals (Marina del Ray, CA) have started large scale production of FDA approved GMP phage. The availability of high titer purified phage greatly increases the practicality and lowers the expense of this system of bacterial detection. Additionally, this system of bacterial detection can also be used in phage therapy to rapidly test bacterial susceptibility to particular phage for treatment purposes.

Photoacoustic flow cytometers are relatively economical to build and are much simpler than many common laboratory equipment. Laser sources are the greatest cost and all parts are commercially available. Total cost of a laboratory setup is around $30,000 while commercial setups could be produced for much less. This low equipment cost suggests photoacoustic flow cytometry could become common clinical tools, similar to x-ray or ultrasound machines.

6.6 Bacteriophage Attachment Variability

An additional advantage when used with PAFC, bacteriophage size plays an important role. Single free floating phage particles are below the detection threshold of our photoacoustic system. Bacteriophage attach to outer surface antigens on the surface of bacterial cells allowing for multiple bacteriophage to bind to a single cell. Regarding the number of bacteriophage attaching

to an individual cell, Max Delbrück demonstrated in the 1930's that bacteriophage binding to surface receptors followed a pattern where the vast majority of bacterial cells will have a full complement of bacteriophage bound and very few will have more or less bound[259]. When labeled bacteriophage aggregate on the surface of bacterial cells, they form a large enough optical absorber to create a detectable acoustic response. Due to this phenomenon, acoustic signals are only detected from target bacteria of our bacteriophage of interest and not from unbound bacteriophage. A threshold was set for the acoustic signal amplitude at 2.5 times the noise floor, meaning that even bacterial cells with far fewer bacteriophage attached create a detectable and quantifiable signal.

Additionally, the bacterial cell suspension is diluted so that the expected value of cells in the detection volume is one, following a Poisson distribution. Assuming a uniform distribution of cells from a well mixed sample, the vast majority of detections will have a single bacterial cell, though a few might have two. A negligible number will have three or more. With our simple amplitude threshold detection, the method is not dependent on relative numbers of attached bacteriophage, as long as there are enough to reach threshold. We are considering automated classifiers for the photoacoustic signals; though our work is too preliminary to provide enough data for a robust classifier at this point.

6.7 Chapter Conclusions

Combining the growth curve data and PAFC results leads us to postulate that Heterogenous A and B strains are heterogeneous in their expression for the *mecA* gene. Our results suggest that strain Heterogeneous Resistant A in Figure 22, panel 3 expresses resistance derived from the *mecA*

gene at a higher penetrance while Heterogeneous Resistant B in Figure 22, panel 4 expresses the *mecA* gene at a low penetrance. These results demonstrate our ability to identify antibiotic resistance in *Staph. aureus* in less than 4 hours. This 4-hour period includes 2 hours of incubation with and without antibiotic, followed by photoacoustic testing, which is less than 2 hours. Additionally, these results show an ability to identify heterogeneous resistant strains that are often misidentified. Correct identification of heterogeneous resistant *Staph. aureus* could potentially save hospitals money and resources.

6.7.1 Future Work

We will extend the ability to determine antibiotic sensitivity to other types of bacteria and resistance. Additionally, RNA-Seq will be performed to further correlate the level of gene expression penetrance with growth curves and cells detected from PAFC. Vancomycin resistant strains, though less common, are dramatically harder to treat and use up hospitals limited resources[260]. Vancomycin resistant Enterococcus, carbapenem resistant Enterobacteriaceae, and multi-drug resistant Pseudomonas aeruginosa are listed as serious threats by the CDC and would benefit from early detection and susceptibility determination. On both an individual and global scale, rapid identification and characterization is essential. The potential for world wide crippling pandemics from bacterial pathogens is of central concern to the CDC and WHO[239]. Multi-drug resistant bacterial infections regularly have mortality rates closer to 50% and transmission rates similar to that of flu and SARS-COV-19 which have mortality rates closer to 1%[261]. There is a clear need for better and more advanced rapid diagnostics to protect individual patients. The disk diffusion method has been the gold standard since 1956 but requires 16-24 hours

after cultures are grown[262]. PAFC has the potential to supplant the gold standard by directly counting the difference between cells in treated and untreated cultures in less than four hours.

6.8 Conflict of Interest Statement

6.8.1 Financial Disclosure

Robert Edgar, Dr. John Viator, Dr. John Kellum, and Dr. John Hempel have equity in J3RM, LLC, a company formed to commercialize photoacoustic methods for bacterial detection and identification. No other authors have financial interests related to this technology.

6.8.2 Acknowldegment

Research reported in this publication was supported by National Cancer Institute of the National Institutes of Health under award number 1R01CA161367-01.

7.0 Differentiating Methicillin Resistant and Susceptible Staphylococcus aureus from Ocular Infections using Photoacoustic Labeling

Robert H. Edgar[a], Anie-Pier Samson[b], Vishal Jhanji[c], Regis P. Kowalski[c], John Kellum[d], Lauren Sugden[b], John Viator[a,b],*

[a]University of Pittsburgh, Swanson School of Engineering: Bioengineering, 3700 O'Hara Street, Pittsburgh, PA,4United States, 15261

[b]Duquesne University, 600 Forbes Ave, Pittsburgh, PA, United States, 15282

[c] University of Pittsburgh, School of Medicine, Ophthalmology, 203 Lothrop Street, Pittsburgh, PA 15213

[d] Spectral Medical, 135 The West Mall, Unit 2, Toronto, Ontario M9C 1C2, Canada

7.1 Chapter Abstract

Antibiotic resistance in bacterial species constitutes a growing problem in clinical treatment of infections. Not only does it limit therapeutic options, but application of ineffective antibiotics allows resistant species to progress prior to prescribing more effective treatment to patients. Methicillin resistance in *Staphylococcus aureus* is a major problem in clinical infections as it is the most common hospital acquired infection. We developed a photoacoustic method using bacteriophage probes for rapid determination of methicillin resistance in *S.aureus* with thirteen clinical samples obtained from keratitis patients. The *S. aureus* isolates were classified from culture isolation as methicillin resistant and susceptible using cefoxitin disk diffusion testing. The

photoacoustic method enumerates bacterial cells. as resistant strains. Using k-means clustering on the data, we achieved 100% classification of *S. aureus* resistance. This method may be generalized to other bacterial species using appropriate bacteriophages and testing for resistance using other antibiotics.

7.2 Chapter Introduction

Methicillin-resistant *Staphylococcus aureus* (MRSA) infections are on the rise in both community and hospital settings[263, 264]. Several studies have shown an increased rate of MRSA infections and that they account for the majority of clinically treated eye infections, and the second most prevalent health care associated infection after *Pseudomonas aeruginosa*[265-267].

Resistance to antibiotics is a natural process that has accelerated by human use of antibiotics for medicine and agriculture. In an effort to slow the rate of growth of antibiotic resistance, rapid identification and assessment of bacteria is essential. New antibiotics have been slow to develop with only two completely novel antibiotics brought into use in the last 75 years, possibly due to regulatory hurdles and small economic value to the industry [27]. In the United States, an estimated $30 billion is spent annually on dealing with antibiotic resistant bacteria[28].

One subset of bacteria is primarily responsible for the majority of multi-drug resistant infections. The ESKAPE pathogens (*Enterococcus faecium, Staphylococcus aureus, Klebsiella pneumonia, Acinetobacter baumannii, Pseudomonas aeruginosa*, and *Enterobacter*) are responsible for the majority of nosocomial infections and mostly likely to be multi-drug resistant[27]. An estimated 90% of human antibiotic use is broad spectrum prescribed by general practice doctors [28]. From food processing plants to hospital beds, the speed at which bacterial

contamination can be identified is the most important factor in treatment and control. Rapid bacterial identification negates the need for broad-spectrum antibiotic use and allows for targeted therapy. Detection of these pathogens not only requires their identification but also the susceptibility to antibiotics. Ideally, rapid bacterial detection and identification of resistance would be fast enough to negate the use of broad-spectrum antibiotics, therefore allowing point of care facilities to test and not require expensive equipment.

We have developed a photoacoustic method for detection of dilute particles in body fluids[10, 11]. Much of this work has been used for detection of circulating tumor cells (CTCs), primarily melanoma cells, as their native optical absorber, melanin, makes them suitable for sensitive photoacoustic detection and enumeration. This photoacoustic method is a type of flow cytometry in which cell suspensions are irradiated with nanosecond laser light that targets optically absorbing particles. These particles subsequently generate acoustic waves. These laser-induced acoustic waves are then detected using ultrasonic transducers. These signals are then counted, providing information about the number of particles. This number has been used to indicate disease state in cancer patients by determining the relative number of CTCs over time. Using bacteriophage that are engineered to absorb laser light, we specifically label bacterial cells in a sample and are able to perform the same type of photoacoustic flow cytometry[8,9].

Most competing technologies using polymerase chain reaction (PCR), fluorescence in situ hybridization (FISH), or bacterial culture require amplification, either in terms of genetic material or organism number [27–30]. This requirement introduces significant delays in returning results and may introduce contamination. Moreover, both PCR or FISH involve analysis of molecular material, rather than the culprit bacteria themselves.

There are other research attempts for early detection of bacterial infection, including size, mechanical property, electrical, and acoustic types of classification [31–34]. While these methods are innovative and exploit powerful techniques, they fundamentally work as enrichment tools, as these properties are all subject to high levels of biological variability. Consequently, discrimination must be done with higher sensitivity and lower specificity, so that most bacterial cells are selected, at the cost of excess blood cell contamination. The major shortcoming in all such methods is that they do not select for bacteria, but for ranges of properties of bacterial cells that are shared with normal cell types.

In this study, we obtained thirteen samples of *S. aureus* from patients who were treated for microbial keratitis. We tested each sample photoacoustically and determined whether these samples were methicillin resistant with 100% accuracy.

7.3 Materials and Methods

7.3.1 Photoacoustic System

Our photoacoustic system is shown in Figure 23 and consisted of a laser coupled to an optical fiber directed at a flow chamber through which saline suspensions were directed. An acoustic transducer was coupled to detection electronics for data processing and analysis.

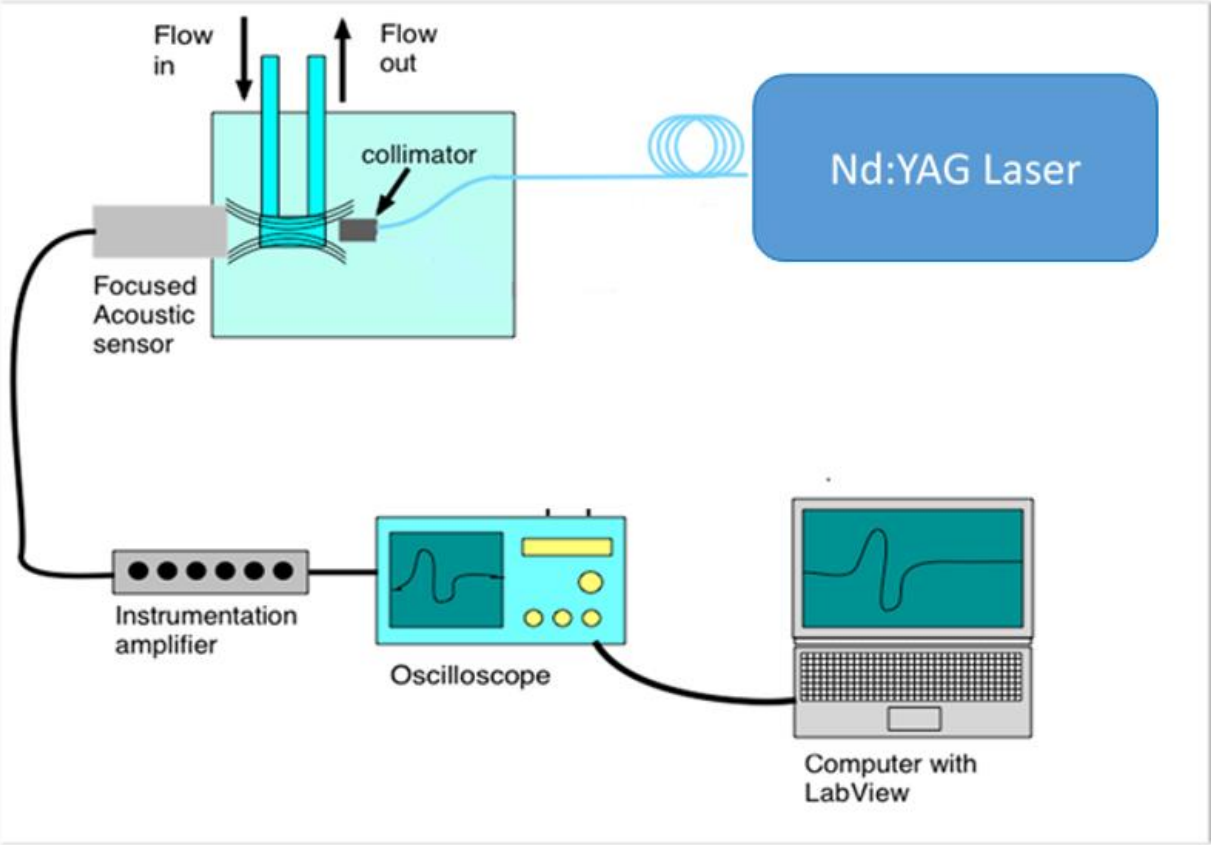

Figure 24 Schematic of Photoacoustic flow setup

The system was calibrated using 10 µm dyed polystyrene microspheres Polybead, Warrington, Pennsylvania) and phosphate buffered saline (Fisher Scientific, Pittsburgh, Pennsylvania) as positive and negative controls. As a control for bacteriophage binding, we used American Type Culture Collection strain 35556 (*Staphylococcus aureus* strain SA113). Modified bacteriophage SP1 was used as tags at a ratio of 1000 bacteriophage per *S. aureus* cell. Bacteriophage were added to each culture and incubated at room temperature for 10 minutes to ensure phage binding. The combined culture and bacteriophage mixture was passed through the PAFC system at a flow rate of 60 mml/min.

The photoacoustic flow cytometer used a frequency doubled Nd:YAG laser operating at 532 nm with a 5 ns pulse duration and a 20 Hz pulse repetition rate. These laser parameters are appropriate for inducing acoustic waves in labeled bacteriophage attached to bacterial cells. Laser light was launched into a 1000-micron optical fiber with a numerical aperture of 0.22. The optical fiber was directed to a flow chamber made from 3D printed polylactic acid (PLA) filament. The chamber is shown in Figure 24. An immersion acoustic transducer (Olympus, Waltham, Massachusetts) fixed to the flow chamber with a center frequency of 2.25 MHz and a focal length of 0.5 inches was used to sense the generated acoustic waves.

Rather than sending a continuous flow of cell suspension through the flow chamber, we induced two phase flow by introducing an immiscible fluid to the saline suspension. We used mineral oil, thus creating alternating droplets of cell suspension and oil[268, 269]. These alternating droplets created a fluidic conveyor belt that allowed for localized detection of photoacoustic events. This arrangement allowed for microfluidic capture of droplets that generated photoacoustic waves which identified bacterial cells of interest.

The transducer was coupled to a high frequency digitizer and amplifier (National Instruments, Austin, Texas) connected to a desktop computer (Dell, Round Rock, Texas). Photoacoustic waves were identified by a LabVIEW (National Instruments, Austin, Texas) program made for this photoacoustic flow cytometer.

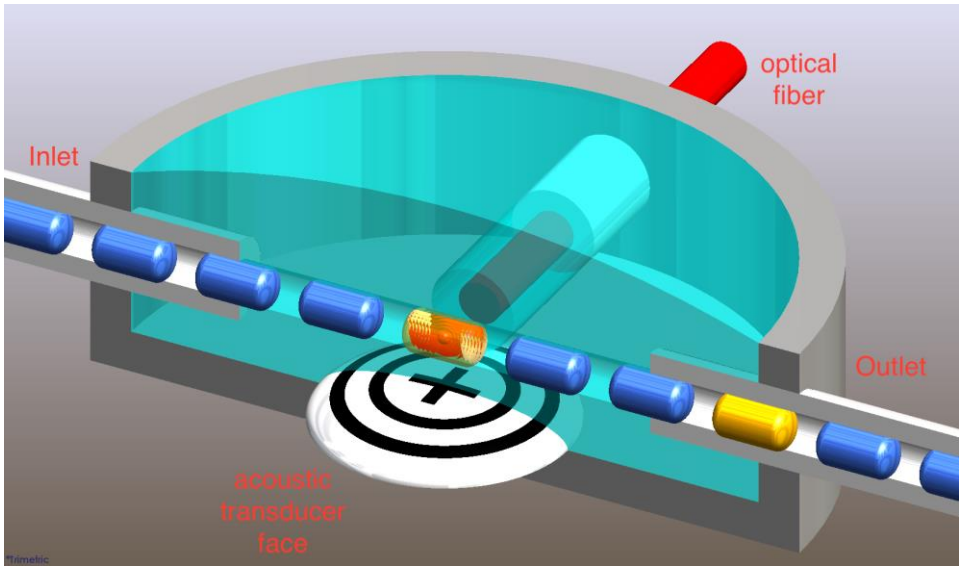

Figure 25 Photoacoustic flow cytometry excitation chamber

Photoacoustic events were classified by a simple threshold of the voltage signal from the transducer. The threshold was set at three times the standard deviation of the noise floor. Each photoacoustic wave was assumed to be generated from a single bacterial cell, which was reasonable from the dilute concentration of bacterial cells. The bacterial count was recorded for each patient sample which as split into two subsamples, one of which was treated with oxacillin, and one was untreated. These numbers were used for determination of antibiotic resistance.

7.3.2 Sample Preparation

S. aureus samples were obtained from The Charles T. Campbell Eye Microbiology Laboratory, University of Pittsburgh Medical Center, Pittsburgh, PA, USA.. A total of thirteen samples were tested for the mecA gene using PCR, thus determining their methicillin resistance before photoacoustic testing. Streaks of each *S.aureus* strain were grown on mannitol salt agar

plates. Single colonies from each streak plate were used to regrow strains in mannitol salt broth for 2 hours in a shaking water bath at 36.5 C. This period ensured cells were growing and entering exponential growth phase. Oxacillin was added at a final concentration of 1 µmg/ml to half of each culture and grown for an additional 2 hours. Before processing through PAFC system, 100 µl from each culture was removed and used for growth analysis in an H1 plate reader (Biotek, Winooski, Vermont). Growth curves were made for each culture by taking the optical density of each treated and untreated culture every minute over a 16-hour period. We determined that two hours of antibiotic treatment was sufficient to determine differential growth rates from prior experimentation. . Prior to performing photoacoustic testing, treated and untreated samples were incubated side-by-side for two hours. Photoacoustic testing of treated and untreated samples for each isolate were alternated, so that both samples were tested within twenty minutes to allow for similar growth times. Thus, total bacteria number could be compared properly.

Table 8 Staph strains with both treated and untreated detections

Isolate	Untreated Detections	Treated Detections	k-means	mecA verified by PCR	Concordant for k-means and PCR
K3255	798	53	1	No	Yes
K3251	726	7	1	No	Yes
B1899	611	404	2	Yes	Yes
K3282	818	689	2	Yes	Yes
K3266	119	18	1	No	Yes
K3268	88	110	2	Yes	Yes
K3270	144	134	2	Yes	Yes
K3279	198	175	2	Yes	Yes
K3261	170	135	2	Yes	Yes
K3262	183	10	1	No	Yes
K3237	137	44	1	No	Yes
K3287	210	2	1	No	Yes
K3280	227	179	2	Yes	Yes

7.3.3 Bacteriophage Preparation

Bacteriophage were produced using SA113 (ATCC, Old Town Manassas, Virginia) and Bacteriophage lysates were concentrated using polyethylene glycol 8000(PEG) precipitation.

Differential centrifugation and cesium chloride gradients were used to further concentrate and purify stocks to a concentration greater then $5x10^{11}$ plaque forming units per milliliter (PFU/mL). These bacteriophage concentration methods are previously described by Edgar *et al.,* Nielson *et al.* and Yamamoto *et al.[202, 222, 223].* Bacteriophage were modified to increase absorbance of 532 nm laser light by adding Direct Red 81 dye (Sigma Aldrich, Saint Louis, Missouri). SP1 bacteriophage were grown using SA113. Purified phage of 1x 10^12 plaque forming unites per milliliter (PFU/ml) were added to a saturated solution of Direct Red 81 dye. Virion particles were then pelleted and resuspended in buffer (10 mM Tris, pH 7.5, 10 mM $MgCl_2$, 68 mM NaCl). This process was repeated to ensure the removal of unbound dye. The absorbance spectrum of dyed phage was determined using the H1 plate reader and compared to that of undyed phage particles. Dyed phage were titred to ensure no detrimental effects were observed from the dying process. Dyed phage were retested for their ability to infect after 150 days and no difference in titer was observed.

7.3.4 K-means Clustering

In order to interpret the photoacoustic data provided by the flow cytometer, we used k-means clustering to guide our differentiation between methicillin resistant and susceptible samples[270]. Although a simple interpretation of the number of bacteria after oxacillin treatment compared to the number in the untreated subsample should obviously indicate whether the bacteria was methicillin resistant or not, we used a formal method to automatically determine resistance. K-means, like other clustering methods, takes data points in a space of one or more dimensions and determines natural groupings of those points by proximity. Given a number of clusters, k, the

algorithm separates all points into that number of groups. Since we are only interested in resistant and susceptible groups, we chose k=2.

We took the ratio of treated detection numbers over untreated numbers resulting in 13 numbers, approximately in the range of 0 to 1. Lower numbers would indicate that oxacillin was effective in decreasing the *S. aureus* population. However, there was no *ad hoc* threshold for determining antibiotic resistance. We applied k-means with two clusters to this data set. We used the Matlab function, kmeans, which uses Lloyd's algorithm. For simplicity, we used Euclidean distance for measuring and establishing iterative clusters. This analysis resulted in two clearly defined clusters for MRSA and methicillin susceptible samples.

7.4 Chapter Results

Table 7 lists each of the clinical isolates obtained from the patients. We indicate how many photoacoustic events and, hence, how many bacterial cells were detected in the Oxacillin treated and untreated subsamples. Photoacoustic testing resulted in bacterial counts ranging from 2 to 689 at 2 hours when incubated with Oxacillin compared to 88 to 818 when samples incubated without antibiotics. Since the sample size was small and the distribution was not obviously Gaussian, we performed a nonparametric test to compare the means of the bacterial counts before and after treatment with Oxacillin. Using a Wilcoxon matched pairs signed rank test, we calculated a p-value of 0.0007.

Furthermore, we observed two distinct subpopulations when incubated with Oxacillin. In one subgroup growth rates were similar between treated and untreated conditions, with a mean ratio of treated to untreated of 0.87, while the second group was markedly different with a mean

ratio of 0.10. Once again, due to the limited sample size, we performed a nonparametric test of the two groups. Using a Mann-Whitney test, we calculated a p-value of 0.0012. Seven of the 13 clinical isolates were found to be methicillin resistant using PCR testing for *mecA* gene. Isolates with the *mecA* gene corresponded to the subgroup with similar growth rates.

To confirm the groupings by photoacoustic detection results, we used an unbiased clustering method, k-means. The k-means column in Table 1 shows whether these numbers determined a ratio that clustered in group 1 or 2, as determined by the Matlab algorithm. The k-means algorithm resulted in 100% concordance with the known antibiotic resistance using mecA genetic analysis

7.5 Chapter Discussion

The spread of MRSA is an increasing clinical problem. Detection and treatment of MRSA have lagged behind the spread of infections [271].The resistance of bacteria is compounded by prescription of non-targeted antibiotics. Rapid identification of bacterial infection is a pressing need in clinical care. It is only after identification of the pathological agent that virulence, antibiotic resistance, and other relevant factors can be considered when determining optimal therapy [22]. Misdiagnosis can result in delayed therapy which can cause sepsis, multiple organ failure, and possibly death. Evaluating patients suspected of bacterial infection is a complex process with unique aspects of each case that may confound proper diagnosis. A system that can immediately identify the bacterial pathogen will result in better outcomes for millions of patients each year.

Over 1.5 million cases of sepsis occur annually in the United States alone [23]. For patients enrolled in clinical trials, hospital mortality has fallen to about 20% [24]. However, sepsis trials

fail to recruit patients where the clinical diagnosis is missed and often exclude the most severely affected. Even so, mortality exceeds 30% at 90 days and 40% at one year. In the US alone, sepsis is estimated to cost more than $24 billion in hospitalization alone. Long term sequelae in survivors includes chronic lung disease, such as fibrosis, and end-stage kidney disease.

A major reason to identify MRSA is that it requires treatment with vancomycin or other non-penicillin, non- cephalosporin, anti-staphylococcal agents. These agents can produce major toxicity especially to the kidney and can result in renal failure [25]. By contrast, methicillin susceptible infection can be treated with a variety of cephalosporins and avoid the risk of renal failure. However, determination of methicillin susceptibility vs MRSA can take up to 72 hours and when the infection is not in the bloodstream, it sometimes cannot be determined at all. For example, cultures are often negative with pneumonia.

Our photoacoustic system has the potential to identify and determine antibiotic resistance from patient samples. In this study, we retrospectively determined antibiotic susceptibilities for 13 clinical isolates using bacteriophage tags and our photoacoustic flow cytometry system. Each isolate had previously been determined to be methicillin resistant or susceptible through PCR of the mecA gene. Additionally, we made growth curves of each isolate in the presence or absence of oxacillin to reconfirm the PCR classification of resistance. In each case, 16-hour growth curves confirmed the PCR classification as susceptible or resistant.

Photoacoustic flow cytometry analysis showed higher number of detections in treated cultures of resistant bacteria than in susceptible bacteria. Simple visual inspection and *ad hoc* classification of results differentiated susceptible and resistant strains. To further strengthen this observation, we used k-means clustering to provide an objective means for separating the set of samples into two groups, namely, resistant and susceptible strains. K-means analysis of the

photoacoustic events produced two clusters that grouped perfectly with the previously determined antibiotic resistance. Although k-means clustering was consistent with the prior determined nature of the samples, in the future, we will develop a classifier, rather than a clustering method, so that we can determine resistance or susceptible to antibiotics from single samples in the clinic.

7.5.1 Applications in Ophthalmology

S. aureus is a common cause of bacterial keratitis, conjunctivitis, and endophthalmitis. The samples used in this study were obtained from clinical cases of keratitis. While vancomycin is often used for treatment of MRSA keratitis, it is associated with corneal toxicity [26]. The clinical significance cannot be understated, as MRSA keratitis is often part of a series of comorbidities that affect visual function. While photoacoustics can certainly identify the foundational bacterial infection and provide insight into factors that can be used to manage therapy for the infection, we are investigating ways to adapt the photoacoustic method for wider application in keratitis, which manifests in a complex environment that is still clinically challenging.

7.6 Chapter Conclusion

Rapid identification and early treatment of bacterial infections has been a goal for medicine since resistant strains emerged. Control of many bacterial strains has been put into jeopardy with the rise of antibiotic resistant strains. Early detection of bacterial strains and characterization of resistance is fundamental to modern clinical treatment[239]. Our method exploits the specificity of naturally derived bacteriophage probes and the robust nature of laser induced ultrasonics to

provide a rapid, unambiguous method for objective identification of bacterial species and their antibiotic susceptibility.

8.0 Conclusions:

8.1 Bacterial Detection

Detection of bacterial contamination early and accurately is imperative to reduce negative impacts on patients, production and general well-being. Left unchecked, bacterial contamination can become a life threatening condition in a matter of hours. Hospitals and manufacturers of medical devices and pharmaceuticals have been searching for better methods of detecting and characterizing contamination since modern medicine and manufacturing evolved.

Bacterial cultures grown from patient samples have been the “gold standard” to which all other detection methods are judged. Patient samples are streaked on an agar plate or are used directly to inoculate a liquid culture. Growth takes anywhere from 18 to 48 hours for bacterial identification. Classification by gram staining as gran-negative or gram-positive is often used as an early characterization step. Gram staining requires 16 hours of growth and provides suggestions as to types of antibiotic classes that are likely to work against an unknown bacterial strain.

Many techniques and systems have recently been developed to enhance upon gram staining and culture growth. The simplest enhancement over simple bacterial culturing is the use of selective media that inhibit the growth of non-target bacteria. Selective media can also provide selective carbon sources that only target bacteria are able to use therefore selecting against the growth of non-target bacteria that are unlikely to be causing a bacterial infection. An adaptation of selective media is chromogenic media in which pathogenic bacteria selectively metabolize synthetic chromogenic enzyme substrates, enabling differentiation and identification of bacteria based on colorimetric phenotypes[14]. MALDI-ToF mass spectroscopy has developed into a

useful and formidable tool in bacterial identification. Clinical use of MALDI-ToF relies on an ever increasing database of bacterial profiles [8].

Several molecular methods of bacterial identification have been developed in the last decade such as Real Time PCR, microarrays, and Fluorescence *In Situ* Hybridization (FISH) [10, 12, 16]. Despite the promised increase in speed and accuracy, each of these methods have been plagued with detractions that limit their practical use. PCR has been shown to be very effective and accurate when it works, but unknown inhibitors and amplification biases have limited its practical use [15, 16, 200, 272]. FISH has shown great promise but been inhibited by high costs and unacceptably high false negative rates [11]. Several commercially available microarrays have produced fantastic results by massively multiplexing probes and targets. Despite the high accuracy, these microarrays still require a positive culture and are therefore limited to an 18-20 hour response time [12, 13].

The majority of rapid diagnostic methods require some amplification of either bacterial cells or bacterial cells in the case of PCR based technology. Some of the more advanced technologies rely on observing the bacterial growth of micro colonies or observing the differential growth rates in antibiotic treated and untreated cultures. PhenoTest BC relies upon observation of micro colonies using in-situ hybridization and morphokinetic cell analysis using dark field imaging to identify and determine antibiotic sensitivity[17]. PhentoTest BC still requires 1.5 hours for bacterial identification, a positive blood culture, and an additional 7 hours to determine antibiotic sensitivity. T2 Biosystems promises to deliver results directly from patient samples in 3-6 hours but is still being proven in the hospital setting and requires expensive specialized machinery with a very high cost per test ranging between $140 and $200[19].

There is currently a great need for more rapid bacterial diagnostics, particularly diagnostic systems that can deliver results at the point of care within a timeframe of one hospital visit[28, 239]. Resistance to antibiotics is a natural process that has been greatly accelerated by human and agricultural use, and the lag time between hospital admission and bacterial contamination directly results in the overuse of broad-spectrum antibiotics. Because of the need to begin effective treatment of patients with infections before bacterial identification and antibiotic sensitivity test are complete, broad spectrum antibiotics are estimated to account for 90% of the prescribed antibiotics[28]. Heavy reliance on broad-spectrum antibiotics in clinical and agricultural settings have accelerated the emergence of antibiotic resistant bacterial strains. The ESKAPE pathogens (*Enterococcus faecium, Staphylococcus aureus, Klebsiella pneumonia, Acinetobacter baumannii, Pseudomonas aeruginosa, and Enterobacter)* are the most frequent culprits of antibiotic resistant infections [27, 273]. The development of new antimicrobial agents and diagnostics have been outpaced by the emergence of antibiotic resistant bacteria[274]. Determination of antimicrobial susceptibility is essential to future goals of managing and treating resistant bacterial strains. Additional challenges come with resistant bacteria in the form of heterogeneous populations both in genetic content as well as gene expression. Antimicrobial susceptibility can often differ between expression of resistant genes. This presents a major problem for current methods of antibiotic resistance determination[275].

Photoacoustics flow cytometry has many advantages of traditional fluorescent flow cytometry. Fluorescent flow cytometry is fundamentally the detection of light from fluorescent molecules excited by some other light source. Photons are capable of traveling the length of the universe and yet be stopped by and absorbed by a single cell. Sound waves, on the other hand, are conducted by materials and propagate through conductive media. Sound waves decrease in

intensity as they move further from their source of origination meaning that there is a practical distance limit for detection. Simply stated, light travels very far but is easily blocked while sound does not travel as far but cannot be easily inhibited. For this reason, sound waves are ideal for detection method in complex and crowded samples. This ability of sound waves to propagate and be detected in complex and concentrated samples is a major advantage of photoacoustic flow cytometry. Fluids like blood and urine are complex environments, which contain many proteins and cells, that can be problematic for fluorescent flow cytometry. Additionally, Photoacoustic flow cytometry is ideal for finding rare particles in a sample as in the case with free-floating cancer cells [190, 192, 235, 269] or low levels of bacterial contamination in blood[202, 257]. This capacity is unmatched by traditional fluorescent flow cytometry that requires several orders of magnitude more cells and concentrated homogenous samples. Photoacoustic flow cytometry's ability to enumerate cells in dilute samples is a major strong point and advantage for this technology.

Bacteriophage have been shown to be useful bacterial tags for use with photoacoustics[202, 257]. Their relative size means that unbound and bound bacteriophage can easily be differentiated within a sample. By modulating the detection threshold so that only bacterial cells that have multiple bacteriophage bound we eliminate the detection of any unbound bacteriophage. This eliminates any background signal noise from unbound bacteriophage and allows us to use an over-abundance of bacteriophage and even bacteriophage against multiple targets. Bacteriophage, and particularly bacteriophage host attachment proteins, have been shown to be stable over long periods of time and demonstrate un-paralleled stability[202, 209, 210, 243]. Bacteriophage as molecular tags have many advantages over antibodies. Antibodies often target the most abundant surface molecules of bacteria which are also those most likely to cause an immune response and

thus be under selective pressure to change [227, 228]. Bacteriophage, on the other hand, have evolved to target essential surface epitopes which are necessarily difficult for the bacterial host to change [229]. Bacteriophage have also been shown to target cell surface pumps used by antibiotic resistant bacteria to eliminate antibiotics from the cell. Bacteriophage have been shown to lower antibiotic resistance in many cases[276]. Resistance to bacteriophage does evolve, though at a much slower rate than antibody avoidance, but always has a detrimental fitness effect on the bacteria [230]. Bacteriophage binding is much stronger than that of antibodies with a binding constant closer to 10—50 nM, while antibodies have a binding constant, kD, in the range of 1—10 nM [233, 234]. Antibodies are less stable then bacteriophage binding proteins[167] and more expensive to produce[232].

Our system of photoacoustic flow cytometry coupled with bacteriophage tags has multiple uses outside of the simple enumeration of bacteria in a sample. Chapter 6 and 7 demonstrate the ability to not only discriminate and enumerate bacteria but also to determine antibiotic susceptibility. By using a short growth period (2 hours) and subjecting some cultures to a predetermined minimum inhibitory concentration (MIC) of antibiotic, our system is able to determine and even classify bacterial resistance. An ability to differentiate between homogeneous expressing resistant bacteria from heterogeneous expressing resistant bacteria is a major advantage. Heterogeneous resistant bacterial strains can be potential pitfalls for hospitals with reimbursement rates and penalties for hospital acquired infections. Heterogeneous resistant bacteria are often misdiagnosed as hospital acquired infections and therefore are no longer a reimbursable expense for hospitals[249]. Photoacoustic flow cytometry coupled with bacteriophage tags represents the fastest as well as the most cost effective method to suggest heterogeneous resistance. Sequencing of multiple bacterial colonies using RNAseq can be used in

combination with photoacoustic flow cytometry to definitively demonstrate and measure heterogeneous resistance. Once our method can be further validated it can serve as a faster and cost effective option of determination of resistance expression.

Additional advancements with the use of functionalized microspheres with bound phage tails add flexibility and robustness to our system. Functionalized microspheres allow for bacteria to be tagged and enumerated without the possibility of lysis. Further downstream processing is then possible by collecting the detected bacterial cells. Collected cells can then be sequenced or further grown to determine their genetic or gene expression profiles. Isolation and collection of these differentially expressing cells will be fundamental to performing reliable RNAseq on heterogeneously expressing strains. Functionalized microspheres also allow for the attachment of multiple types of bacteriophage tails and the ability to produce microspheres that bind to a wide variety of bacterial species. This approach allows the photoacoustic flow cytometry system to rapidly identify bacterial strains and contamination, with fewer tests by performing a dichotomous decision tree analysis. By refining the number of tests that need to be run in order to identify contamination, we have decreased the time to identification.

Our photoacoustic flow system coupled with bacteriophage or functionalized microspheres as tags will ideally be developed for point of care use. The entire flow system along with the pulsed laser and focused transducers are all commercially available and relatively low cost. Currently, prototypes of our photoacoustic flow cytometry system cost around $30,000 and this price could be greatly reduced with bulk manufacturing. The laboratory bench top space required for such a system is on par with a real time PCR machine or plate reader. There are no special stability or temperature requirements that come with other systems like MALDI-ToF or T2 Biosystems. This system is designed to be used with human blood samples with minimal processing. The blood

processing required is a standard laboratory Ficoll gradient that is used for many other procedures in blood labs. Due to the simple sample preparation, the small size, and low equipment cost this system is well suited to be used at a point of care facility.

The previous published papers and chapters in this work have pointed to the role of this technology in hospital setting and rapid diagnosis of bacterial infections. High death rates associated with sepsis and septic shock are large factors in the push for rapid diagnostic systems. The rise of antibiotic resistance and need for antimicrobial stewardship also pushed for the need to determine rapid antibiotic susceptibility. In addition, there is a role for this technology to enable other forms on antimicrobial stewardship such as phage therapy. Phage therapy is the application of bacteriophage to control bacterial infections. One of the major historical drawbacks to phage therapy has been determining bacterial susceptibility to each type of bacteriophage. One possible option for phage therapy is to collect a large number of bacteriophage that infect all the strains and sub-strains of bacteria you are targeting and combine them into a phage cocktail. In this scenario, the phage cocktail continually needs to be updated and checked against available clinical isolates to make sure the cocktail still has the same coverage. An alternative approach is to test each patient sample against large library of bacteriophage to determine a specific single bacteriophage that has high virulence against the patient bacterial sample. Photoacoustic flow cytometry when used with bacteriophage can determine bacteriophage binding much faster than a traditional plaque assay. In the future, phage therapy may be able to be used at point of care facilities with the addition of photoacoustic flow cytometry to ensure phage efficacy against each patient sample. Additionally, titration of bacteriophage into patient bacterial samples could represent a way to determine bacteriophage dosage for each patient. This will greatly increase the viability of phage therapy.

8.2 Future Directions

Despite the advancements in both microbiology and engineering that this project has seen, there is more work to develop it in the future. Substantial work will continue to be done in many areas to develop this technology to become the standard of care in hospitals around the world. Three main areas of development for this system are the engineering of the physical flow system, the development of bacteriophage and functionalized microsphere tags, and the determination of heterogeneity in samples.

Photoacoustic flow cytometry has not had the years of development, research, and refinement that have progressed fluorescent flow cytometry to be ubiquitous in research facilities. Currently, the rate at which samples can be processed is limited by the flow rate of the system. The repetition rate of the laser is matched to the current flow rate of 60 µl/min. With minimal improvements the laser repetition rate could be increased by 20-fold and flow rates increased to match. Processing at this speed will require additional adjustments and improvements to the software and programs used to record and collect signal detections. The outcome of this optimization work would will bring the sample processing time from 16 min/mL down to 48 sec/mL.

Further engineering improvements to the fluidics system and flow cell will greatly increase the system stability. Current flow cell design uses ultrasound gel as a medium to transfer acoustic waves from the quartz tube to the transducer. The quartz tubes are problematic due to their fragile nature and difficulty in assembling. Likewise, the acoustic gel often dries out needs to be replaced. Replacement of the acoustic gel requires removal of accumulated air bubbles. This manual process is both time consuming and difficult. Initial work has started replacing both the quartz tube and the acoustic gel with polydimethylsiloxane (PDMS) and patching the acoustic impedance to that

of the acoustic gel. Building of flow chambers from PDMS will remove the need for the quartz tube and the continual replacement of acoustic gel. This would make the flow cell reusable over long periods of time and commercially viable. Upgrades to the rest of the flow system using stainless steel tubing allowing for increased pressures and faster flow rates would also allow for increased stability and reproducibility.

For our signal detection, we have primarily used a thresholding set at 1.5 times the background noise as this has been empirically shown to be useful and effective. Initial work classifying signals using total peak area, peak height and other metrics have shown promise. Machine learning models to classify signals has shown the most progress. Training sets of positive and negative signals used with a machine learning approach showed initial detection well above 90%. Continued work and training sets using microspheres show a differentiation of signals from microspheres and signals from tagged bacteria of greater than 70%. This initial work shows great promise and hopes to be a read advancement in the signal detection and processing for our photoacoustic flow cytometry system.

Photoacoustic flow cytometry coupled with bacteriophage for the detection and enumeration of bacteria was shown in chapter 6 to be an indicator of resistance gene expression. Heterogeneous gene expression of resistance genes has been identified as an area of concern and problem for hospitals [277-279]. Expression levels of heterogeneous mixtures are notoriously difficult to determine using current methods. RNAseq requires the extraction of total RNA from a population and will show a single intermediary number. A method of differentiating high expressing cells from low expressing cells and separating them is required to get a true picture of the levels of gene expression in a heterogeneous mixture. In order to conclusively prove the correlation between our photoacoustic results and heterogeneous expression we will need to obtain

RNAseq data from identical cultures used on our system. The RNAseq data will both correlate the results of photoacoustics as well as be dependent upon the system to obtain pure samples of similarly expressing cells.

Future efforts of development of our system will also require an expansion of the bacteriophage and the target bacteria that we use. Ultimately, bacteriophage that target all of the ESKAPE pathogens will be useful to expand the abilities of detection. A large library of bacteriophage will be required and continually maintained against clinical isolates on a regular basis to provide assurance of accuracy. Currently, bacteriophage stocks are produced and purified in a laboratory setting using standard PEG precipitation and $CsCl_2$ gradients. Wide adoption of this method and system will require the use of commercially available GMP (Good Medical Practice) produced bacteriophage. Therefore, initial testing with GMP produced bacteriophage will provide assurance that this method can be expanded and started soon.

The work presented within this document shows the development of the photoacoustic detection of bacteria and several advancements to that detection. Initially, simple detection and enumeration of bacteria was achieved. Following on from detection, antibiotic susceptibility was able to be accurately and rapidly determined using our system. Advancements in antibiotic susceptibility by determining homogenous versus heterogeneous expressing strains was also achieved. Finally, functionalized microspheres were developed to further progress the detection and rapid characterization of bacteria. It is my hope that the continued development of this system will allow for point of care use and allow doctors to prescribe targeted antibiotics or bacteriophage in a single office visit timeframe. Detection of bacterial contamination early and accurately is imperative to reduce negative impacts of patients, production, and general well-being.

Appendix A

9.0 Predicting Metastasis in Melanoma by EnumeratingCirculating Tumor Cells Using Photoacoustic FlowCytometry

Robert H. Edgar,[1,2] Ahmad Tarhini,[3] Cindy Sander,[4] Martin E. Sanders,[5] Justin L. Cook,[1] andJohn A. Viator, PhD [1,2,5*]

[1]*Department of Engineering, Duquesne University, Pittsburgh, Pennsylvania 15282*
[2]*Department of Bioengineering, University of Pittsburgh, 300 Technology Dr, Pittsburgh, Pennsylvania 15213*
[3]*H. Lee Moffitt Cancer Center and Research Institute, Tampa, Florida 33612*
[4]*Hillman Cancer Center, University of Pittsburgh Medical Center, 5115 Centre Ave, Pittsburgh, Pennsylvania 15232*
[5]*Acousys Biodevices Inc., 1777 Highland Drive, Ann Arbor, Michigan 48108*

Background and Objectives: Enumerating circulating tumor cells has been used as a method of monitoring progression of various cancers. Various methods for detecting circulating melanoma cells (CMCs) have been reported, but none has had sufficient sensitivity to determine if the presence of rare CMCs in the blood of Stage I–III melanoma patients predicts if those patients eventually develop metastatic disease.

Study Design: We quantified CMCs in serial blood samples from 38 early stage melanoma patients to determine ifCMC numbers predict development of metastatic melanoma. CMCs were enumerated using a photoacoustic flowcytometric detection system that uses a laser to induce high frequency acoustic signals in pigmented CMCs.

Results: We observed that detection of greater than2 CMCs/ml of blood from patients with Stage I–III melanoma predicts metastatic disease. Of the 11 patients we studied who had two or fewer CMCs detected at all time points tested, none progressed to metastatic disease over a mean follow-up of 1288 days. In contrast, 18 of the 27 patients (67%) having more than 2 CMCs/ml at one or more time points progressed to metastatic disease over a mean follow-up of 850 days.

Conclusions: Photoacoustic flow cytometry can detect rare CMCs in the blood of Stage I–III melanoma patientsand detection of these cells is predictive of subsequent development of metastatic disease. Lasers Surg. Med.

Key words: cancer staging; microfluidic; optoacoustics

INTRODUCTION

The study of circulating tumor cells (CTCs) has been ongoing for many years, with technologies for their detection having varying degrees of success and utility. Detection and capture of CTCs or their cellular components may have utility in monitoring cancer recurrence orprogression, and may inform clinicians of the molecular nature of cancer in individual patients with respect to potential drug response [1,2]. More specifically, CTCs have generated much interest with respect to their poential utilization as a diagnostic for detection, capture, and genetic analysis for monitoring for recurrence and progression. A recent study by Lucci et al. reported a strong correlation of CTCs in melanoma patients and re- lapse of disease. This study was conducted with

the CellSearch system, and it was found that more than one CTC in baseline blood samples of recently surgically treated 243 Stage III melanoma patients correlated highly with advancement toward metastasis [3]. Their work paralleled our own findings, though ours were per- formed on serial sampling of blood from patients. The results of Lucci et al. and our work coincide with many other efforts in CTC research, showing that research interest in CTC assays continues, as a successful method using small blood samples may provide valuable in- formation without departing from current clinical care.

As melanoma metastasis is responsible for the vast majority of skin cancer deaths, the detection and quantification of circulating melanoma cells (CMCs) for monitoring disease relapse may have great utility in patient care [4]. Many efforts for detection and monitoring of melanoma have focused on polymerase chain reaction (PCR) methods, which exploit prior information about DNA and RNA sequences in melanoma. These techniques allow for multiple biomarkers to be assayed, and are supported by substantial industry interest. However, clinical use of PCR detection methods is confounded by their lack of ability to document objectively and quantitatively the actual presence of low numbers of circulating cancer cells in a patient.

Other detection technologies use size filtration or specific antibody-coated surfaces to capture CTCs for later imaging, enumeration, and analysis [5,6,7]. Although there are many antibody-capture techniques for counting CTCs, a label-free method, such as photoacoutic flow cytometry, eliminates the need for predicting the presence of specific cell surface markers in heterogeneous populations of cells. Additionally, some antibody-based detection methods require immobilization of the CTCs on a substrate. Maintaining CTCs in an unbound, suspended state has potential advantages in analyzing cells for various biological functions that might be perturbed by antibodies binding to cell surface molecules capable of transducing signals to the captured cells.

Photoacoustic detection is based on transduction of absorbed light from a laser source into ultrasonic waves. It has the ability to specifically detect materials based on their optical absorption. Materials that produce a robust acoustic signal, such as melanin crystals in melanoma cells, can be detected and analyzed using their photoacoustic properties [8]. Photoacoustic flow cytometry uses this principle to detect rare particles in body fluids in a fluidic system [9,10,11]. This type of flow cytometry is distinct from standard fluorescent flow cytometric methods as the laser excitation can simultaneously irradiate a large number of cells while actively identifying only rare particles, such as melanoma cells in blood, that have specific optical absorption. This advantage makes photoacoustic flow cytometric detection of CMCs rapid and sensitive, allowing detection of a single melanoma cell spiked into a 10 ml sample of blood in only a few minutes of processing time, as previously reported [12].

We have enhanced our photoacoustic flow cytometer to induce two-phase flow in order to enable cell capture for later analysis [12]. This two-phase flow introduces an immiscible fluid, such as mineral oil, to the flow system to create alternating bubbles of cell suspension and oil. This train of droplets is sequentially irradiated with laser light. Bubbles that generate photoacoustic waves are assumed to have cells of interest and are sorted down-stream. Other bubbles are discarded as waste.

We used this sensitive acoustic flow cytometric detection system to assay for CMCs in serial blood samples from 38 Stage I–III melanoma patients. Our goal was to determine if CMC enumeration over time has predictive value for progression to metastatic disease. Our analysis showed a predictive association of detected CMCs with whether patients remained free of metastatic disease, or experienced disease relapse with metastases.

MATERIALS AND METHODS

Photoacoustic Flow Cytometry

Photoacoustic generation is the process of inducing acoustic waves in a medium after irradiation with light. Virtually all photoacoustic methods use laser energy and most modern manifestations used rapid pulse laser systems. While there are several distinct physical processes to induce photoacoustic waves, our method uses thermo- elastic expansion [12,13]. This process comes about whenrapid laser heating of an optical absorber results in thermal expansion of the material, resulting in pressure waves. It is this process that occurs in photoacoustic flowcytometry, where pulsed laser light gets selectively absorbed by melanoma granules, generating sound waves. In order to detect and enumerate any circulating melanoma cells in the patient samples, we used a Q-switched Nd:YAG laser operating at 532 nm with a pulse durationof 5 nanoseconds to induce acoustic waves in melanoma cells under flow. The system is shown diagrammatically in Figure 1.

Laser light was launched into a 1000 μm, multimode optical fiber with a numerical aperture of 0.39 (Thorlabs, Newton, NJ). The laser energy typically varied from 1.9 to

2.1 mJ. Laser light was directed to a quartz tube through which the sample flowed. This tube had a 10 μm wall thickness. The thin wall enabled maximum transfer of energy from the flow within the tube to an acoustic sensor. The quartz tube was immersed in acoustic-matching gel (Sonotech LithoClear; NEXT Medical Products Company, North Branch, NJ). The optical fiber was bent as a meansto mix modes, resulting in a near-Gaussian beam. Fluencewas calculated to be 0.014 mJ/cm^2.

Two syringe pumps were used to create two-phase flow, that is, fluid sample separated by an immiscible mineral oil, as shown in Figure 1. This change from continuous flow allowed for

sequestration of cellular material into a small volume. If a melanoma cell was detected by a photoacoustic

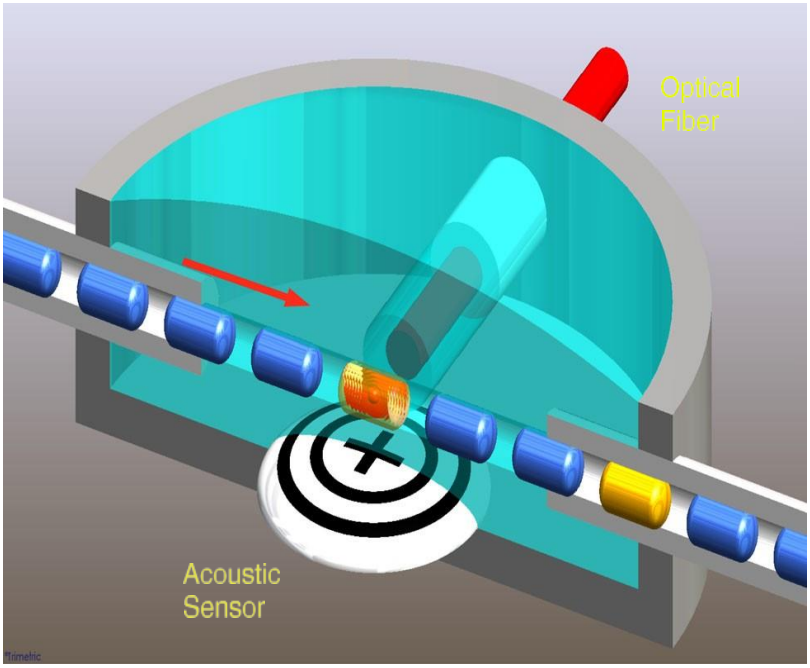

Figure 26 The photoacoustic flow cytometer separates continuous flow of blood cells with air bubbles.

response, this volume was kept using fluidic capture for later analysis. The syringe pumps created alternating flowof sample and mineral oil equal to a 60 µl/min flow rate. The flow rate and fluid properties resulted in approximately 1000 sample bubbles from the milliliter of sample.

The acoustic waves were sensed by a focused ultra- sound transducer with a focal length of 12.5 mm and a center frequency of 5 MHz. These signals were amplified with a gain of 50 using a Tegam 4040B system and was sent to a desktop computer with custom LabVIEW code (National Instruments, Austin, TX) for instrumentation control and data acquisition. Classification of photo-acoustic events was performed using a simple threshold. The noise floor was determined by

irradiating phosphate-buffered saline (PBS), as there is no optical absorption at 532 nm. The threshold was set at three times the noise floor to classify a signal as originating from a CMC. Comprehensive design and descriptions of the photo- acoustic flow cytometer for detection and capture of CMCs are given in O'Brien et al. [12]. The laser beam and the detection volume of the acoustic sensor were aligned to the detection chamber of the photoacoustic flow cytometer. The cell suspension from each sample had approximately 1000 bubbles.

We assumed the number of CMCs in each milliliter sample would be much smaller than 1000, thus, with a well-mixed suspension of cells, two-phase flow would result in most bubbles having no cells. Poisson statistics predicts that there would be a number of bubbles with one CMC, approximately equal to the total number of CMCs. That is, if there are 33 CMCs in a sample, there would be about 32–33 bubbles with one CMC each. There may be a bubble with two or more CMCs, though this possibility would be rare. Poisson statistics is described by

Equation 8.1

$$P(x) = \frac{\lambda^x e^{-\lambda}}{x!}$$

where $P(k)$ is the probability of k CMCs in a droplet and λ is the expected value of CMCs per droplet. In our study, the number of CMCs per sample typically ranged from 0 to 50, so Poisson statistics should apply. In the case of higher numbers of CMCs, Poisson would underestimate the total number, as some bubbles with a photoacoustic response would actually have two or more CMCs, but would be counted as one. However, even with 500 CMCs in a 1 ml sample resulting in 1000 bubbles, having two or more CMCs would have a probability of approximately 0.07.

Prior to each session of testing, we calibrated the photoacoustic system using PBS and 1 μm diameter black latex microspheres suspended in PBS. We ensured that running the photoacoustic system with PBS resulted in nophotoacoustic waveforms, as there is no optical absorptionin that case. When PBS samples resulted in errant photoacoustic responses, we replaced the detection chamber with a new one, as we assumed the previous one became contaminated. We then ran the system with 1 μm, black microspheres (Polysciences, Warrington, PA) to ensure that the photoacoustic responses were recorded, commensurate with the concentration of spheres. This processensured that our system was functioning properly, minimizing false positive and negative signals.

Using this system, we tested 15 healthy volunteers. We separated their whole blood by a centrifugation process that included introduction of Histopaque 1077 to separatethe buffy coat from the red blood cell layer. We also used red blood cell lysis and additional centrifugation to eliminate red blood cells, which would act as optical absorbersat 532 nm and thus provide false positive photoacoustic signals. All samples from healthy volunteers resulted in no photoacoustic detections.

Patient Samples and Preparation

We assayed, in a blinded fashion, archived frozen bloodbuffy coat samples from 38 non-Stage IV melanoma patients who had been followed at the University of Pitts- burgh Medical Center after definitive surgical management. Each sample comprised the buffy coat processed from 1 ml of whole blood. There were two to six samplesfor each patient. These were drawn at varying follow-up time points, over periods of up to 8 years from initial surgical excision of the primary melanoma lesions.

The 38 patients included 3 Stage I, 4 Stage II, and 27 Stage III individuals with melanoma of cutaneous primary lesions. Also included were four patients who had mucosal surface primary melanoma lesions. Blinded longitudinal clinical information was correlated with results of the blinded CMC assays, to examine whether detection of CMCs in Stage I–III patients was associated with eventual progression and development of metastatic dis- ease. Five of the Stage III patients we studied had received treatment with adjuvant high dose interferon-α postoperatively. This treatment appeared to have no impact on our analysis. The number of days between initial surgical excision of each patient's melanoma and detection of metastasis, for the patients whose disease progressed; or alternatively, between initial surgical excision and the last available blood sample for the patients who remained disease free; was determined by confidential blinded review of medical records. This number ranged from 102 to 2974 days.

Each blood sample was assayed by a standardized protocol. The samples had Histopaque 1077 (Sigma-Aldrich, St. Louis, MO) added prior to centrifugation and buffy coat extraction. Lysing buffer (BD Biosciences, Franklin Lakes, NJ) was also added to ensure removal of erythrocytes. Additionally, DNAase was added to eliminate free DNA fragments that could potentially bind cells together and interfere with acoustic flow cytometric enumeration of CMCs.

CMC Numbers and Date of Metastasis

We compared the data of patient samples with greater than two CMCs that led to advanced disease to those from patients who remained disease-free. We plotted the number of CMCs per sample against the number of days after diagnosis. We did not use the data for patients with fewer than two CMCs as we wanted to determine if the population of patients with greater than two CMCs in any sample was distinct, depending on whether the patients advanced their disease or not. We determined the centroid of the two sets, then determined the Mahalanobis distance of each

centroid to the total data. The Mahalanobis distance determines the distance of points to a reference in multiple dimensions, taking into account the co- variance of the data [13]. As we computed the distance using the total data set, the covariance was computed over the entire set. This distance calculation was done to get a numerical indication whether the two data sets constituted different sets in the sense of cluster analysis.

RESULTS

Data for each of the 38 patients in the study is shown in Tables 1, 2, and 3. These tables are arranged as patients with fewer than two CMCs in any sample, patients with greater than two CMCs in any sample who advanced to metastatic disease, and patients with greater than two CMCs in any sample who did not advance to metastatic disease, respectively. The initial stage of each patient is shown, along with the lowest and highest numbers of CMCs detected for all samples taken from each individual patient, over each patient's indicated time of follow-up. The tables also indicate whether each patient progressed to metastatic disease; and for patients who did progress, the number of days from initial excision to the date metastatic disease was diagnosed. Alternatively, in patients who did not progress to metastatic disease, the table displays the number of days from their initial excision to their last blood sample assayed.

In our data set, failure to detect greater than two CMCs at all time points distinguished a population of patients in which none progressed to metastatic disease. No patients of the eleven who had two or fewer CMCs detected in all of their various time point samples progressed to metastatic disease. In contrast, 18 of the 27 patients (67%), who had greater than two CMCs detected on one or more time points, eventually progressed to metastatic disease during their individual times of follow-up. This categorical difference is statistically significant given a

threshold of 0.05 on post hoc analysis by Fisher's Exact Test, 2 × 2 contingency table; two-tailed P = 0.0002 (Table 4).

The mean and median number of days of follow-up observation for the 11 patients who always had two or fewer CMCs and never progressed to metastatic disease were 1288 and 1186 from the date of initial excision. For the 18 patients with greater than 2 CMCs on at least one occasion who progressed to metastatic disease, the mean and median number of days of observation from initial excision to diagnosis of metastatic disease were 850 and 727. For the nine patients with greater than 2 CMCs on at least one occasion who did not progress to metastatic disease, the mean and median number of days of follow-up from initial excision to their last tested sample were 728 and 495. Therefore, the observation of the categorical difference in incidence of progression to metastatic dis- ease between the groups of patients with greater than 2 CMCs detected at any time point and two or fewer CMCs detected at all time points is not explainable as a result of difference in duration of follow-up time between the patient groups. The group with two or fewer CMCs on all occasions was observed an average of 438 days longer than the group with greater than 2 CMCs on at least one occasion who progressed to metastatic disease. The group with greater than 2 CMCs who did not progress to metastatic disease were followed an average of 122 days less than the group that progressed, with a median follow- up observation of 228 days less. This suggests that some of these patients may have progressed to metastatic dis- ease had they been observed longer. There was also a strong general trend for increasing rates of progression to metastatic disease with increasing thresholds for detected CMCs on at least a single occasion (Table 5).

While examining the CMC data in a converse manner, it

becomes apparent that exceeding a low threshold of2 CMCs/ml is a useful benchmark for predicting increased risk of developing metastatic disease. Detection of greaterthan 2 CMCs on any single occasion, up to detection of 100or fewer CMCs on any occasion, was associated with a riskof development of metastatic disease in the low to mid 60% range. With detection of greater than 100 CMCs on

Table 9 Patients With Fewer Than Two Circulating Melanoma Cells (CMCs) on All Samples

Patient	Stage	Lowest CMC	Highest CMC	Metastasis	Days from diagnosis
1	3B	0	2	No	317
2	3B	0	2	No	152
3	Unknown	0	0	No	2889
4	3B	0	1	No	2974
5	1A	0	1	No	1186
6	3	0	1	No	2480
7	3A	0	1	No	358
8	1A	0	1	No	1876
9	2C	0	1	No	102
10	2B	0	2	No	1583
11	3B	0	2	No	251

Table 10 Patients With Greater than Two Circulating Melanoma Cells (CMCs) in Any Sample Who Advanced to Metastatic Disease

Patient	Stage	Lowest CMC	Highest CMC	Metastasis	Days from diagnosis
12	3	2	61	Yes	192
13	3B	0	16	Yes	212
14	3B	3	209	Yes	1852
15	3C	3	54	Yes	730
16	2C	0	19	Yes	951
17	3	0	7	Yes	786
18	Mucosal	0	34	Yes	266
19	1B	11	301	Yes	723
20	3B	43	234	Yes	547
21	2A	1	3	Yes	1670
22	3A	1	74	Yes	405
23	3A	7	83	Yes	624
24	3	1	3	Yes	2240
25	3C	34	240	Yes	220

26	Mucosal	33	100	Yes	934
27	Mucosal	3	161	Yes	1506
28	3B	0	5	Yes	378

Table 11Patients With Greater Than Two Circulating Melanoma Cells (CMCs) in any Sample Without Advancing to Metastatic Disease

Patient	Stage	Lowest CMC	Highest CMC	Metastasis	Days from diagnosis
29	3C	2	63	No	383
30	3B	11	129	No	213
31	3B	0	4	No	468
32	3C	4	100	No	2490
33	3C	0	56	No	1233
34	3A	0	50	No	435
35	3B	1	423	No	513
36	3A	0	11	No	495
37	3A	0	13	No	205
38	3B	2	4	No	468

any single occasion, the risk of metastasis was 71%; and with detection of greater than 200 CMCs on any single occasion, the risk of metastasis was 80% in the timeframes during which these patients were observed.

In our entire data set, there were 18 metastatic patientsout of a total of 38 patients, for an overall metastasis rate of47.4% in the study. That overall metastasis rate is similar tothe generally quoted 5-year approximately 50% metastasis rate for Stage III melanoma patients. This supports that the patient population in our study was generally representative of typical Stage III melanoma patients. That there werea few Stage IB and Stage II patients in the study population would be expected to skew the overall observed metastasis rate a bit below the standard quoted 50% rate for Stage III patients, which was in fact observed. Also, many of the patients were followed less than the standard 5-year bench-mark, so one would expect a slightly lower overall meta- stasis rate than the historical figure of approximately 50% over 5 years for Stage III patients. Overall, our data setis consistent with the known historical metastasis rate and timeline of Stage III melanoma patients, supporting the validity and general applicability of our findings.

Table 12The 2 × 2 Contingency Table Showing Meta- stasis With Respect to the Circulating Melanoma Cell (CMC) Enumeration Threshold.

	≤2 CMCs	>2 CMCs
Metastasis	0	18
No metastasis	11	9

Threshold. The *P* Value Was Calculated as $P = 0.0002$

CMC Numbers and Date of Metastasis

Figure 2 shows the data for patients who had greaterthan two CMCs on any given sample. For patients who did not advance to metastasis, the points are indicated by plus signs. For those patients who advanced to meta- stasis, the points are indicated by circles. The data point for which metastasis was found is indicated by a filled redcircle. The Mahalanobis distance from the centroid of thenonmetastatic group to the whole set is 0.107, while the distance from the metastatic group is 0.216.

Table 13 The Progression of Circulating Melanoma Cell (CMC) Number Corresponding to Eventual Metastasis

Number of CMCs	Number that metastatic	Percentage metastatic
2 or fewer CMCs in all samples	0 of 11	0
3 or fewer CMCs in all samples	2 of 13	15
4 or fewer CMCs in all samples	3 of 15	20
5 or fewer CMCs in all samples	4 of 16	25
7 or fewer CMCs in all samples	5 of 17	29
19 or fewer CMCs in all samples	7 of 21	33
50 or fewer CMCs in all samples	8 of 22	36.4
100 or fewer CMCs in all samples	13 of 31	41.9

DISCUSSION

Detection and analysis of markers in blood is a rich fieldof investigation for cancer research [16–19]. More specifically, detection and capture of CMCs in blood may aid in disease staging, monitoring and design of therapy, and prediction of metastasis of melanoma [20]. Our study, using photoacoustic flow cytometry to detect and enumerate CMCs, provides evidence of a low risk of progression to metastatic disease in patients whose CMCs

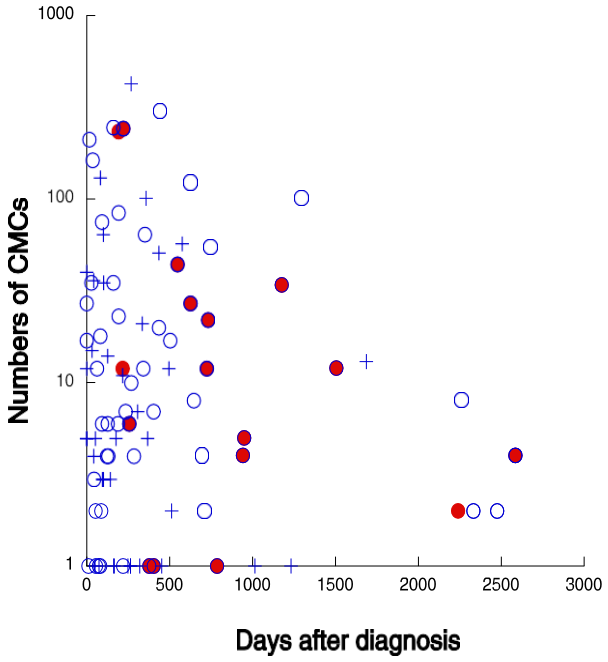

A plot of sample points from patients with at least one occasion of having two or more circulating melanoma cells (CMCs) detected. Plus signs are from those patients who were never diagnosed with metastasis. Samples from patients who didbecome metastatic are indicated by circles, with red circles specifically showing the day in which metastasis was diagnosed.

Figure 27 . A plot of sample points from patients with at least one occasion of having two or more circulating melanoma cells (CMCs) detected.

never exceed a low threshold of 2 CMCs/ml. However, we would caution against using a single determination of CMCs from a patient's blood sample to assess the risk for progression. It is

possible for patients with initially low levels of CMCs to increase their number of CMCs to above the low threshold, below which we did not observe progression. We did observe progression to metastatic disease in a few patients who initially had no detectable CMCs. Therefore, continued repeated assay of blood for CMCs will be required for monitoring patients for early evidence of progression to metastatic disease. Our analysis only used CMC number as a predictor. It may be possible to develop a more highly predictive model that takes into account other factors, such as the trend of CMC numbers over time, and as well by genetic analysis of panels of individual CMCs, which can be captured and isolated by our photoacoustic system. However, the simple criterion of highest observed CMC number, as we used in this present analysis, has clinical utility and the advantage of simplicity. There might be an advantage in testing more blood volume, allowing better stratification of patient risk. This study tested buffy coats from 1 ml of blood. Taking a greater volume, such as 10 ml, is not burdensome to the patient and could yield additional useful CMC data, especially by capture and phenotypic or genetic analysis of panels of individual CMCs. While we did not analyze captured CMCs for this study, as the goal was to correlate CMC number with the onset of metastasis, photoacoustic flow cytometry is capable of capturing CMCs in suspension.

Sensitivity of the Photoacoustic Flow Cytometer

This cell assay is not concentration dependent, unlike many chemical or biochemical assays. As long as there are pigmented cells of sufficient optical absorption in a volume of fluid, there will be a photoacoustic response when the cell passes through the laser beam. So one cell in a microliter will create a photoacoustic signal in our flow cytometer just as one cell in a liter would create such as signal. However, larger volume samples would result in more bubbles created

by the two-phase flow process, increasing the amount of time needed for the assay. As the two-phase flow results in bubbles of approximately 1 µl using the flow and material parameters employed, this volume is the fundamental sampling unit that is relevant to our method. As the beam expands to cover the entire volume of each bubble, it detects a photoacoustic event in every bubble containing a CMC. Of course, pigmentation level of the cellis important, but this study showed that, given the natural pigmentation of CMCs, a predictive model of metastasis can be derived.

It must be noted that another photoacoustic technology,the Cytophone, developed by Vladimir et al. [21] and by Galanzha et al. [22], has achieved success in performing CMC counting *in vivo*. This accomplishment overcomes many challenges not encountered in our *in vitro* method, and potentially allows for testing of the entire blood volume of a patient. This advantage cannot be under- estimated, as much of the uncertainty of current CTC assays, including our own, comes from the limited volumes sampled.

Benefit of Photoacoustic-Mediated Capture

We have used photoacoustic flow cytometry to perform immunocytochemical analysis, as shown in Figure 3, where green fluorescence illuminates MART1 antigens on the captured cell surface. We estimate that cell loss in the staining procedure could have been 20–50%. Further confounding fluorescent detection is the uncertainty of any given CMC expressing MART1. While imaging some fluorescent cells in the capturedsamples from photoacoustic flow cytometry gave some measure of validation that the method was effective in detecting CMCs, a formal study that includes such validation has numerous sources of error that would make it difficult to assess properly. However, this exploratory staining technique indicates that performing other molecular

assays on captured cells is possible and could potentially be used for design of therapy, such as in testing for BRAF mutations [23,24].

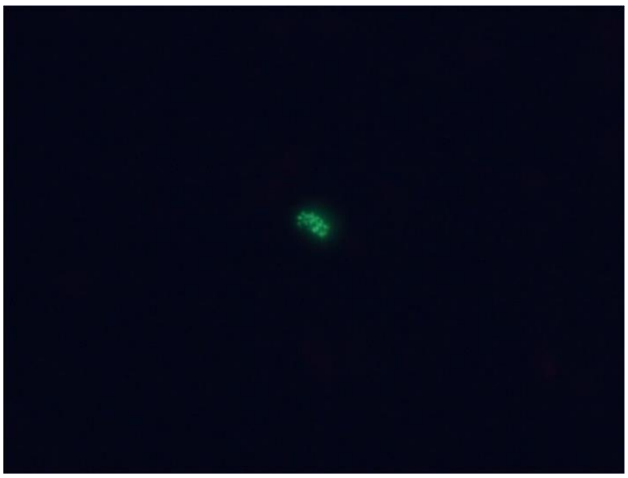

Figure 28 Green fluorescence indicates the presence of MART1 surface markers on a captured circulating melanoma cells from a Stage III melanoma patient.

CMC Numbers and Date of Metastasis

Inspection of Figure 2 shows that most of the non- metastatic cases, indicated by plus signs, occur early in the data set, mostly prior to about 500 days. While there are many points from the metastatic group prior to 500 days, there are many points later. More notable is that the majority of the samples where metastasis is detected occur after 500 days. This observation indicates that the nonmetastatic group might have developed metastasis if this group had been followed longer. There- fore, the threshold measurement of detecting more than two CMCs in any blood sample is a strong indicator of riskof metastasis.

Further indication that the two groups, metastatic and nonmetastatic, are actually in the same population is that the Mahalanobis distance is small. As this distance is not Euclidean, but accounts for the covariance in both dimensions, the values of 0.107 and 0.216 strongly indicate that both groups belong to the same, composite population.

Nonpigmented Melanoma

Photoacoustic flow cytometry generates acoustic waves in melanoma cells due to the content of melanin pigment, which absorbs and transduces optical energy from laser pulses. However, some melanoma cells are nonpigmented or partially pigmented. Most melanomas are highly pigmented, with estimates of amelanotic melanoma being less than 5% [25] or 1.8–8.1%, though this latter figure includes partially pigmented melanoma [26]. We have developed means to enhance melanoma cell detection and induce nonpigmented cancer cells using antibody-labeled, exogenous optical absorbers, such as functionalized dyed microspheres [27,28]. Some researchers have found that undifferentiated and, hence, nonpigmented melanomas are responsible for disease with more metastatic potential. Muller et al. [29] stated that microphthalmia- associated transcription factor (MITF), which is responsible for pigmentation, is relevant to prediction of meta- static potential. Specifically, MITF is known to block proliferation, so lack of MITF may result in nonpigmented CMCs that are more likely to lead to metastasis. However, while relying on pigmentation for photoacoustic signals, our results still provide valuable predictive value in a data set that was not selected beforehand for pigmentation. That is, in a population of patients, regardless of MITF expression, photoacoustic enumeration of CMCs still provides statistically significant classification of patients into metastatic and nonmetastatic groups.

Future Work

Although we have restricted this model of disease progression to the simple, but straightforward, enumeration of the maximum number of CMCs in serial samples, we are planning a prospective study of melanoma patients to include other factors to incorporate a multivariate model for metastasis prediction. We will develop a survival model that uses CMC detection to provide estimates of model parameters that can be used to predict time to metastasis in early-stage melanoma patients. The time to metastasis will be modeled as

$$h(t) = h_0(t)e^{(\beta X_{i,j} + \alpha Z_i)}$$

Where $h(t)$ denotes a baseline function, ß models the correlation of CMC number to time to metastasis, α denotes prior information about the patient, potentially including tumor burden or relevant blood chemistry levels. Z_i is the disease stage of the patient. $X_{i,j}$ is a function derived from a longitudinal model that forms the basis for this model. Estimation of these parameters will yield the relationship of CMC numbers to advancement to metastatic disease and will provide a more sophisticated model for clinical prediction. Prior information about the patient may include sex, age, and treatment regimen. This study will be based on serial data from approximately 100 early-stage melanoma patients.

Furthermore, we have been investigating methods to improve classification of signals and hence, improving the predictive value of photoacoustic flow cytometry. In other work with photoacoustic signals, we used Bayesian methods to classify vascular and pigmented lesions in the skin [30]. We are developing unsupervised learning using convolutional and dense neural networks for feature extraction. This area of investigation offers rich developments in our ability to detect CTCs, but testing and validating the many possible cases is an ongoing process. In this study, however, we

wereable to extract notable inferences using the simple thresholdclassification explained in Materials and Methods

CONCLUSIONS

Photoacoustic flow cytometry was demonstrated to detectand quantify rare CMCs in blood samples of Stage I-III melanoma patients. In our data set, derived from serial blooddraws from 38 Stage I–III melanoma patients, detection of 2or fewer CMCs/ml of blood, on all occasions tested in an individual patient, was never associated with progression to metastatic disease. In contrast, detection of greater than 2 CMCs/ml, on even a single occasion, was statistically significantly associated with eventual progression to metastaticdisease, though not all patients with greater than 2 CMCs had documented progression to metastatic disease over their varying duration individual follow-up periods. In addition, detection of CMCs at higher threshold levels, especially above 100 CMCs/ml, was associated with even higher rates of progression to metastatic disease. In summary, our resultssupport that photoacoustic detection of CMCs in Stage I–IIImelanoma patients is useful for monitoring for early evidence of development of metastatic disease, which potentially may enable earlier and more effective therapeutic intervention.

ACKNOWLEDGMENTS

Research reported in this publication was supported by National Cancer Institute of the National Institutes of Health under award number 1R01CA161367-01 and the Pennsylvania Department of Health CURE grant.

Bibliography

1. Perry, J.D., A Decade of Development of Chromogenic Culture Media for Clinical Microbiology in an Era of Molecular Diagnostics. Clinical Microbiology Reviews, 2017. **30**(2): p. 449-479.

2. Diekema, D.J., et al., Antimicrobial resistance trends and outbreak frequency in United States hospitals. Clinical infectious diseases, 2004. **38**(1): p. 78-85.

3. Kuehnert, M.J., et al., Methicillin-resistant–Staphylococcus aureus hospitalizations, United States. Emerging infectious diseases, 2005. **11**(6): p. 468.

4. Salque, M., et al., Earliest evidence for cheese making in the sixth millennium bc in northern Europe. Nature, 2013. **493**(7433): p. 522-525.

5. Coico, R., Gram Staining. Current Protocols in Microbiology, 2006. **00**(1): p. A.3C.1-A.3C.2.

6. Orenga, S., et al., Enzymatic substrates in microbiology. Journal of Microbiological Methods, 2009. **79**(2): p. 139-155.

7. Tran, A., et al., Cost Savings Realized by Implementation of Routine Microbiological Identification by Matrix-Assisted Laser Desorption Ionization–Time of Flight Mass Spectrometry. Journal of Clinical Microbiology, 2015. **53**(8): p. 2473-2479.

8. Chen, Y., et al., Rapid Identification of Bacteria Directly from Positive Blood Cultures by Use of a Serum Separator Tube, Smudge Plate Preparation, and Matrix-Assisted Laser Desorption Ionization–Time of Flight Mass Spectrometry. Journal of Clinical Microbiology, 2015. **53**(10): p. 3349-3352.

9. Hou, T.-Y., C. Chiang-Ni, and S.-H. Teng, Current status of MALDI-TOF mass spectrometry in clinical microbiology. Journal of Food and Drug Analysis, 2019. **27**(2): p. 404-414.

10. Kempf, V.A., K. Trebesius, and I.B. Autenrieth, Fluorescent In situ hybridization allows rapid identification of microorganisms in blood cultures. Journal of clinical microbiology, 2000. **38**(2): p. 830-838.

11. King, R.L., et al., False-negative rates for MYC fluorescence in situ hybridization probes in B-cell neoplasms. Haematologica, 2019. **104**(6): p. e248-e251.

12. Blaschke, A.J., et al., Rapid identification of pathogens from positive blood cultures by multiplex polymerase chain reaction using the FilmArray system. Diagnostic microbiology and infectious disease, 2012. **74**(4): p. 349-355.

13. Kostić, T., et al., Thirty-minute screening of antibiotic resistance genes in bacterial isolates with minimal sample preparation in static self-dispensing 64 and 384 assay cards. Applied Microbiology and Biotechnology, 2015. **99**(18): p. 7711-7722.

14. Váradi, L., et al., Methods for the detection and identification of pathogenic bacteria: past, present, and future. Chemical Society Reviews, 2017. **46**(16): p. 4818-4832.

15. Al-Soud, W.A. and P. Rådström, Purification and Characterization of PCR-Inhibitory Components in Blood Cells. Journal of Clinical Microbiology, 2001. **39**(2): p. 485-493.

16. Espy, M.J., et al., Real-Time PCR in Clinical Microbiology: Applications for Routine Laboratory Testing. Clinical Microbiology Reviews, 2006. **19**(1): p. 165-256.

17. Sullivan, K.V. and J. Dien Bard, New and novel rapid diagnostics that are impacting infection prevention and antimicrobial stewardship. Current Opinion in Infectious Diseases, 2019. **32**(4): p. 356-364.

18. Pancholi, P., et al., Multicenter Evaluation of the Accelerate PhenoTest BC Kit for Rapid Identification and Phenotypic Antimicrobial Susceptibility Testing Using Morphokinetic Cellular Analysis. Journal of clinical microbiology, 2018. **56**(4): p. e01329-17.

19. Manning, B., et al., Automated Detection of Candida auris Direct from Whole Blood by T2MR. Open Forum Infectious Diseases, 2017. **4**(Suppl 1): p. S609-S610.

20. Giuliano, C., C.R. Patel, and P.B. Kale-Pradhan, A Guide to Bacterial Culture Identification And Results Interpretation. P & T : a peer-reviewed journal for formulary management, 2019. **44**(4): p. 192-200.

21. Mahony, J.B., et al., Cost Analysis of Multiplex PCR Testing for Diagnosing Respiratory Virus Infections. Journal of Clinical Microbiology, 2009. **47**(9): p. 2812-2817.

22. Tang, M., et al., Diagnostic Accuracy of MALDI-TOF Mass Spectrometry for the Direct Identification of Clinical Pathogens from Urine. Open medicine (Warsaw, Poland), 2020. **15**: p. 266-273.

23. Harris, D.M. and D.J. Hata, Rapid identification of bacteria and Candida using PNA-FISH from blood and peritoneal fluid cultures: a retrospective clinical study. Ann Clin Microbiol Antimicrob, 2013. **12**: p. 2.

24. Järvinen, A.-K., et al., Rapid identification of bacterial pathogens using a PCR- and microarray-based assay. BMC Microbiology, 2009. **9**: p. 161-161.

25. Sabat, A.J., et al., Targeted next-generation sequencing of the 16S-23S rRNA region for culture-independent bacterial identification - increased discrimination of closely related species. Scientific Reports, 2017. **7**(1): p. 3434.

26. Drevinek, P., et al., Direct detection of ESKAPEc pathogens from whole blood using the T2Bacteria Panel allows early antimicrobial stewardship intervention in patients with sepsis. MicrobiologyOpen, 2021. **10**(3): p. e1210.

27. Bassetti, M., et al., New antibiotics for bad bugs: where are we? Annals of clinical microbiology and antimicrobials, 2013. **12**: p. 22-22.

28. World Health, O., The evolving threat of antimicrobial resistance : options for action. 2012, World Health Organization: Geneva.

29. Edwards, R.A. and F. Rohwer, Viral metagenomics. Nat Rev Micro, 2005. **3**(6): p. 504-510.

30. Angly, F.E., et al., The Marine Viromes of Four Oceanic Regions. PLoS Biol, 2006. **4**(11): p. e368.

31. Sullivan, M.B., et al., Three <italic>Prochlorococcus</italic> Cyanophage Genomes: Signature Features and Ecological Interpretations. PLoS Biol, 2005. **3**(5): p. e144.

32. Šimoliūnas, E., et al., <italic>Klebsiella</italic> Phage vB_KleM-RaK2 — A Giant Singleton Virus of the Family <italic>Myoviridae</italic>. PLoS ONE, 2013. **8**(4): p. e60717.

33. Secor, P.R. and A.A. Dandekar, More than Simple Parasites: the Sociobiology of Bacteriophages and Their Bacterial Hosts. mBio, 2020. **11**(2): p. e00041-20.

34. Barr, J.J., et al., Bacteriophage adhering to mucus provide a non–host-derived immunity. Proceedings of the National Academy of Sciences, 2013. **110**(26): p. 10771-10776.

35. Van Belleghem, J.D., et al., Interactions between Bacteriophage, Bacteria, and the Mammalian Immune System. Viruses, 2018. **11**(1): p. 10.

36. Krut, O. and I. Bekeredjian-Ding, Contribution of the Immune Response to Phage Therapy. The Journal of Immunology, 2018. **200**(9): p. 3037-3044.

37. Lengeling, A., A. Mahajan, and D.L. Gally, Bacteriophages as Pathogens and Immune Modulators? mBio, 2013. **4**(6): p. e00868-13.

38. Barr, J.J., et al., Bacteriophage adhering to mucus provide a non-host-derived immunity. Proceedings of the National Academy of Sciences of the United States of America, 2013. **110**(26): p. 10771-10776.

39. Barr, J.J., M. Youle, and F. Rohwer, Innate and acquired bacteriophage-mediated immunity. Bacteriophage, 2013. **3**(3): p. e25857-e25857.

40. Scott, A.E., et al., Bacteriophage influence Campylobacter jejuni types populating broiler chickens. Environmental Microbiology, 2007. **9**(9): p. 2341-2353.

41. Cenens, W., et al., Expression of a Novel P22 ORFan Gene Reveals the Phage Carrier State in <italic>Salmonella</italic> Typhimurium. PLoS Genet, 2013. **9**(2): p. e1003269.

42. Nanda, A.M., K. Thormann, and J. Frunzke, Impact of Spontaneous Prophage Induction on the Fitness of Bacterial Populations and Host-Microbe Interactions. Journal of Bacteriology, 2015. **197**(3): p. 410-419.

43. Dedrick, R.M., et al., Prophage-mediated defence against viral attack and viral counter-defence. Nature microbiology, 2017. **2**: p. 16251-16251.

44. Gentile, G.M., et al., More Evidence of Collusion: a New Prophage-Mediated Viral Defense System Encoded by Mycobacteriophage Sbash. mBio, 2019. **10**(2): p. e00196-19.

45. Montgomery, M.T., et al., Yet More Evidence of Collusion: a New Viral Defense System Encoded by Gordonia Phage CarolAnn. mBio, 2019. **10**(2): p. e02417-18.

46. Mavrich, T.N. and G.F. Hatfull, Bacteriophage evolution differs by host, lifestyle and genome. Nature microbiology, 2017. **2**: p. 17112-17112.

47. Thingstad, T., Elements of a theory for the mechanisms controlling abundance, diversity, and biogeochemical role of lytic bacterial viruses in aquatic systems. Limnology and Oceanography [Limnol. Oceanogr.], 2000. **45**(6): p. 8.

48. Weigele, P.R., et al., Genomic and structural analysis of Syn9, a cyanophage infecting marine Prochlorococcus and Synechococcus. Environmental Microbiology, 2007. **9**(7): p. 1675-1695.

49. Wilhelm, S.W. and C.A. Suttle, Viruses as regulators of nutrient cycles in aquatic environments. 2000.

50. Cenens, W., et al., Phage–host interactions during pseudolysogeny: Lessons from the Pid/<italic>dgo</italic> interaction. Bacteriophage, 2013. **3**(1): p. e25029.

51. Lawrence, J.G. and H. Hendrickson, Lateral gene transfer: when will adolescence end? Molecular Microbiology, 2003. **50**(3): p. 739-749.

52. Suttle, C.A., Marine viruses — major players in the global ecosystem. Nature Reviews Microbiology, 2007. **5**(10): p. 801-812.

53. Fillol-Salom, A., et al., Bacteriophages benefit from generalized transduction. PLoS pathogens, 2019. **15**(7): p. e1007888-e1007888.

54. Hendrix, R.W., et al., Evolutionary relationships among diverse bacteriophages and prophages: All the world's a phage. Proceedings of the National Academy of Sciences, 1999. **96**(5): p. 2192-2197.

55. Matilla, M.A., X. Fang, and G.P.C. Salmond, Viunalikeviruses are environmentally common agents of horizontal gene transfer in pathogens and biocontrol bacteria. The ISME Journal, 2014. **8**(10): p. 2143-2147.

56. Edgar, R.H. and University of Pittsburgh, EVOLUTION OF BACTERIOPHAGE HOST ATTACHMENT USING DET7 AS A MODEL. 2014. p. 1 online resource (58 pages).

57. Casjens, S.R. and P.A. Thuman-Commike, Evolution of mosaically related tailed bacteriophage genomes seen through the lens of phage P22 virion assembly. Virology, 2011. **411**(2): p. 393-415.

58. Petty, N.K., et al., A generalized transducing phage for the murine pathogen Citrobacter rodentium. Microbiology, 2007. **153**(9): p. 2984-2988.

59. Flores, C.O., et al., Statistical structure of host–phage interactions. Proceedings of the National Academy of Sciences, 2011.

60. Salmond, G.P.C. and P.C. Fineran, A century of the phage: past, present and future. Nature Reviews Microbiology, 2015. **13**(12): p. 777-786.

61. Strauss, B.S., A Physicist's Quest in Biology: Max Delbrück and "Complementarity". Genetics, 2017. **206**(2): p. 641-650.

62. Nelson, D., Phage Taxonomy: We Agree To Disagree. Journal of Bacteriology, 2004. **186**(21): p. 7029-7031.

63. Adriaenssens, E. and J.R. Brister, How to Name and Classify Your Phage: An Informal Guide. Viruses, 2017. **9**(4): p. 70.

64. Cabilly, S., The basic structure of filamentous phage and its use in the display of combinatorial peptide libraries. Molecular Biotechnology, 1999. **12**(2): p. 143-148.

65. Filamentous Bacteriophages: Biology and Applications, in eLS.

66. Crick, F.H.C., L. Barnett, S. Brenner, and Watts-Tobin, General Nature of the genetic Code for Proteins. Nature. Nature, 1961. **192**: p. 1227-1232.

67. Johnson, J.E. and J.A. Speir, Quasi-equivalent viruses: a paradigm for protein assemblies. Journal of Molecular Biology, 1997. **269**(5): p. 665-675.

68. Caspar, D.L.K., A, Physical Principles in the construction of regular viruses. Cold Spring Harbor Symp. Quant. Biol, 1962. **27**: p. 1-24.

69. Pauling, L., Aggregation of globular proteins. Disc. Farad. Soc, 1953. **15**: p. 49-53.

70. Mannige, R.V. and C.L. Brooks, Geometric considerations in virus capsid size specificity, auxiliary requirements, and buckling. Proceedings of the National Academy of Sciences, 2009. **106**(21): p. 8531-8536.

71. Caspar, D.L.D. and A. Klug, Physical Principles in the Construction of Regular Viruses. Cold Spring Harbor Symposia on Quantitative Biology, 1962. **27**: p. 1-24.

72. Twarock, R., Mathematical virology: a novel approach to the structure and assembly of viruses. Philosophical Transactions of the Royal Society A: Mathematical, Physical and Engineering Sciences, 2006. **364**(1849): p. 3357-3373.

73. Alam, T.I., et al., The headful packaging nuclease of bacteriophage T4. Molecular Microbiology, 2008. **69**(5): p. 1180-1190.

74. Lane, T. and F. Eiserling, Genetic control of capsid length in bacteriophage T4. VII. A model of length regulation based on DNA size. J Struct Biol, 1990. **104**(1-3): p. 9-23.

75. Becker, A., et al., Bacteriophage lambda DNA packaging: The product of the FI gene promotes the incorporation of the prohead to the DNA-terminase complex. Journal of Molecular Biology, 1988. **199**(4): p. 597-607.

76. Hendrix, S.C.a.R., Control Mechanism in dsDNA Bacteriophage Assembly, in The Bacteriophages, R. Calendar, Editor. 1988, Plenum Press: Berkeley.

77. Shore, D., et al., Determination of capsid size by satellite bacteriophage P4. Proceedings of the National Academy of Sciences of the United States of America, 1978. **75**(1): p. 400-404.

78. Wang, S., J.R. Chang, and T. Dokland, Assembly of bacteriophage P2 and P4 procapsids with internal scaffolding protein. Virology, 2006. **348**(1): p. 133-140.

79. Sifang Wang [1], J.R.C., Terje Dokland, Assembly of bacteriophage P2 and P4 procapsids with internal

scaffolding protein. Virology, 2005. **348**: p. 133–140.

80. Walker, D.H., Jr. and T.F. Anderson, Morphological Variants of Coliphage P1. J. Virol., 1970. **5**(6): p. 765-782.

81. Choi, K.H., et al., Determinants of Bacteriophage [phi]29 Head Morphology. Structure, 2006. **14**(11): p. 1723-1727.

82. Sullivan, W., Scientists Examine Tiny Viruses For Messages From Outer Space, in New York Times. 1979: New York City.

83. Cherwa, J. and B. Fane, Microviridae: Microviruses and Gokushoviruses. 2011.

84. G. Effantin1, P.B., E. Neumann1, L. Letellier2 and and J. F. Conway1, Bacteriophage T5 Structure Reveals Similarities with

HK97 and T4 Suggesting Evolutionary Relationships. Journal of Molecular Biology, 2006. **361**: p. 993–1002.

85. Abrescia, N.G.A., et al., Insights into assembly from structural analysis of bacteriophage PRD1. Nature, 2004. **432**(7013): p. 68-74.

86. Hofer, U., The sting is in the phage's tail. Nature Reviews Microbiology, 2016. **14**(8): p. 477-477.

87. Tavares, P., The Bacteriophage Head-to-Tail Interface, in Virus Protein and Nucleoprotein Complexes, J.R. Harris and D. Bhella, Editors. 2018, Springer Singapore: Singapore. p. 305-328.

88. Simpson, A.A., et al., Structure of the bacteriophage φ29 DNA packaging motor. Nature, 2000. **408**(6813): p. 745-750.

89. Lebedev, A.A., et al., Structural framework for DNA translocation via the viral portal protein. The EMBO journal, 2007. **26**(7): p. 1984-1994.

90. Feiss, M. and V.B. Rao, The Bacteriophage DNA Packaging Machine, in Viral Molecular Machines, M.G. Rossmann and V.B. Rao, Editors. 2012, Springer US: Boston, MA. p. 489-509.

91. Lin, S., et al., Altering the speed of a DNA packaging motor from bacteriophage T4. Nucleic acids research, 2017. **45**(19): p. 11437-11448.

92. Hegde, S., et al., Portal-Large Terminase Interactions of the Bacteriophage T4 DNA Packaging Machine Implicate a Molecular Lever Mechanism for Coupling ATPase to DNA Translocation. Journal of Virology, 2012. **86**(8): p. 4046-4057.

93. van Ooij, C., Uncorking the phage capsid. Nature Reviews Microbiology, 2009. **7**(7): p. 481-481.

94. Sun, S., et al., Structure and function of the small terminase component of the DNA packaging machine in T4-like bacteriophages. Proceedings of the National Academy of Sciences, 2012. **109**(3): p. 817-822.

95. Kondabagil, K.R. and V.B. Rao, A critical coiled coil motif in the small terminase, gp16, from bacteriophage T4: insights into DNA packaging initiation and assembly of packaging motor. Journal of molecular biology, 2006. **358**(1): p. 67-82.

96. Cuervo, A., et al., Structural characterization of the bacteriophage T7 tail machinery. The Journal of biological chemistry, 2013. **288**(36): p. 26290-26299.

97. Sciara, G., et al., Structure of lactococcal phage p2 baseplate and its mechanism of activation. Proceedings of the National Academy of Sciences of the United States of America, 2010. **107**(15): p. 6852-6857.

98. Belcaid, M., A. Bergeron, and G. Poisson, The evolution of the tape measure protein: units, duplications and losses. BMC Bioinformatics, 2011. **12**(9): p. S10.

99. Casjens, S.R. and R.W. Hendrix, Bacteriophage lambda: Early pioneer and still relevant. Virology, 2015. **479-480**: p. 310-330.

100. Pell, L.G., et al., The X-Ray Crystal Structure of the Phage λ Tail Terminator Protein Reveals the Biologically Relevant Hexameric Ring Structure and Demonstrates a Conserved Mechanism of Tail Termination among Diverse Long-Tailed Phages. Journal of Molecular Biology, 2009. **389**(5): p. 938-951.

101. Leiman, P.G., et al., Morphogenesis of the T4 tail and tail fibers. Virology Journal, 2010. **7**(1): p. 355.

102. Thompson, J.E., et al., The K5 Lyase KflA Combines a Viral Tail Spike Structure with a Bacterial Polysaccharide Lyase Mechanism. Journal of Biological Chemistry, 2010. **285**(31): p. 23963-23969.

103. Seckler, R., Folding and Function of Repetitive Structure in the Homotrimeric Phage P22 Tailspike Protein. Journal of Structural Biology, 1998. **122**(1-2): p. 216-222.

104. Andres, D., et al., An essential serotype recognition pocket on phage P22 tailspike protein forces Salmonella enterica serovar Paratyphi A O-antigen fragments to bind as nonsolution conformers. Glycobiology, 2013. **23**(4): p. 486-494.

105. Andres, D., et al., Tail morphology controls DNA release in two Salmonella phages with one lipopolysaccharide receptor recognition system. Molecular Microbiology, 2012. **83**(6): p. 1244-1253.

106. Baxa, U., et al., Interactions of phage P22 tails with their cellular receptor, Salmonella O-antigen polysaccharide. Biophysical Journal, 1996. **71**(4): p. 2040-2048.

107. Andres, D., et al., Carbohydrate binding of Salmonella phage P22 tailspike protein and its role during host cell infection. Biochem Soc Trans, 2010. **38**(5): p. 1386-1389.

108. Miller, S., B. Schuler, and R. Seckler, Phage P22 tailspike protein: removal of head-binding domain unmasks effects of folding mutations on native-state thermal stability. Protein Sci, 1998. **7**(10): p. 2223-32.

109. Inamdar, M.M., W.M. Gelbart, and R. Phillips, Dynamics of DNA Ejection from Bacteriophage. Biophysical Journal, 2006. **91**(2): p. 411-420.

110. Xu, J. and Y. Xiang, Membrane Penetration by Bacterial Viruses. Journal of Virology, 2017. **91**(13): p. e00162-17.

111. Maghsoodi, A., et al., How the phage T4 injection machinery works including energetics, forces, and dynamic pathway. Proceedings of the National Academy of Sciences, 2019. **116**(50): p. 25097-25105.

112. Roos, W.H., et al., Viral capsids: Mechanical characteristics, genome packaging and delivery mechanisms. Cellular and Molecular Life Sciences, 2007. **64**(12): p. 1484.

113. Twort, F.W., An investigation on the nature of ultra-microscopic viruses. The Lancet, 1915. **186**(4814): p. 1241-1243.

114. d'Herelle, M., Sur un microbe invisible antagoniste des bacilles dysentériques. Acta Kravsi, 1961.

115. Wilkinson, L., Félix d'Herelle and the origins of molecular biology. Medical History, 2001. **45**(2): p. 294-295.

116. Summers, W.C., The strange history of phage therapy. Bacteriophage, 2012. **2**(2): p. 130-133.

117. Ruska, H., Die Sichtbarmachung der bakteriophagen Lyse im Übermikroskop. Naturwissenschaften, 1940. **28**(3): p. 45-46.

118. D'Herelle, F. and G.H. Smith, The bacteriophage and its behavior. 1926, Baltimore, Md. :: The Williams & Wilkins Company.

119. Eaton, M.D. and S. Bayne-Jones, BACTERIOPHAGE THERAPY: REVIEW OF THE PRINCIPLES AND RESULTS OF THE USE OF BACTERIOPHAGE IN THE TREATMENT OF INFECTIONS. Journal of the American Medical Association, 1934. **103**(24): p. 1847-1853.

120. Krueger, A.P. and E.J. Scribner, THE BACTERIOPHAGE: ITS NATURE AND ITS THERAPEUTIC USE. Journal of the American Medical Association, 1941. **116**(19): p. 2160-2167.

121. Morton, H.E. and F.B. Engley, The Protective Action of Dysentery Bacteriophage in Experimental Infections in Mice. Journal of bacteriology, 1945. **49**(3): p. 245-255.

122. Franklin, R.E. and R.G. Gosling, The structure of sodium thymonucleate fibres. I. The influence of water content. Acta Crystallographica, 1953. **6**(8-9): p. 673-677.

123. Sidhu, S.S., Engineering M13 for phage display. Biomol Eng, 2001. **18**(2): p. 57-63.

124. Serwer, P., et al., Enhancing and initiating phage-based therapies. Bacteriophage, 2014. **4**(4): p. e961869-e961869.

125. Strich, J.R. and D.S. Chertow, CRISPR-Cas Biology and Its Application to Infectious Diseases. J Clin Microbiol, 2019. **57**(4).

126. Barrangou, R., et al., CRISPR Provides Acquired Resistance Against Viruses in Prokaryotes. Science, 2007. **315**(5819): p. 1709-1712.

127. Mojica, F.J., et al., Intervening sequences of regularly spaced prokaryotic repeats derive from foreign genetic elements. J Mol Evol, 2005. **60**(2): p. 174-82.

128. Ulitzur, N. and S. Ulitzur, New rapid and simple methods for detection of bacteria and determination of their antibiotic susceptibility by using phage mutants. Applied and environmental microbiology, 2006. **72**(12): p. 7455-7459.

129. Svircev, A., D. Roach, and A. Castle, Framing the Future with Bacteriophages in Agriculture. Viruses, 2018. **10**(5).

130. Adriaenssens, E.M., et al., A suggested new bacteriophage genus: "Viunalikevirus". Archives of virology, 2012. **157**(10): p. 2035-2046.

131. Matilla, M.A. and G.P.C. Salmond, Bacteriophage ϕMAM1, a viunalikevirus, is a broad-host-range, high-efficiency generalized transducer that infects environmental and clinical isolates of the enterobacterial genera Serratia and Kluyvera. Applied and environmental microbiology, 2014. **80**(20): p. 6446-6457.

132. Tam, W., et al., Tail tip proteins related to bacteriophage λ gpL coordinate an iron-sulfur cluster. J Mol Biol, 2013. **425**(14): p. 2450-62.

133. de Vries, G.E., C.K. Raymond, and R.A. Ludwig, Extension of bacteriophage lambda host range: selection, cloning, and characterization of a constitutive lambda receptor gene. Proceedings of the National Academy of Sciences of the United States of America, 1984. **81**(19): p. 6080-6084.

134. Oechslin, F., Resistance Development to Bacteriophages Occurring during Bacteriophage Therapy. Viruses, 2018. **10**(7): p. 351.

135. Yang, Y., et al., Development of a Bacteriophage Cocktail to Constrain the Emergence of Phage-Resistant Pseudomonas aeruginosa. Frontiers in microbiology, 2020. **11**: p. 327-327.

136. Wright, R.C.T., et al., Resistance Evolution against Phage Combinations Depends on the Timing and Order of Exposure. mBio, 2019. **10**(5): p. e01652-19.

137. Clark, J.A., Visual characteristics of inhomogeneous acoustic waves. Journal of Sound and Vibration, 1980. **70**(2): p. 267-273.

138. Boner, P.J., Kepler on the origins of comets: Applying earthly knowledge to celestial events. Nuncius, 2006. **21**(1): p. 31-47.

139. Chandrasekhar, S., Radiative transfer. 2013: Courier Corporation.

140. White, R.M., Generation of Elastic Waves by Transient Surface Heating. Journal of Applied Physics, 1963. **34**(12): p. 3559-3567.

141. Sigrist, M.W. and F.K. Kneubühl, Laser-generated stress waves in liquids. The Journal of the Acoustical Society of America, 1978. **64**(6): p. 1652-1663.

142. Niemi, J., T. Löfqvist, and P. Gren, Investigation of the photoacoustic signal dependence on laser power. Advanced Laser Technologies 2007. Vol. 7022. 2008: SPIE.

143. Bell, C.E. and B.S. Maccabee, Shock Wave Generation in Air and in Water by CO2 TEA Laser Radiation. Applied Optics, 1974. **13**(3): p. 605-609.

144. Paltauf, G., H. Schmidt-Kloiber, and M. Frenz, Photoacoustic waves excited in liquids by fiber-transmitted laser pulses. The Journal of the Acoustical Society of America, 1998. **104**(2): p. 890-897.

145. Hetnarski, R.B., M.R. Eslami, and G. Gladwell, Thermal stresses: advanced theory and applications. Vol. 41. 2009: Springer.

146. Viator, J.A., Characterization of photoacoustic sources in tissue using time domain measurements. 2001.

147. Bolaños, J.G., et al., An optoacoustic point source for acoustic scale model measurements. The Journal of the Acoustical Society of America, 2013. **133**(4): p. EL221-EL227.

148. Mansfeld, F.M., T.P. Davis, and M. Kavallaris, Chapter Two - Nanotechnology in Medical Research, in Micro and Nanotechnology in Vaccine Development, M. Skwarczynski and I. Toth, Editors. 2017, William Andrew Publishing. p. 21-45.

149. Bell, A.G., On the production and reproduction of sound by light. American Journal of Science, 1880. **s3-20**(118): p. 305-324.

150. Tam, A.C., Applications of photoacoustic sensing techniques. Reviews of Modern Physics, 1986. **58**(2): p. 381-431.

151. Fan, Y., et al., Development of a laser photothermoacoustic frequency-swept system for subsurface imaging: Theory and experiment. The Journal of the Acoustical Society of America, 2004. **116**(6): p. 3523-3533.

152. Lashkari, B. and A. Mandelis, Photoacoustic radar imaging signal-to-noise ratio, contrast, and resolution enhancement using nonlinear chirp modulation. Optics Letters, 2010. **35**(10): p. 1623-1625.

153. Treeby, B.E., et al., Automatic sound speed selection in photoacoustic image reconstruction using an autofocus approach. Journal of biomedical optics, 2011. **16**(9): p. 090501.

154. Hoelen, C.G. and F.F. de Mul, Image reconstruction for photoacoustic scanning of tissue structures. Applied Optics, 2000. **39**(31): p. 5872-5883.

155. Farnia, P., et al., High-quality photoacoustic image reconstruction based on deep convolutional neural network: towards intra-operative photoacoustic imaging. Biomedical Physics & Engineering Express, 2020. **6**(4): p. 045019.

156. Bell, M.A.L., et al., Localization of transcranial targets for photoacoustic-guided endonasal surgeries. Photoacoustics, 2015. **3**(2): p. 78-87.

157. Schmid, T., et al., Optical absorbance measurements of opaque liquids by pulsed laser photoacoustic spectroscopy. Analytical chemistry, 2009. **81**(6): p. 2403-2409.

158. Xia, J., J. Yao, and L.V. Wang, Photoacoustic tomography: principles and advances. Electromagnetic waves (Cambridge, Mass.), 2014. **147**: p. 1-22.

159. Song, L., et al., Ultrasound-array-based real-time photoacoustic microscopy of human pulsatile dynamics in vivo. Journal of Biomedical Optics, 2010. **15**(2): p. 021303.

160. Kim, C., et al., Deeply penetrating in vivo photoacoustic imaging using a clinical ultrasound array system. Biomedical optics express, 2010. **1**(1): p. 278-284.

161. Jeon, S., et al., Review on practical photoacoustic microscopy. Photoacoustics, 2019. **15**: p. 100141.

162. Chuangsuwanich, T., et al., Photoacoustic imaging of lamina cribrosa microcapillaries in porcine eyes. Applied optics, 2018. **57**(17): p. 4865-4871.

163. Jiao, S., et al., Simultaneous multimodal imaging with integrated photoacoustic microscopy and optical coherence tomography. Optics letters, 2009. **34**(19): p. 2961-2963.

164. Yang, J.-M., et al., Photoacoustic endoscopy. Optics letters, 2009. **34**(10): p. 1591-1593.

165. Yaseen, M.A., et al., Optoacoustic imaging of the prostate: development toward image-guided biopsy. Journal of biomedical optics, 2010. **15**(2): p. 021310.

166. Yang, J.-M., et al. Volumetric photoacoustic endoscopy of upper gastrointestinal tract: ultrasonic transducer technology development. in Photons Plus Ultrasound: Imaging and Sensing 2011. 2011. International Society for Optics and Photonics.

167. Wang, L. and H. Wu, Biomedical Optics: Principles and Imaging, 10–15 John Wiley & Sons. New Jersey, 2007.

168. Sheinfeld, A., S. Gilead, and A. Eyal, Simultaneous spatial and spectral mapping of flow using photoacoustic Doppler measurement. Journal of biomedical optics, 2010. **15**(6): p. 066010.

169. Yao, J., et al., In vivo photoacoustic imaging of transverse blood flow by using Doppler broadening of bandwidth. Optics letters, 2010. **35**(9): p. 1419-1421.

170. Yao, J., K.I. Maslov, and L.V. Wang. Noninvasive quantification of metabolic rate of oxygen (MRO2) by photoacoustic microscopy. in Photons Plus Ultrasound: Imaging and Sensing 2011. 2011. International Society for Optics and Photonics.

171. Patel, C., E. Burkhardt, and C. Lambert, Spectroscopic measurements of stratospheric nitric oxide and water vapor. Science, 1974. **184**(4142): p. 1173-1176.

172. Palzer, S., Photoacoustic-based gas sensing: A review. Sensors, 2020. **20**(9): p. 2745.

173. Schmitt, K., et al., Compact photoacoustic gas sensor based on broadband IR source. Procedia Engineering, 2011. **25**: p. 1081-1084.

174. Sigrist, M.W., Trace gas monitoring by laser-photoacoustic spectroscopy. Infrared Physics & Technology, 1995. **36**(1): p. 415-425.

175. Rusk, N., The fluorescence microscope. Nature Cell Biology, 2009. **11**(1): p. S8-S9.

176. Lagercrantz, C., Photo-electric counting of individual microscopic plant and animal cells. Nature, 1948. **161**(4079): p. 25-26.

177. Coulter, W.H., Means for counting particles suspended in a fluid. 1953, Google Patents.

178. Givan, A.L., Principles of flow cytometry: an overview. Methods in cell biology, 2001. **63**: p. 19-50.

179. Maciorowski, Z., P.K. Chattopadhyay, and P. Jain, Basic Multicolor Flow Cytometry. Curr Protoc Immunol, 2017. **117**: p. 5.4.1-5.4.38.

180. Crosland-Taylor, P.J., A Device for Counting Small Particles suspended in a Fluid through a Tube. Nature, 1953. **171**(4340): p. 37-38.

181. Cao, R., et al., Expanding the potential of standard flow cytometry by extracting fluorescence lifetimes from cytometric pulse shifts. Cytometry Part A, 2014. **85**(12): p. 999-1010.

182. Galanzha, E.I., et al., In vivo magnetic enrichment and multiplex photoacoustic detection of circulating tumour cells. Nature nanotechnology, 2009. **4**(12): p. 855-860.

183. Morgan, S.P. and I.M. Stockford, Intrumentation for in vivo flow cytometry-a sickle cell anemia case study. Advanced Optical Flow Cytometry, 2011.

184. Tuchin, V.V., A. Tárnok, and V.P. Zharov, Towards in vivo flow cytometry. Journal of biophotonics, 2009. **2**: p. 457.

185. Zharov, V.P., et al., Photothermal nanotherapeutics and nanodiagnostics for selective killing of bacteria targeted with gold nanoparticles. Biophysical journal, 2006. **90**(2): p. 619-627.

186. Tuchin, V.V., Optical clearing of tissues and blood using the immersion method. Journal of Physics D: Applied Physics, 2005. **38**(15): p. 2497.

187. Galanzha, E.I. and V.P. Zharov, Circulating tumor cell detection and capture by photoacoustic flow cytometry in vivo and ex vivo. Cancers, 2013. **5**(4): p. 1691-1738.

188. Galanzha, E.I., et al., In vivo, noninvasive, label-free detection and eradication of circulating metastatic melanoma cells using two-color photoacoustic flow cytometry with a diode laser. Cancer research, 2009. **69**(20): p. 7926-7934.

189. Sarimollaoglu, M., et al., Nonlinear photoacoustic signal amplification from single targets in absorption background. Photoacoustics, 2014. **2**(1): p. 1-11.

190. Viator, J.A., et al., Photoacoustic detection of circulating melanoma cells as a predictor of metastasis in stage III patients. Journal of Clinical Oncology, 2017. **35**(15_suppl): p. e21053-e21053.

191. O'Brien, C.M., et al., Capture of circulating tumor cells using photoacoustic flowmetry and two phase flow. Journal of Biomedical Optics, 2012. **17**(6): p. 0612211-0612219.

192. Edgar, R.H., et al., Capture and Isolation of Circulating Melanoma Cells Using Photoacoustic Flowmetry. Methods in Molecular Biology (Clifton, NJ), 2021. **2265**: p. 203-212.

193. Ventola, C.L., The antibiotic resistance crisis: part 1: causes and threats. P & T : a peer-reviewed journal for formulary management, 2015. **40**(4): p. 277-283.

194. Bearson, B.L. and B.W. Brunelle, Fluoroquinolone induction of phage-mediated gene transfer in multidrug-resistant Salmonella. International Journal of Antimicrobial Agents, 2015. **46**(2): p. 201-204.

195. Mancini, N., et al., The Era of Molecular and Other Non-Culture-Based Methods in Diagnosis of Sepsis. Clinical Microbiology Reviews, 2010. **23**(1): p. 235-251.

196. Kollef, M.H., Broad-Spectrum Antimicrobials and the Treatment of Serious Bacterial Infections: Getting It Right Up Front. Clinical Infectious Diseases, 2008. **47**(Supplement_1): p. S3-S13.

197. Guo, X.-G. and Q.-F. Liu, Gram Stain and Molecular Method for the Diagnosis of Bacterial Pneumonia. Chinese Medical Journal, 2016. **129**(15): p. 1884-1884.

198. Won, H., et al., Rapid Identification of Bacterial Pathogens in Positive Blood Culture Bottles by Use of a Broad-Based PCR Assay Coupled with High-Resolution Melt Analysis. Journal of Clinical Microbiology, 2010. **48**(9): p. 3410-3413.

199. Chang, Y.-T., et al., Rapid Identification of Bacteria and Candida Pathogens in Peritoneal Dialysis Effluent from Patients with Peritoneal Dialysis-Related Peritonitis by Use of Multilocus PCR Coupled with Electrospray Ionization Mass Spectrometry. Journal of Clinical Microbiology, 2014. **52**(4): p. 1217-1219.

200. Murai, K., et al., Cost-effectiveness of diagnostic strategies using quantitative real-time PCR and bacterial culture to identify contagious mastitis cases in large dairy herds. Preventive Veterinary Medicine, 2014. **113**(4): p. 522-535.

201. Porreca Kratz, A.M., K.V. Sullivan, and J.C. Gallagher, Clinical impact of matrix-assisted laser desorption ionization time-of-flight mass spectrometry for the management of inpatient pneumonia without additional antimicrobial stewardship support. Infect Control Hosp Epidemiol, 2019. **40**(9): p. 1053-1055.

202. Edgar, R., et al., Bacteriophage-mediated identification of bacteria using photoacoustic flow cytometry. Journal of Biomedical Optics, 2019. **24**(11): p. 115003.

203. Singer, M., et al., The third international consensus definitions for sepsis and septic shock (sepsis-3). JAMA, 2016. **315**(8): p. 801-810.

204. Millenbaugh, N.J., et al., Photothermal killing of Staphylococcus aureus using antibody-targeted gold nanoparticles. International journal of nanomedicine, 2015. **10**: p. 1953.

205. Galanzha, E.I., et al., In vivo magnetic enrichment, photoacoustic diagnosis, and photothermal purging of infected blood using multifunctional gold and magnetic nanoparticles. 2012.

206. Nima, Z.A., et al., Bioinspired magnetic nanoparticles as multimodal photoacoustic, photothermal and photomechanical contrast agents. Scientific reports, 2019. **9**(1): p. 1-12.

207. Cai, Q., et al., Chemotaxis-instructed intracellular Staphylococcus aureus infection detection by a targeting and self-assembly signal-enhanced photoacoustic probe. Nano letters, 2018. **18**(10): p. 6229-6236.

208. Schmidt, A., et al., Bacteriophage tailspike protein based assay to monitor phase variable glucosylations in Salmonella O-antigens. BMC Microbiology, 2016. **16**(1): p. 207.

209. Bartual, S.G., et al., Structure of the bacteriophage T4 long tail fiber receptor-binding tip. Proceedings of the National Academy of Sciences, 2010. **107**(47): p. 20287-20292.

210. Thomas, G.J., et al., Conformational stability of P22 tailspike proteins carrying temperature-sensitive folding mutations. Biochemistry, 1990. **29**(17): p. 4181-4187.

211. Bonilla, N., et al., Phage on tap–a quick and efficient protocol for the preparation of bacteriophage laboratory stocks. PeerJ, 2016. **4**: p. e2261.

212. Hodyra-Stefaniak, K., et al., Mammalian Host-Versus-Phage immune response determines phage fate in vivo. Scientific Reports, 2015. **5**: p. 14802.

213. Shao, Y. and I.-N. Wang, Bacteriophage Adsorption Rate and Optimal Lysis Time. Genetics, 2008. **180**(1): p. 471-482.

214. Chatterjee, A.N., Use of Bacteriophage-resistant Mutants to Study the Nature of the Bacteriophage Receptor Site of Staphylococcus aureus. Journal of Bacteriology, 1969. **98**(2): p. 519-527.

215. Casjens, S.R., et al., Genome Sequence of Salmonella enterica Phage Det7. Genome Announcements, 2015. **3**(3): p. e00279-15.

216. Meysman, P., et al., Expression divergence between Escherichia coli and Salmonella enterica serovar Typhimurium reflects their lifestyles. Molecular biology and evolution, 2013. **30**(6): p. 1302-1314.

217. Manohar, S. and D. Razansky, Photoacoustics: a historical review. Advances in Optics and Photonics, 2016. **8**(4): p. 586-617.

218. Paltauf, G., H. Schmidt-Kloiber, and H. Guss, Light distribution measurements in absorbing materials by optical detection of laser-induced stress waves. Applied Physics Letters, 1996. **69**(11): p. 1526-1528.

219. Kruger, R.A., Photoacoustic ultrasound. Medical Physics, 1994. **21**(1): p. 127-131.

220. Weight, R.M., et al., Photoacoustic detection of metastatic melanoma cells in the human circulatory system. Optics Letters, 2006. **31**(20): p. 2998-3000.

221. Gutierrez-Juarez, G., et al., Detection of melanoma cells in vitro using an optical detector of photoacoustic waves. Lasers in Surgery and Medicine, 2010. **42**(3): p. 274-281.

222. Castro-Mejía, J.L., et al., Optimizing protocols for extraction of bacteriophages prior to metagenomic analyses of phage communities in the human gut. Microbiome, 2015. **3**: p. 64.

223. Yamamoto, K.R., et al., Rapid bacteriophage sedimentation in the presence of polyethylene glycol and its application to large-scale virus purification. Virology, 1970. **40**(3): p. 734-744.

224. Mirande, M., M. Lazard, and J.-P. Waller, Small-scale purification of bacteriophage λ DNA by an airfuge centrifugation step in cesium chloride gradients. Gene Analysis Techniques, 1988. **5**(4): p. 80-82.

225. Goldwasser, E. and F.W. Putnam, Physicochemical Properties of Baeteriophages. III. Diffusion of Bacteriophage T6. Journal of Biological Chemistry, 1951. **190**(1): p. 75-81.

226. Chase, G.R. and D.G. Hoel, Serial dilutions: error effects and optimal designs. Biometrika, 1975. **62**(2): p. 329-334.

227. Rostova, E., et al., Kinetics of Antibody Binding to Membranes of Living Bacteria Measured by a Photonic Crystal-Based Biosensor. Biosensors, 2016. **6**(4): p. 52.

228. Butela, K. and J. Lawrence, Population genetics of Salmonella: selection for antigenic diversity. Bacterial population genetics in infectious disease, 2010: p. 287-319.

229. Orndorff, P.E., Use of bacteriophage to target bacterial surface structures required for virulence: a systematic search for antibiotic alternatives. Current genetics, 2016. **62**(4): p. 753-757.

230. Labrie, S.J., J.E. Samson, and S. Moineau, Bacteriophage resistance mechanisms. Nature Reviews Microbiology, 2010. **8**: p. 317.

231. Kreisberg, J.F., et al., The interdigitated beta-helix domain of the P22 tailspike protein acts as a molecular clamp in trimer stabilization. Protein science : a publication of the Protein Society, 2002. **11**(4): p. 820-830.

232. Production, M.A., A Report of the Committee on Methods of Producing Monoclonal Antibodies. Institute for Laboratory Animal Research, National Research Council, 1999: p. 1-57.

233. Hubbs, N.B., M.M. Whisby-Pitts, and J.L. McMurry, Kinetic Analysis of Bacteriophage Sf6 Binding to Outer Membrane Protein A Using Whole Virions. bioRxiv, 2019: p. 509141.

234. Landry, J., et al., Measuring affinity constants of 1450 monoclonal antibodies to peptide targets with a microarray-based label-free assay platform. Journal of immunological methods, 2015. **417**: p. 86-96.

235. Edgar, R.H., et al., Predicting Metastasis in Melanoma by Enumerating Circulating Tumor Cells Using Photoacoustic Flow Cytometry. Lasers Surg Med, 2020.

236. TF, A. and M. NA. On the structure and osmotic properties of phage particles. in Annales de L'institut Pasteur. 1953.

237. Wang, H., et al., Early detection and classification of live bacteria using time-lapse coherent imaging and deep learning. Light: Science & Applications, 2020. **9**(1): p. 118.

238. Hussain, M.A. and C.O. Dawson, Economic Impact of Food Safety Outbreaks on Food Businesses. Foods (Basel, Switzerland), 2013. **2**(4): p. 585-589.

239. Kadri, S.S., Key Takeaways From the U.S. CDC's 2019 Antibiotic Resistance Threats Report for Frontline Providers. Critical care medicine, 2020. **48**(7): p. 939-945.

240. Anany, H., et al., Print to detect: a rapid and ultrasensitive phage-based dipstick assay for foodborne pathogens. Analytical and Bioanalytical Chemistry, 2018. **410**(4): p. 1217-1230.

241. Anany, H., et al., Biocontrol of Listeria monocytogenes and Escherichia coli O157:H7 in meat by using phages immobilized on modified cellulose membranes. Appl Environ Microbiol, 2011. **77**(18): p. 6379-87.

242. Brovko, L.Y., H. Anany, and M.W. Griffiths, Bacteriophages for detection and control of bacterial pathogens in food and food-processing environment. Adv Food Nutr Res, 2012. **67**: p. 241-88.

243. Walter, M., et al., Structure of the Receptor-Binding Protein of Bacteriophage Det7: a Podoviral Tail Spike in a Myovirus. Journal of Virology, 2008. **82**(5): p. 2265-2273.

244. Moller, A.G., J.A. Lindsay, and T.D. Read, Determinants of Phage Host Range in Staphylococcus Species. Applied and environmental microbiology, 2019. **85**(11): p. e00209-19.

245. Munita, J.M. and C.A. Arias, Mechanisms of Antibiotic Resistance. Microbiology spectrum, 2016. **4**(2): p. 10.1128/microbiolspec.VMBF-0016-2015.

246. El-Halfawy, O.M. and M.A. Valvano, Non-genetic mechanisms communicating antibiotic resistance: rethinking strategies for antimicrobial drug design. Expert opinion on drug discovery, 2012. **7**(10): p. 923-933.

247. Abraham, E.P. and E. Chain, An enzyme from bacteria able to destroy penicillin. 1940. Rev Infect Dis, 1988. **10**(4): p. 677-8.

248. Jensen, S.O. and B.R. Lyon, Genetics of antimicrobial resistance in Staphylococcus aureus. Future Microbiology, 2009. **4**(5): p. 565-582.

249. Cassidy, A., Medicare's hospital-acquired condition reduction program. 2015: Project HOPE.

250. Alder, J., The use of daptomycin for Staphylococcus aureus infections in critical care medicine. Critical care clinics, 2008. **24**(2): p. 349-363.

251. Kaur, R., et al., Daptomycin susceptibility of methicillin resistant Staphylococcus aureus (MRSA). The Indian journal of medical research, 2012. **136**(4): p. 676-677.

252. Viator, J.A., et al., Clinical testing of a photoacoustic probe for port wine stain depth determination. Lasers in Surgery and Medicine: The Official Journal of the American Society for Laser Medicine and Surgery, 2002. **30**(2): p. 141-148.

253. Goldschmidt, B.S. and J.A. Viator, Capture and Isolation of Circulating Melanoma Cells Using Photoacoustic Flowmetry. 2015.

254. Samson, E.B., et al., Photoacoustic spectroscopy of β-hematin. Journal of Optics, 2012. **14**(6): p. 065302.

255. Lilleengen, K., TYPING OF SALMONELLA DUBLIN AND SALMONELLA ENTERITIDIS BY MEANS OF BACTERIOPHAGE. Acta Pathologica Microbiologica Scandinavica, 1950. **27**(4): p. 625-640.

256. Leppänen, M., et al., Imaging Bacterial Colonies and Phage–Bacterium Interaction at Sub-Nanometer Resolution Using Helium-Ion Microscopy. Advanced Biosystems, 2017. **1**(8): p. 1700070-n/a.

257. Edgar, R., et al., Identification of MRSA infection in blood using photoacoustic flow cytometry. SPIE BiOS. Vol. 10878. 2019: SPIE.

258. Sader, H.S., R.K. Flamm, and R.N. Jones, Antimicrobial activity of daptomycin tested against Gram-positive pathogens collected in Europe, Latin America, and selected countries in the Asia-Pacific Region (2011). Diagnostic Microbiology and Infectious Disease, 2013. **75**(4): p. 417-422.

259. Ellis, E.L. and M. Delbruck, The growth of bacteriophage. Journal of General Physiology, 1939. **22**(3): p. 365-384.

260. McGuinness, W.A., N. Malachowa, and F.R. DeLeo, Vancomycin Resistance in Staphylococcus aureus. The Yale journal of biology and medicine, 2017. **90**(2): p. 269-281.

261. Colomb-Cotinat, M., et al., Estimating the morbidity and mortality associated with infections due to multidrug-resistant bacteria (MDRB), France, 2012. Antimicrobial Resistance & Infection Control, 2016. **5**(1): p. 1-11.

262. Khan, Z.A., M.F. Siddiqui, and S. Park, Current and Emerging Methods of Antibiotic Susceptibility Testing. Diagnostics (Basel, Switzerland), 2019. **9**(2): p. 49.

263. Kahanov, L., et al., Staphylococcus aureus and community-associated methicillin-resistant Staphylococcus aureus (CA-MRSA) in and around therapeutic whirlpools in college athletic training rooms. Journal of athletic training, 2015. **50**(4): p. 432-437.

264. Turner, N.A., et al., Methicillin-resistant Staphylococcus aureus: an overview of basic and clinical research. Nat Rev Microbiol, 2019. **17**(4): p. 203-218.

265. Asbell, P.A., et al., Increasing prevalence of methicillin resistance in serious ocular infections caused by Staphylococcus aureus in the United States: 2000 to 2005. J Cataract Refract Surg, 2008. **34**(5): p. 814-8.

266. Haas, W., et al., Monitoring antibiotic resistance in ocular microorganisms: results from the Antibiotic Resistance Monitoring in Ocular micRorganisms (ARMOR) 2009 surveillance study. Am J Ophthalmol, 2011. **152**(4): p. 567-574.e3.

267. Peleg, A.Y. and D.C. Hooper, Hospital-acquired infections due to gram-negative bacteria. The New England journal of medicine, 2010. **362**(19): p. 1804-1813.

268. Thorsen, T., et al., Dynamic pattern formation in a vesicle-generating microfluidic device. Phys Rev Lett, 2001. **86**(18): p. 4163-6.

269. O'Brien, C.M., et al., Capture of circulating tumor cells using photoacoustic flowmetry and two phase flow. Journal of Biomedical Optics, 2012. **17**(6): p. 061221.

270. Arthur, D. and S. Vassilvitskii. k-means++: the advantages of careful seeding. in SODA '07. 2007.

271. Corrigendum to Twenty-Year Trends in Antimicrobial Susceptibilities Among Staphylococcus aureus From the SENTRY Antimicrobial Surveillance Program. Open forum infectious diseases, 2019. **6**(5): p. ofz202-ofz202.

272. Başpınar, E.Ö., et al., Comparison of culture and PCR methods in the diagnosis of bacterial meningitis. Brazilian Journal of Microbiology, 2017. **48**(2): p. 232-236.

273. van Belkum, A., et al., Innovative and rapid antimicrobial susceptibility testing systems. Nature Reviews Microbiology, 2020. **18**(5): p. 299-311.

274. Theuretzbacher, U., et al., Analysis of the clinical antibacterial and antituberculosis pipeline. The Lancet Infectious Diseases, 2019. **19**(2): p. e40-e50.

275. Nicoloff, H., et al., The high prevalence of antibiotic heteroresistance in pathogenic bacteria is mainly caused by gene amplification. Nature Microbiology, 2019. **4**(3): p. 504-514.

276. Torres-Barceló, C., The disparate effects of bacteriophages on antibiotic-resistant bacteria. Emerg Microbes Infect, 2018. **7**(1): p. 168.

277. Marchese, A., et al., Heterogeneous vancomycin resistance in methicillin-resistant Staphylococcus aureus strains isolated in a large Italian hospital. Journal of clinical microbiology, 2000. **38**(2): p. 866-869.

278. Takesue, Y., et al., Impact of a hospital-wide programme of heterogeneous antibiotic use on the development of antibiotic-resistant Gram-negative bacteria. Journal of Hospital Infection, 2010. **75**(1): p. 28-32.

279. Vali, L., et al., Characterization of Heterogeneous MRSA and MSSA with Reduced Susceptibility to Chlorhexidine in Kuwaiti Hospitals. Frontiers in Microbiology, 2017. **8**(1359).